UNIVERSITÁ DEGLI STUDI DI PADOVA -

KUNGLIGA TEKNISKA HÖGSKOLAN

DIPARTIMENTO DI INGEGNERIA INDUSTRIALE

CORSO DI LAUREA MAGISTRALE IN INGEGNERIA DEI MATERIALI

TESI DI LAUREA

# SUBZERO TENSILE PROPERTIES OF A WELDED DUPLEX STAINLESS STEEL

*Relatore interno: IRENE CALLIARI*

*Relatore esterno: ROLF SANDSTRÖM*

*Tutor: JOHAN PILHAGEN*

*Laureando: PAOLO CASAROTTO*

*Matr. n. 622339 - IR*

Anno Accademico 2011/2012

# SUBZERO TENSILE PROPERTIES OF A WELDED DUPLEX STAINLESS STEEL

*PAOLO CASAROTTO*

**Abstract**. In this work, tensile properties of different welds on duplex LDX2101 are studied. LDX2101 is intended for general industrial purposes due to its mechanical properties, corrosion resistance and cost. Compared to most common duplex grades, LDX2101 is alloyed with less nickel and more nitrogen. The main difference between the welds is the decreasing nickel content: the different mechanical behaviors are interesting to be investigated due to the cost of the element. All welds have the same X geometry, are performed predominantly with submerged arc welding and are not subjected to post-heat treatment. Specimens are extracted according to three different orientations from each weld type. Materials are tested at temperatures between 20 ° C and -40 ° C.

**Abstract**. Nel presente lavoro vengono studiate le proprietà tensili di diversi tipi di saldatura su acciaio duplex LDX2101. Questo acciaio è destinato a generici usi industriali, qualora particolari proprietà meccaniche, resistenza alla corrosione ed economicità vengano richieste. Rispetto ai gradi duplex più comuni, LDX2101 è alligato con quantità inferiore di nickel e superiore di azoto. La principale differenza tra le saldature studiate è il tenore decrescente di nickel: i diversi comportamenti meccanici sono interessanti da indagare dato il costo dell'elemento. Le saldature presentano tutte la stessa geometria ad X, sono effettuate prevalentemente con tecnica ad arco sommerso e sono prive di post-trattamento termico. Campioni sono estratti secondo tre diverse orientazioni da ogni tipo di saldatura. I materiali vengono testati a temperature comprese tra 20°C e -40°C.

KTH - Materialvetenskap / Università di Padova – Dipartimento di ingegneria industriale

*Academic year 2011/2012*

*Key words*: Duplex stainless steels, Welds, Tensile properties, Low temperatures

# Index

# 1 INTRODUCTION

Duplex stainless steels have a biphasic microstructure consisting of δ-ferrite and γ-austenite in quantity of nearly 50%-50% in order to achieve excellent mechanical properties.

Duplex steels were already known and marketed during the '30s. The first duplex steel was produced in Sweden for use in paper industry due to good anti-corrosion properties.

Between the '60s and the '70s, a world-wide nickel shortage, alongside the development of oil and gas extraction in the North Sea, encouraged the use of corrosion-resistant steels with lower nickel content. Moreover, production techniques like Argon and Vacuum Oxygen Decarburitazion (AOD and VOD) were introduced, leading to high quality and high reproducibility thanks to lower carbon and controlled nitrogen contents.

Years '80s saw the development of a new generation of duplex steels, with improved properties due to nitrogen addition.

During 2000-2010, duplex steel production nearly doubled in volume. Today, the most common duplex grade is 2205 (UNS S31803/S32205), with a composition 22% Cr – 5% Ni – 3% Mo – 0,16% N. 2205 is often taken as reference to compare other duplex grades. New studies keep broadening knowledge about duplex steels.

There are two main ideas standing at the base of duplex steels production and development. Mechanically, the two-phases microstructure increases tensile properties, hinders cracks propagation and leads to toughness-increasing mechanisms. Regarding the corrosion behavior, ferritic steels have higher stress-corrosion resistance than austenitic ones, which otherside have more resistance to general corrosion: so, duplex steels can reach a compromise.

Despite their niche production, duplex steels can be used to make pipelines, heat exchangers, boilers, scrubbers, stirrers, shafts, engine parts, propellers, tanks, digesters in a lot of fields, such as paper, gas, biofuel, nuclear, food and pharmaceutic industries. A key field for their use is the offshore oil extraction.

Duplex steels have higher specific strengths than other stainless steels and they are competitive regarding costs .

Their pitting and crevice corrosion resistance is comparable to those of austenitic stainless steels. An industrially accepted measure to quantify pitting resistance is the PRE (pitting resistance equivalent): duplex steels usually show values around 40, while the austenitic grade 316 stands at about 24.

Pieces in working condition usually contain welds, so studying weld properties is essential in order to understand the usability of duplex steels.

Some duplex steels stand well subzero temperatures, anyway they are generally suggested to not be used below -40° C having lower ductility than austenitic steels, [1]. Tensile tests at low temperatures are difficult to perform, so deep studies about tensile properties of differently welded duplex stainless steels at subzero temperatures still cannot be found in literature.

A duplex grade that is still case of study is the lean grade LDX2101®: it has slightly lower mechanical and corrosive properties than 2205, but has the great advantage to be cheaper because of lower nickel content. LDX2101 is usually welded with filler containing 7% of nickel in order to reach good phase balance. Since nickel is a strategic metal, it is worthy investigating if using lower nickel containing fillers permits to reach satisfactory mechanical properties. Moreover, tensile properties can be used to model the toughness behavior of materials.

The aim of this work is studying tensile properties at low temperatures of LDX2101 duplex stainless steel welded with different nickel contents. The materials have been provided to the Swedish Royal Institute of Technology by the Finnish company Outokumpu, current leader in duplex steels production.

The reported information about history of duplex steels are drawn from [2].

# 2 TENSILE TESTS

## 2.1 General points

Tensile tests are the most common mechanical tests performed on materials. They quantify properties such as yield strength, ultimate tensile strength, elastic modulus and elongation to fracture of a material once defined testing conditions are set. Datas coming from these tests are commonly reported in material specifications: they are often used to compare candidate materials for mechanical applications or to discriminate the effectiveness of different processes for the production of materials.

Tensile datas can also be used to study the behavior under non-uniaxial tensile conditions of isotropic materials; for instance, the shear yield strength of steels can be esteemed taking half of the tensile yield strength value, if more reliable experimental datas are not available.

Knowing the elastic modulus of materials is essential to predict the deformation of workpieces, to calculate their flexural stiffness or to estimate hygrothermal stresses during their lifetime.

In statically stressed workpieces, the yield strength, corrected with a suitable safety coefficient, should never be exceeded. Moreover, the yield strength is used to plot the Wohler curve for dynamically stressed pieces.

The ultimate tensile strength is less important to design structures, but knowing it can be useful to design plastic deformation processes.

The total elongation to fracture helps to judge the ductility of a material and the quality of the process used to obtain it.

All these properties are influenced by experimental conditions, such as temperature and testing strainrate. Temperature usually lowers the elastic modulus, the yield and the tensile strengths while increasing the total elongation, that is the opposite of what higher strainrates do.

## 2.2 Stress-strain curves

The output datas of tensile tests are elaborated to plot stress-strain curves from which mechanical properties can be obtained. Stress vs strain curves have the advantage of being

independent of specimen size.

The most important curve consists of the engineering (or nominal) stress in relation to the nominal strain. The former and the latter are respectively defined as Eqs. (1) and (2):

$$\sigma_{ing} = \frac{F}{A_0} \tag{1}$$

$$\varepsilon_{ing} = \frac{\Delta L}{L_0} \tag{2}$$

where $A_0$, $L_0$, $\Delta L$ and $F$ are the initial area, the initial length of the specimen, the elongation and the force value respectively. The initial part of the curve for a metal alloy has usually a steep slope and it is quite straight: it corresponds to the elastic behavior of the material. Once released within this range, the specimen should spring back as it was without any permanent deformation, due to the relaxation of stretched atomic bonds. In practice, metals that behave perfectly elastically do not exist. The slope of the first part of the curve is the elastic or Young's modulus and a typical value for steels is 200 GPa. After the elastic range, the plastic deformation starts and the slope of the curve decreases.

The yield strength is the engineering load at which the stress trend should start deviating from linearity. This deviation is not always definite. In some materials like structural steels, the yielding is clearly viewable in the curve as a portion of zig-zag load connected to progressive formation of Lüders bands at 45° in respect of the specimen axis. In other materials, like duplex stainless steels, the transition is gradual. Current standards, [3], say that the yield strength can be taken as the load in which a straight line parallel to the elastic portion passing through 0,002 elongation abscissa value intersects the curve. This means that the yield strength is taken as the load from which the specimen, once unloaded, keeps a permanent 0,2% nominal elongation.

The point of maximum engineering load is called ultimate tensile strength. The necking of a specimen usually occurs in correspondance of this value, after which the load starts decreasing. The yield strength is often named Rp0,2 and the ultimate tensile strength Rm.

For tested specimens it is also possible to draw the true stress-strain curve, of course. The advantage of dealing with this kind of curve is that strain values are additive and refer

moment by moment to the actual specimen length. True stress values account for the actual stress-bearing capacity of the material. True curves can be obtained from direct measures that require complex instruments or can be deduced from engineering ones, as in this work.

The actual stress is defined as in Eq. (3):

$$\sigma = \frac{F}{A} \tag{3}$$

where A is the current section when force F is applied. Actual strain is defined in Eq. (4):

$$\varepsilon = \ln \frac{L}{L_0} \tag{4}$$

and it is meaningful until necking is reached. Eq. (4) comes from taking an infinitesimal increment of length dL, dividing it by the total length L and integrating from the initial length $L_0$ to the final L.

In case the elongation - elastic or plastic - is uniform in the gauge length, a direct relation between engineering and true stresses and strains subsists and true measures can be deduced by engineering ones. During uniform deformation, the volume is assumed to be constant, i.e.

$$V = A_0 L_0 = A L \tag{5}$$

and consequently Eq. (6) is valid.

$$\frac{A_0}{A} = \frac{L}{L_0} \tag{6}$$

As a matter of common sense, Eq. (7) is valid, too.

$$L = L_0 + \Delta L \tag{7}$$

Considering Eqs. (2), (6) and (7), Eq. (8) can be obtained.

$$\frac{A_0}{A} = 1 + \varepsilon_{ing} \tag{8}$$

Eq. (3) can be rewritten as Eq. (9).

$$\sigma = \frac{F}{A_0} \frac{A_0}{A} \tag{9}$$

Using Eqs. (1), (8) and (9), the true stress is obtained, Eq. (10).

$$\sigma = \sigma_{ing}\left(1+\varepsilon_{ing}\right) \tag{10}$$

Recalling Eqs. (4), (6) and (8), the true strain is obtained with Eq. (11).

$$\varepsilon = \ln\left(1+\varepsilon_{ing}\right) \tag{11}$$

It must be underlined that the assumption of constant volume, even if quite reliable, has an empirical base: if true values are deduced from engineering ones, systematic errors rise.

After the necking of the specimen, formulas to deduce true values are no longer valid. Firstly, the so calculated stress would be the stress at the base of the necked zone, not in the restricted section. After necking, then, the elongation is concentrated in the necked zone: Eq. (4) would be serviceable only if L and $L_0$ were relative to a very short zone without section variations placed in the middle of the necked area. So, in the absence of direct measurements, the true curve after necking should be drawn connecting the necking point to the final point of coordinates ($\sigma_f$, $\varepsilon_f$) calculated a posteriori measuring the restricted area $A_f$ at failure:

$$\sigma_f = \frac{F}{A_f} \tag{12}$$

$$\varepsilon_f = \ln\frac{A}{A_f} \tag{13}$$

Eq. (13) can be obtained from Eqs. (4) and (6).

Actually, even being able to measure the necked section in real-time, neither Eq. (3) would be actually correct to depict the stress in the material: the necking introduces a three-dimensional stress state, while regions out of the necked zone unload elastically. So, the stress in the necked material would be slightly greater than Eq. (3) would say. There are analytical (the so-called "Bridgeman correction") and numerical approaches to calculate the "real" true stress after necking, but these considerations go beyond the aim of this work.

When the strain is low, differences between true and engineering stresses and strains are negligible and the elastic modulus can be deduced from both curves. Engineering curves can be obtained from direct simple measurements and engineering properties are conservative and commonly used. So, this work firstly pays attention to them.

An interesting measure is the total percent elongation to fracture, Eq. (14):

$$T.E. = \frac{L - L_0}{L} x\,100 \tag{14}$$

In literature, A5 total elongation values are usually found. A5 elongation is defined as Eq. (14) where the initial length of the specimen is given by Eq.(15):

$$L_0 = 5{,}65\sqrt{S_0} \tag{15}$$

where $S_0$ is the inital cross-section.

Other measure can be important to study the tensile behavior of materials, but have not been studied due to lack of proper tools and complexity of measurements on a big number of tests. They are for instance the Poisson modulus, i.e. the ratio between transversal and longitudinal strains in the elastic range, and the percent reduction of area at fracture.

# 3 DUPLEX STAINLESS STEELS

## 3.1 General points

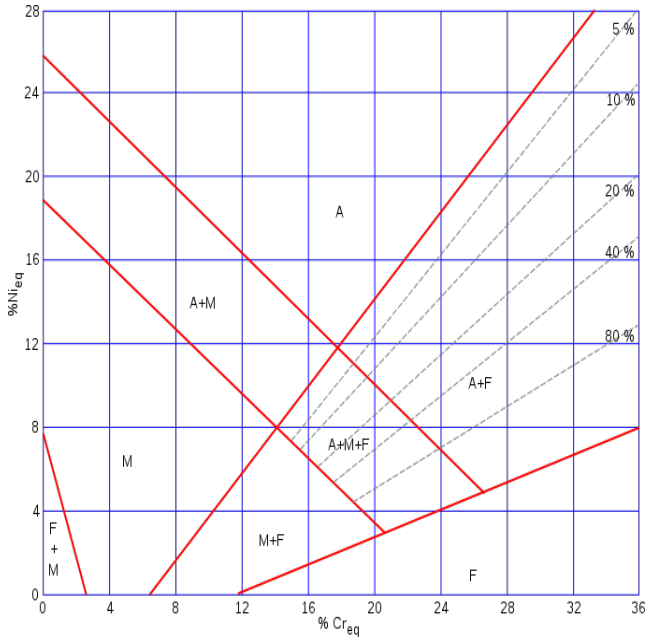


*Fig. 1: Schaeffler diagram: A+F is the area of existence of duplex stainless steels,* [4]

Information in 3.1 and 3.2 is taken from [2]. Duplex stainless steels compostition always contemplates Ni, Cr and Mo: the former element is an austenite stabilizer and the latter are ferrite stabilizers. The usual percent ranges of these elements are respectively 4÷6%, 18÷28% and 1,5÷3%. Beside these elements, many other ones contribute to determine the ferrite/austenite ratio and the final properties. Since Ni and Cr are the alloying elements present in larger amount, the contribution of other alloying elements to the formation to the phase balance is depicted by Eqs. (16) and (17).

$$Ni_{eq} = \% Ni + 35\% C + 20\% N + 0{,}5\% Mn + 0{,}25\% Cu \quad (16)$$

$$Cr_{eq} = \% Cr + \% Mo + 1{,}5\% Si + 0{,}7\% Nb \quad (17)$$

C and N are both important in austenite stabilization, even if scarce in respect of Ni. Cr and Mo have equal ferrite stabilizing effect and the other ferrite stabilizers are scarce in duplex steels.

The Schaeffler diagram shows the field of existance of duplex steels in relation to $Ni_{eq}$ and $Cr_{eq}$ (zone A+F), see Fig. 1.

The structure of duplex stainless steels consists of austenite (γ phase) and δ-ferrite phase. The ideal volume proportion should be 50%-50%. As seen Fig. 1, suitable proportions of ferrite and austenite stabilizers (mainly chromium and nickel) must be provided in order to obtain a double phase structure after solidification.

During cooling, duplex steels first solidify as ferrite; later, austenite starts nucleating and growing. Three morphologies are possible for the austenite depending on the temperature at which it forms. From higher to lower temperatures they are: grain boundaries allotriomorphs, Widmanstätten side plates and intragranular precipitates, [5]. The formation of the first two austenite morphologies requires a small driving force, i.e. it can occur in large amount with little cooling, if the latter is slow enough. Intragranular austenite requires instead a greater degree of cooling and tends to form if the latter is fast.

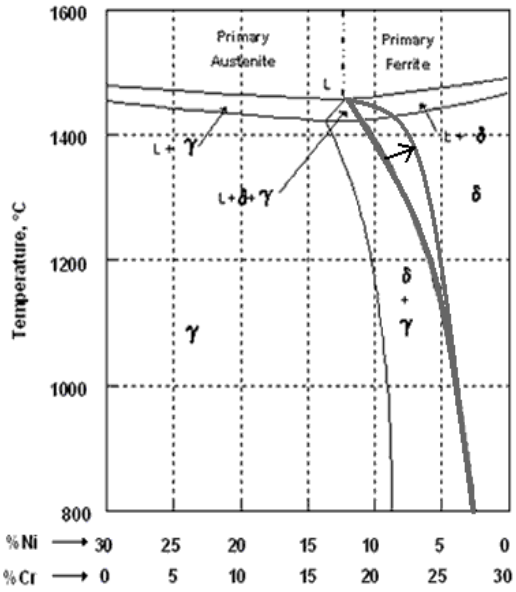


*Fig. 2: Diagram of phase existance,* [6]

### 3.2 Influence of alloying elements

Here follows an overview about the effects of the main duplex alloying elements: all of these can have both positive and negative effects on mechanical and corrosion properties of duplex steels. Their mechanical effects come mostly from their contribution to the phase balance, see Eqs. (16) and (17). The relative quantities of these elements lead to obtain slightly different duplex steels.

*Chromium*

This element improves the localised corrosion resistance by formation of a passive oxy-hydroxide film. The limit for Cr content is due to enhancement of detrimental intermetallic precipitations (see 3.3).

*Molybdenum*

Mo increases pitting and crevice corrosion resistance in chloride solutions thanks to its contribution to the formation of the oxy-hydroxide layer, with molybdate ions incorporated in

it. The limit of Mo content is 4%, because it enhances σ phase precipitation above 1000° C.

*Nickel*

In duplex steels, the ferrite/austenite balance should be kept within 0,4 and 0,6. Nickel must be added in relation to the content of chromium and other ferrite stabilizers in order to achieve the right balance. Nickel increases of course $Ni_{eq}$ and also raises the solvus line (see the arrow in Fig. 2). This means that Ni permits the austenite formation at higher temperatures and increases its quantity at equilibrium, [7]. The raise of the solvus also means that high temperature austenite morphologies (see 3.1) are more stable and so are promoted during cooling. An excess in Ni can lead to excessive austenite level with Cr and Mo that concentrate in the remaining ferrite, so that intermetallic precipitation may be enhanced. Nickel has also direct positive effects on the corrosion resistance. Unfortunately, Ni can accelerate α' precipitation in the ferrite, see 3.3.

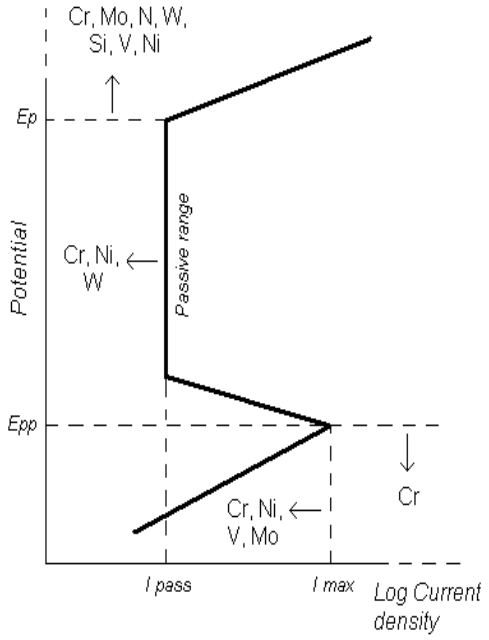


*Fig. 3: Effect of alloying elements on the polarization curve,* [8]

*Nitrogen*

This element increases the corrosion resistance since it enlarges the passive range, see Fig. 3. N has a sinergic influence with Mo on pitting resistance. N is a strong austenite stabilizer: this role is particularly important in welding because of the enhanced austenite reformation during cooling, in particular within the HAZ. N can have even more intense effect as Ni in raising the solvus line, see Fig. 2. This means that equilibrium austenite content at lower temperatures can be equal to that at higher temperatures: therefore acceptable austenite content can even be achieved with rapid cooling rates, as its nucleation and growth at higher temperatures is encouraged, [7]. Fundamental effects of N in duplex steels are the stabilization against intermetallic precipitations and the reduction of Cr-partitioning between austenite and ferrite. An increase in N content can also reduce nitrides formation: this contradictory effect is due to the

increased content of austenite, which solubilizes more the N itself. Being an interstitial element, N increases mechanical strengths. Cr and Mn help to not reach the N solubility limit: if their quantities are too low, N can cause out-gassing and, after solidification, porosity.

*Manganese*

Mn addition can improve abrasion and wear resistance, as well as strength without loss of ductility if σ phase precipitation is avoided. Mn can also increase N solubility, avoiding the risk of out-gassing, particularly problematic in welding. The combined presence of N and Mn improves the pitting resistance, but excess of Mn in respect of N leads to MnS formation which instead decreases the pitting resistance. So, N content sets limit to Mn content: for example, 3% Mn should not be exceeded for 0,1% N. Mn increases tendency to σ phase formation.

*Copper*

This element can reduce both the general and the crevice corrosion in non-oxidising environments. Copper addition should be limited to 2%, because higher levels reduce hot ductility and enable precipitation hardening.

*Tungsten*

W helps to improve pitting and crevice corrosion resistance. In acid chloride solutions it reacts to form insoluble $WO_3$ which goes to the passive film strengthening it. Unfortunately, W encourages $\gamma_2$ formation in heat treated weld metal and intermetallic precipitations between 700° and 1000° C. W content of 2% should never be exceeded.

*Silicon*

It is effective for concentrated nitric acid and high temperature oxidation resistance. It is preferable limiting it to 1%, since it is involved in σ phase formation.

Carbon content is limited at 0,02÷0,03% in order to avoid Cr carbides which can act as pitting and intergranular corrosion starters. Phosphorus and sulphur contents are also controlled, even if not totally suppressed in order to allow more weld bead penetration.

### 3.3 Intermetallic phases

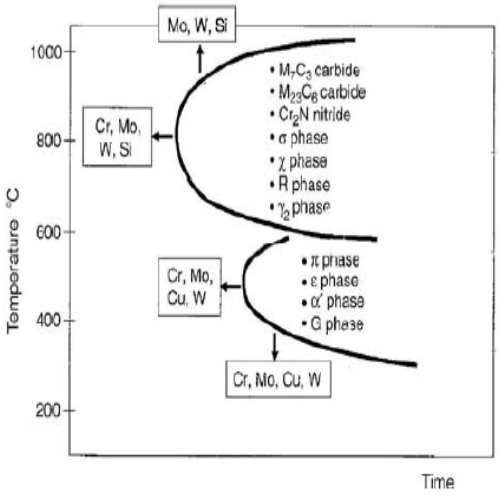


*Fig 4: TTT diagram of secondary phases in duplex steels,* [9]

At temperatures between 550° and 1050°C, duplex steels may be subjected to formation of secondary phases. Precipitations can also occur at temperatures down to 300° C. Unfortunately, 1÷3% of secondary phases in duplex steels are usually enough to cause dangerous drops of elongation to fracture as well as of corrosion properties.

Here follows a brief description of the main phases that can be found in duplex steels with relative temperature ranges of formation. Information, unless otherwise indicated, is taken from [2] and [10].

*Precipitations within 550°÷1050° C range*

*σ* is a hard intermetallic phase with average composition 32% Cr, 55% Fe, 6% Mo and with a tetragonal lattice. It forms between 600°÷1000°C, with a peak at 850°C, [11]. Its lattice parameters can show big variations depending on the presence of different interstitial or substitutional atoms. σ phase can precipitate at δ/γ grain boundaries, austenitised δ/δ sub-grain boundaries and δ/δ grain boundaries in deacreasing order of preference. σ nuclei can grow in coarse plates, lamellaes in a $\sigma+\gamma_2$ eutectoid or σ+δ lamellar aggregates. Since ferrite is richer than austenite in Cr and Mo, σ preferentially grows in it. σ phase is brittle and non-magnetic. σ is the most common cause of elongation to fracture drop in duplex steels. The critical cooling rate that should be exceeded in order to avoid σ precipitation is 0,35°C/s for duplex steels with average chromium content, [12].

*χ* has cubic lattice and is rich in Cr (24%) and Mo (15%). χ has similar temperature formation range as σ (700°÷900°C), with the same peak at 850°C and grows in the ferrite. It forms in less quantity than σ, so it is difficult to distinguish the two phases, at least with light microscopy. χ formation locally subtracts Mo to the ferrite, making it more prone to be transformed to austenite. χ can also act as precursor of σ. The critical cooling rate that should be exceeded in order to avoid χ precipitation is 0,1÷0,15°C/s, [12]: if the critical cooling rate

for σ is provided, χ cannot form for sure.

$\gamma_2$ precipitates between 600°÷900°C. Between 700°÷900°C, it can form an eutectoid with σ, cause it absorbs Ni rejecting Cr and Mo, in turn absorbed by σ; $\gamma_2$ can precipitate with $Cr_2N$ for the same reason. Between 650°÷800°C, Widmanstätten $\gamma_2$ precipitates in a diffusive way from ferrite, absorbing Ni. At 600°÷650°C, $\gamma_2$ precipitates from ferrite without diffusion.

*$Cr_2N$* and *CrN* form between 700°÷950°C from ferrite supersaturated in N. The N solubility drops as temperature decreases during cooling. In particular, the former nitride can precipitate as needles in ferrite grains even if quench is fast.

*$M_{23}C_6$* forms between 650°÷950°C and it can be avoided with low C content (actually the latter is quite low in duplex steels) and fast cooling rate since around 800°C it takes nearly 1 minute to precipitate. M stands for metal atom.

*$M_7C_3$* form in the range 950°÷1050°C and can be avoided with low C content and fast cooling rate, since its precipitation takes 10 minutes to start.

*R* is composed of Fe, Cr and Mo and forms between 550°÷650°C. It reduces the localized corrosion resistance.

*Precipitations within 300°÷650° C range*

*π* is a phase containing Mo, Fe and N with precipitation temperature around 600°C. It takes long time to start precipitating, so it is not a usual problem.

*ε* precipitates at around 500°C. It is very rich in Cu and can also improve mechanical properties, but its precipitation takes more than 100 hours so it is definitely not common.

*τ* forms after long permanence in the range 550°÷650°C.

*α′* comes from spinodal decomposition of ferrite in the range 300°÷525°C and it is often linked to the presence of $Cr_2N$.

*G* precipitates in the range 300°÷400°C at the interface between ferrite and α' due to enrichment of Ni and Si.

# 4 WELDING METHODS

The welding methods used on the tested materials are MIG (metal arc inert gas, often indicated with the more generic term GMAW, gas metal arc welding) and SAW (submerged arc welding). Both of them exploit an electric arc and a consumable electrode, i.e. the electrode itself provides the filler material. These two methods are here introduced. Information, unless otherwise indicated, is taken from [4].

## 4.1 MIG

This technique is popular due to relatively low cost equipment, good controllability and high production rates. The electric power involved is high and the equipment is not portable. The welds are realized with a welding torch, that can be handled manually or with a mechanical arm.

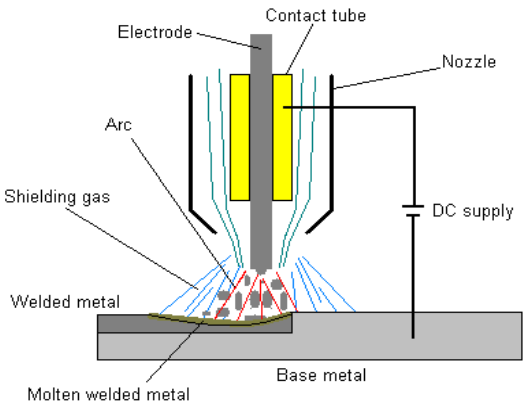


*Fig. 5: Scheme of MIG welding*

During MIG welding, a wire-drive makes the wire-electrode sliding inside a copper contact tube as the fusion takes place. The tube is electrically connected to the workpiece. The contact tube must be adherent to the wire in order to transfer current to it, but must let it slide without interruptions. The electric arc between the electrode and the workpiece is necessary to close the electric circuit and melt the filler material. A shielding gas is made to flow on the weld during the process. The current can cause the fusion of the electrode only when the polarity is reversed, i.e. electrons are directed towards the electrode heating it. The current is usually continuous, but alternating current is often used in duplex steel welding. The electrode usually has similar chemical composition to the base metal and is additioned with deoxidizing agents to avoid welding defects. The filler deposition may be performed either with spray (common duplex welding), globular (with large metal droplets dripping from the wire) or short circuit mode (with the wire immersed in the molten pool). Typical MIG welding speed rates are 2÷10 m/min, maximum 30 m/min. Up to 20 kg/h can be deposited.

Variations of arc length, i.e. distance between the welding torch and the workpiece, cause changes in arc voltage, which in turn cause current and heat input variations. Automatic systems for controlling the wire feed rate in relation to the arc voltage are available.

In respect to submerged arc welding, 4.2, MIG permits a direct observability of the arc and can be performed with non-planar, non-horizontal geometries.

*Shielding gases*

A key aspect in MIG is the presence of shielding gas. The latter is used in order to protect the molten pool from atmospheric gases such as $O_2$ and $N_2$, which can cause porosity and precipitation of embrittling phases.

The choice of the shielding gas depends on the type of material that must be welded and the process. Pure He and Ar cannot be used with stainless steels. The former allows great energy transfer because its ionization heat is high, but the arc would not be very stable and spatter would be encouraged. The second does not allow ideal welding penetration, although it protects the weld effectively being heavier than air. Pure $CO_2$ causes spattering and encourages oxides formation, but is inexpensive. Other shielding gases that can be added in the gas mixture are $H_2$, $N_2$ and $O_2$. An oxygen content up to 5% is usually required for the arc stability. $CO_2$ and $O_2$ allow faster metal transfer to the workpiece; they are oxidizing gases and so have chemical activity. If they are used, the welding technique is more properly called MAG, i.e. metal-arc active gas.

The shielding gas is distributed evenly with a nozzle to avoid inconsistent flow, which would cause inadequate protection of the weld area. Factors that lead to greater demand for gas feed rate are: flat surfaces (because they disperse gas quickly), high welding speed and larger He amount in the mixture (because it is lighter than air).

An excellent technique to improve corrosion resistance is using a back-shield gas, i.e. a gas made flow at the opposite side than the welding one. This gas can be 100% $N_2$ or being additioned with $H_2$: the nitrogen should stabilize the austenite, which content is often critical in duplex welds. Anyway, the flow rate must not be as high as to cause mixing of the melted metal and so spitting, porosity or hydrogen embrittlement.

*MIG on duplex steels*

So far, the usual way to perform MIG welds on duplex steels is the pulsed spray mode, as stated in [13].

The spray technique requires high voltage and direct current. The electrode is quickly reduced to small drops and the wire feed rate is high. The final quality of the weld is high and the spatter is avoided, because there are no large drops impacting the molten pool. The technique does not cause much nitrogen loss and so permits welds with good corrosion resistance. The heat input is high and the melted area is wide: spray MIG is used predominantly for welds on flat horizontal areas.

The pulsed mode evolves from the spray mode: it requires alternating current to melt the wire and makes a small droplet dripping from the electrode at each pulse. This method allows the use of lower current than usual spray MIG, lowering the total heat input and thus decreasing the size of molten pool and HAZ. Pulsed spray is also geometrically versatile and suitable to weld thin pieces. Pulsed spray mode requires nearly 10 l/min shielding gas feed rate. The obtainable welding speed rate is 5m/min. Current frequencies of 30÷400 Hz are required.

*MIG welding defects*

Defects can start cracks and reduce resistant sections, so it is worthy introducing them.

- *Porosity*. Air can contaminate the weld with nitrogen and oxygen, the water with hydrogen coming from its dissociation; other gases can come from contaminants in the filler or impurities in the shielding gas. The welding is not a process in thermodynamic equilibrium: the amount of gas in the molten pool is higher than calculable. With the decrease in temperature the solubility decreases, so gases tend to gather in bubbles: these can leak due to convective motions or remain trapped in the weld if the metal solifidifies before their expulsion. The pores are stress concentrators. Gases may also remain in the weld as dissolved monoatomic species: in this case they do not lead to pores, but to interstitial hardening, stabilization of phases or formation of fragile compounds. Pores can be avoided increasing the time for cooling, selecting materials carefully, or increasing the shielding gas flow rate.

- *Hot cracks*. They come from tensions in the workpiece due to thermal variations: they

originate if stresses are greater than the strength of the material. Hot cracks are usually parallel to the welding direction and form when some areas (usually at the center of the bead) cools more slowly than others: these areas solidify after the surrounding material, causing dangerous stresses. Hot cracks may be due to the presence of low-melting elements such as S and P (that concentrate in the liquid center of the weld) or to excessive welding speed of the torch which leaves thin trails of molten material behind itself. Hot cracks can also generate at grain boundaries, which are richer in low-melting elements: those areas solidify later, causing same problems as before. In order to avoid hot cracks, materials with as little S and P content as possible should be used and lower welding speed or faster cooling should be provided.

- *Lack of fusion*. This defect comes from weak bond between filler and base metal. In case of multipass, lack of fusion may involve subsequent passes. MIG melts the filler material more than the workpiece metal so it can give this defect. In order to avoid it, it is important working on clean pre-heated pieces, with appropriate electrodes and geometric profiles.

- *Undercut*. This defect, due to high heat input, consists of notching at the edges of the weld bead: these zones can concentrate stresses in work.

### 4.2 SAW

This mechanized process is widely used in duplex welding because of its high productivity. The process produces nearly no smoke and light pollution, therefore the impact on the work environment is reduced. The edges that must be jointed are covered with dry granular flux having low melting point. The electrode, consisting of filler metal, is immersed in the flux. The electric arc snaps between electrode and workpiece fusing the granular material which becomes conductive: the function of the latter is triggering and protecting the arc, i.e. the same function as the shielding gas in MIG. The flux also permits to avoid spark and spatter. Once the arc is stabilized, the power feed can be increased in order to transfer more energy to the weld. SAW exploits reverse polarity, so that the electrode is invested by current, is heated and can melt. The current (500÷2000 A) can be both AC and DC. Considerations made describing MIG about electrodes are still valid.

High depth of penetration can be reached: SAW is suitable for large or highly stressed workpieces. SAW is generally automatized. Deposition rates are the best among all welding techniques: up to 45 kg/h. Preparation of the edges is practically not requested and distortion of finished pieces is reduced. More than 50% of the flux can be recovered. The use of SAW is usually limited to flat horizontal surfaces because of the large molten pool and the use of flux.

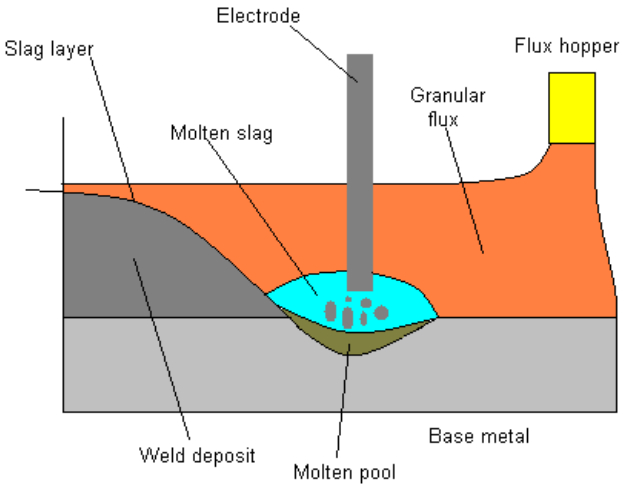


*Fig. 6: Scheme of SAW welding*

*Fluxes*

Information in this paragraphs is taken from [14]. Granular materials used in SAW must have low melting point and they must be incompatible with the melted metal in order to float on it. After welding, the slag should be brittle enough to be removed mechanically. Fluxes consist mainly of $MnO\text{-}SiO_2$ or $CaO\text{-}SiO_2$. Compounds that can be added contain Mn and Ca that have deoxidizing function. Compounds of Ca and Mn can react with S and P to purify the molten pool. Na and K silicates can improve the arc stability.

Fluxes are not well classified. They can be acid, basic or neutral. The former has high silica content, which subtracts Cr from the molten pool. The basic ones are low in silica and they should not alter significantly the Cr content. The neutral ones are addiotioned with Cr.

*Weld defects in SAW*

- *Porosity* (same considerations as for MIG welding).
- *Hot cracks*.
- *Lack of fusion*.
- *Inclusions*. This is the most common defect in SAW. The welding is turbulent, so some flux powder always moves to the molten pool. Thanks to chemical incompatibility and convection, it should leave the pool just floating on it, but few flux granules can

remain trapped in the metal as it solidifies. The joint resistance can vary from the one calculated by the designer in relation to quantity, dimension and disposition of inclusions. These defects are common in zones less involved by convection during welding.

### 4.3 General issues about duplex welding

Duplex steels require an approximate 50/50 ferrite/austenite balance and they are alloyed with big quantities of elements that can form intermetallic compounds. The cooling rate is the basic parameter which influences both phase balance and precipitations. The parameter usually refers to $\Delta_{12/8}$, i.e. the time to make the joint cross the 1200°÷800°C range (the austenite forms in this range). $\Delta_{12/8}$ is just indicative since cooling cannot be uniform in the entire joint. In order to reach satisfying austenite quantity and avoid secondary phases, $\Delta_{12/8}$ should stay between 4÷15 s, i.e. the cooling rate should be 27÷100°C/s, [15]. Cooling rate is controlled by factors like geometry, heat input, pre-heat and interpass temperature, besides obviously chemical composition.

A general problem in welding is the formation of the heat affected zone (HAZ). The temperature profile decreases gradually from the molten pool towards the base metal: right out of the fusion line, a portion of solid metal undergoes to undesired heat treatment. Classic problems in the HAZ are excessive grain growth, incorrect phase balance and precipitation of secondary phases, see 3.3. Coarser grains lead to drop of strength. However, the HAZ in duplex steels is usually narrow and does not represent a crucial problem, see 6.2.

Large weld thicknesses cannot be performed with a single pass: this would require too much energy and would promote welding defects. Other problems that can occur are for example excess of dilution and segregations. Dilution occurs when filler is used during welding, because of mixing with base material. If the filler is excessively diluted, the welding does not acquire the desired properties. Segregations can occur in the stagnant zone between melted and solid metal, where mixing is reduced. Various elements may concentrate in the aforesaid zone, resulting in stabilization of certain phases, unwanted secondary phases and hydrogen concentration.

The multipass technique, i.e. welding with more subsequent passes, can significantly reduce problems connected to HAZ, dilution and segregation. Therefore, it is widely used to weld large thicknesses. The multipass ensures chemical homogenization since it mixes the weld

area at each pass, gives more controllability, minimizes the molten pool and allows to use adequate heat input for the material. The sequence of welding must be carefully planned to ensure metallurgical characteristics and high productivity. After the root pass, filler of the same type is often used but with faster welding process.

Regarding distortions during welding, duplex steels have lower thermal expansion coefficient and similar heat conductivity as austenitic steels, so their welding give less risks.

A fundamental parameter that influences productivity and microstructure is the heat input. It is also called arc energy if the heat is intended to come from the welding procedure only. It is defined as Eq. (18).

$$H.I. = \frac{V * I}{s * 1000} \tag{18}$$

where V is the voltage [V], I the current [A], s the travel speed [mm/s] to give [kJ/mm].

An increase in heat input lowers the cooling rate: this can enhance austenite formation. Unfortunately, a higher H.I. affects more HAZ and weld metal, lowers the productivity rate and leads to deformations and excessive molten pool size. The welding process may not be the only heat source: there can be heat from previous passes or pre-heat (see below). These contributions must be quantified in order to provide the correct global heat input. There are tables that connect the heat input with the desired $\Delta_{12/8}$ and plate thickness. LDX2101 is sensitive to H.I.: the latter should not exceed 1,5 kJ/mm. Duplex steels cannot be welded with too low heat input, as well: the cooling rate would be too high, resulting in dangerous ferrite level. The minimum H.I. suggested for LDX2101 is 0,3 kJ/mm, [1].

Pre-heat is sometimes performed in order to increase the global heat input, to let hydrogen flow out of the pieces harmlessly and to reduce stresses in the weld and so improving mechanical properties. Pre-heat, anyway, is not usually performed in duplex steels welding.

The interpass temperature, i.e. the temperature between subsequent passes, has an important role in determining final properties. It should be high enough to provide enough heat input to the weld, but not as high as to affect negatively HAZ and weld zone. For LDX2101, interpass temperature should be limited at 150°C. A higher I.T. slows too much the cooling after welding, making the HAZ more prone to secondary precipitations in the lower temperature range described in 3.3, [16].

# 5 EXPERIMENTAL SECTION

## 5.1 Experimental apparatus

The typical specimen for tensile tests on steels is dog-bone shaped: the gauge length, i.e. the straight portion between the two ends, has reduced section in order to make deformation and failure occur there. The gauge length should be at least four times longer than the diameter in order to get an axial stress-flow and the transition with the ends should be longer than the diameter, [3].

*Fig. 7: Machine for tensile tests*

Specimens tested in this work have gauge length of nearly 36 mm. This length is short because of the high cost of the plates from which specimens are extracted. The diameter is nearly 5 mm, even if [3] suggests it to be at least 6 mm. The ends are threaded and longer than the diameter, as standards require.

The mechanism of the tensile machine in Fig. 7 is electromechanical: screws commanded by an electric motor drive a crosshead in the upper part of the machine. The electric motor and a gear reduction system allow variable testing speedrates and an electronic closed loop servo-system aims to control the crosshead speedrate. A load cell situated on the top of the crosshead generates load signal. The machine is connected to a pc and a software controls movements and acquires datas.

*Fig. 8: Grip*

The specimen is connected to the crosshead and to the lower part of the rig. A removable grip is used to connect the specimens to the top, see Fig. 8. The grip is screwed to the threaded specimens and linked to the crosshead with a cylindrical pin. A good grip must transfer force to the specimen without

making it slip or fail near an end.

It is hard to find in literature useful indications about technical procedures for low temperature tensile tests. A room for low temperatures tests, as in [17], was not available. An idea is keeping the specimen immersed in a liquid environment throughout the whole test, since liquid are easy to keep in temperature and they do not require upperly closed containers. So, a steel bucket open in the upper part and connected to the lower part of the machine is used, Fig. 9. The specimen is connected to the bottom of this container and to the upper crosshead. The liquid chosen to fill the bucket and being refrigerated is alcohol, since it is quite cheap, it does not give undesirable reactions with steel and its freezing point is -114°C, far lower than -40°C which is the lowest temperature reached in the tests. Alcohol is spilled in and out of the bucket with a pump. The bucket is also used for room temperature tests, just without alcohol in it.

*Fig. 9: Testing bucket*

Liquid nitrogen, which temperature is -196°C, is used in order to cool down the alcohol. The nitrogen is contained in a pressure vessel (Fig. 10) and the required amount for a test is tapped from this to a portable insulated pot (Fig. 11).

*Fig. 10: Nitrogen vessel*

Four tools are alternatively immersed in the liquid nitrogen and in the alcohol. They are built following this procedure:

- a piece of aluminium net is cut and rolled to make a cilinder
- the bottom is closed sewing aluminium wire
- metallic bolts and screws are put into the cilinder
- the upper part is sewed with aluminium wire

*Fig. 11: Nitrogen pot*

*Fig. 12: "Infuser"*

- plastic string is tied to the upper part.

These tools are called “infusers”, since they work as cold-infusers, see Fig. 12. Bolts and screws work as heat (or, better, "cold") sinks. They must have good conductivity to shorten the time of immersions in nitrogen and alcohol. They should also have as higher specific heat as possible. Common steels has slightly higher specific heat and triple thermal conductivity than INOX steels. Then, since chromium has high thermal conductivity and is corrosion resistant, bolts and screws made of chromed common steel are used.

*Fig. 13: Stirrer*

These tools are moved from the nitrogen pot to the bucket and then back to the nitrogen when the temperature of the alcohol stops lowering: a termometer immersed in the alcohol checks the temperature in real-time.

To guarantee a uniform and quick cooling of the alcohol, a speed-adjustable stirrer is used, see Fig. 13.

To measure the strain in real-time, a clip-on extensometer is used, Fig. 14. The device is conncected to the specimen with two clasps that detach themselves as the specimen deforms. Length variations are evaluated thanks to an internal strain gage with the desired time frequency and are given as output to the pc. A clasp is made by a gripper and a blade that should guarantee excellent connection without any slippage during the test. When the extensometer is not used and when it is being applicated to a specimen, the proper distance between blades is ensured by an inserted pin. This must be

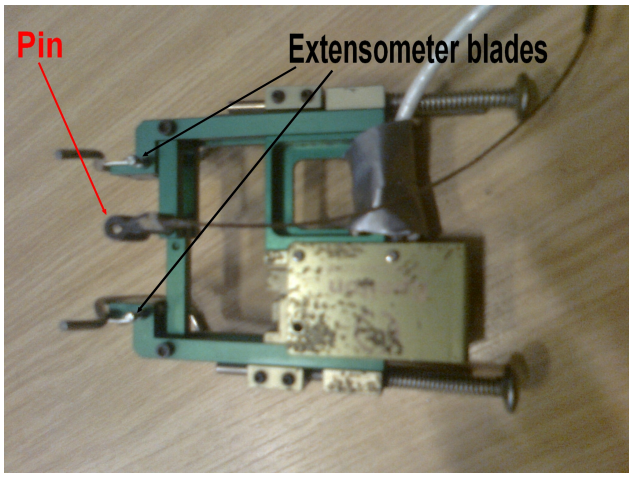


*Fig. 14: Clip-on extensometer*

removed once the extensometer is correctly connected. The sensibility of the extensometer used in this work is 1 μm and the maximum opening range is nearly 3 mm.

More sophisticated ways to measure the displacement (e.g. laser or video extensometers) were not available for this work and it would be impossible using them with the experimental apparatus for low temperatures used. Anyway, clip-on extensometers are reliable in their working range thanks to the good grip given by the blades and they are accepted by standards, [3]. They are also relatively cheap.

## 5.2 Experimental procedure

*Test controls*

Many fundamental testing operations are driven by the software. In order to better understand the testing procedure and the various problem encountered during experiments, it is convenient describing how the sofware works.

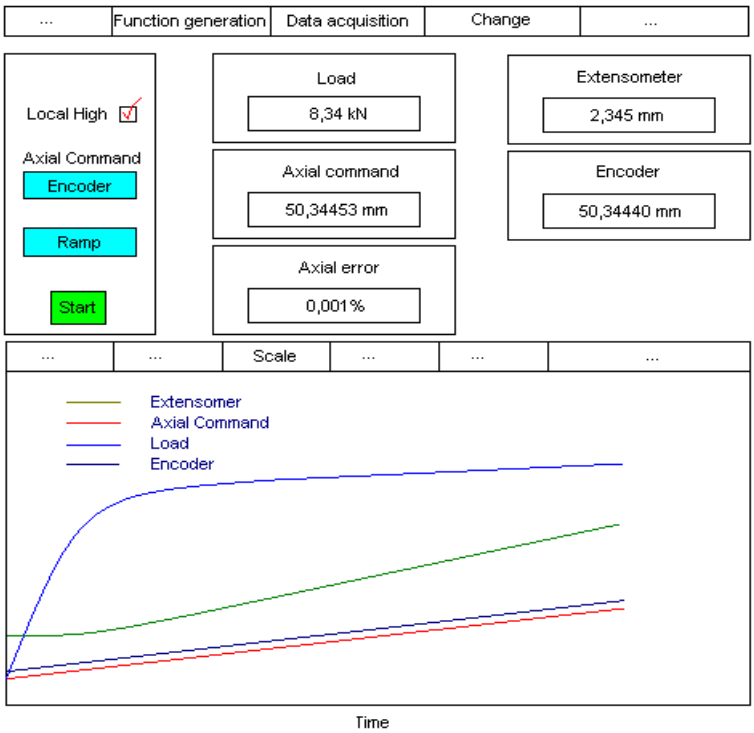


*Fig. 15: Software screen*

When the software is launched, a screen similar as in Fig. 15 pops up. Some windows show the real-time values of Load, Extensometer, Axial command, Encoder and Axial error.

Load is of course the force signal coming from the load cell of the machine.

Extensometer is the opening value of the extensometer blades.

Axial command is the command which is given moment by moment to the crosshead. The tests in this work are performed at constant speedrate of the crosshead, so the axial command is in displacement ("encoder").

The window Encoder shows the current displacement value of the crosshead: the latter

follows the instruction of movement with delay. Anyway, encoder and encoder axial command should be very close to each other moment by moment.

Axial error is the percent difference between axial command and encoder, calculated arithmetically.

These quantities, except load and axial error, are relative to a zero-point: each quantity can be zero-adjusted. For instance, the encoder value before starting the test can differ from zero: the machine takes as zero the point in which the crosshead is situated when the software is launched and not the position corresponding to the start of the test. The encoder values can be adjusted with subsequent pc elaborations, but a starting encoder value different from zero is a problem, see 5.3.

The extensometer value recognized by the pc must be zero when the distance between the blades is actually the nominal extensometer gauge length. Otherwise, the measured strains would be correlated to a gauge length different from the actual one and this would lead to errors.

The encoder axial command must always be equal to the encoder command before starting a test, otherwise the crosshead would suddenly move when the test is made to start damaging the specimen.

Encoder, load and extensometer signals are necessary to draw the tensile curves. The sampling frequency is set to nearly 2500 acquisition per minute.

It is possible to give instructions for stopping the machine if particular conditions are reached, for example a critical force value.

When settings are properly defined, the test can be started. The machine can work in automatic and manual mode: the former means that the machine follows instructions by software, the latter that the machine is driven by manual knobs. Of course, a test must be performed in automatic control.

The evolution of the quantities is shown in the lower part of the screen in Fig. 15. Singular events like sudden peaks or valleys in the extensometer signal mean slippages or malfunctions. They must be checked and remembered during subsequent data elaborations, see 5.3.

*Test procedure*

The tensile behavior of steels shows strainrate dependency, but the latter should not subsist at enough low strain rates. The crosshead speedrate is chosen as 0,01 mm/s. This should be slow enough, since a speedrate commonly used in tensile tests is 0,001 $s^{-1}$, i.e. 0,036 mm/s for specimens 36 mm long.

A dynamic pre-load can be performed in order to align the specimen with the axis of tension and avoid some problems described later in 5.3. It consists of loading the specimen until maximum 20% of the yield strength, [3], and then unloading it back. The pre-load is not usually performed in the tests at low temperatures since keeping in temperature the system is challenging and the pre-load would extend the testing time.

Now that the software functioning has been introduced, it is worthy reporting the progressive list of operations performed to make a test at room temperature. The sequence may vary slightly: this is the one followed in the present work. The big number of operations makes clear that performing a good test requires care.

- Check the machine to be off and in manual mode
- Switch on the hardware leaving the power disabled
- Launch the controlling and acquisition software from pc
- Connect the specimen to the bucket
- Screw the upper grip on the specimen
- Enable the machine power
- Slow down the crosshead and connect it to the upper grip with the cylindrical pin
- Disable the power
- Connect the extensometer to the specimen with its pin on
- Remove the extensometer pin
- Zero-adjust the encoder value

- Zero-adjust the axial command

Pre-load (not always performed)

- Set the machine to stop when a certain force is reached
- Define the proper setting for the pre-load
- Enable the machine power
- Switch from manual to auto mode
- Start the loading
- When the desired loading is reached, command the unloading: reverse the direction of crosshead motion and set limit at 0 kN
- Disable the power

TEST

- Check the machine to be off, in auto mode and in encoder control
- Define the proper setting for the test
- Zero-adjust the encoder value
- Zero-adjust the axial command
- Instruct the software to save the testing datas (this can be done before the preload if registering its datas is desired)
- Enable the power
- Start the loading
- During the test, check if the proceeding is straight and take notes about sudden events
- Stop the datas registration when the specimen breaks
- Disconnect the extensometer
- Switch to manual control

- Lift the crosshead
- Disable the power
- Switch off the hardware
- Disassemble grip and broken fragments of the specimen

The procedure is slightly different for low temperature tests. After having connected the extensometer, alcohol is tapped in the bucket to cover at least the whole specimen and the grip. In order to cool down the system, the infusers are alternatively immersed in the nitrogen pot and in the alcohol bucket, as mentioned. Two infusers are usually changed at once, substituting the ones in alcohol with those in nitrogen when the temperature stops lowering, i.e. when the infusers in alcohol are too warm to keep cooling it. During cooling, the stirrer is set to its highest rotating rate, so that the alcohol can effectively get in touch with the cold infusers. Two infusers can usually lower the temperature of 4°C at a time, taking minutes before having to be substituted. The entire cooling procedure for a single specimen can last more than one hour if starting from room temperature. Alcohol is tapped out and in between subsequent tests remaining relatively cold: it is convenient performing more tests in a row in order to save time for cooling it.

When the right temperature is reached before starting the test, the stirrer is switched off, since turbulences in the alcohol can affect the extensometer signal. A good idea is checking the stability of the signal and waiting till it is stable enough to start. Before starting, specimens are kept in temperature for more than 5 minutes in order to be sure that their entire section is at the same temperature.

As the test is performed, the temperature must be kept at the right value.

*Data elaboration*

Matlab is used to elaborate the datas of tests. Thanks to a script and to functions written using this programming language, it is straightforward carrying out some necessary operations like adjusting signal values and plotting graphs. The use of a properly written program for these operations gives the advantage to make them automatic once tensile datas are delivered as input. Using softwares like Excel to perform all of these operations would require manual inserting of instructions to elaborate the datas of each test: this procedure could potentially

introduce errors. Instead, when instructions are defined once for all, it is not possible introducing further errors.

Here a description about how the script works is reported.

First of all, the script requires to insert specimen 'ID', temperature of the test, diameter of the specimen, crosshead speedrate (the same for all specimens), extensometer offset (shift from the nominal gauge length, readable in Fig. 15 when the device is connected), specimen gauge length (*GL2*), extensometer nominal gauge length and final length of the broken specimen (*FL*). The initial extensometer gauge legth (*GL*) is obtained subtracting the extensometer offset from the nominal gauge length.

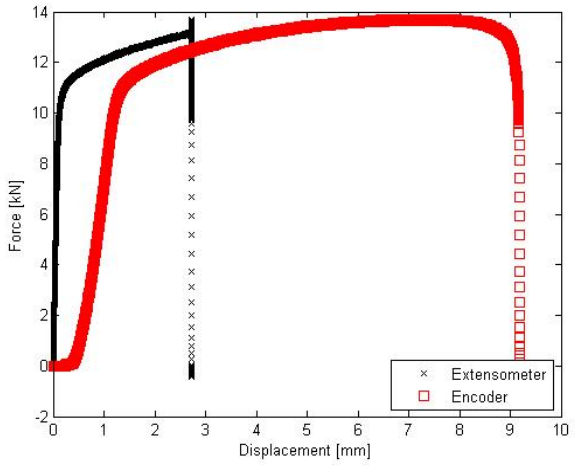


*Fig. 16: Force vs extensometer and encoder signals*

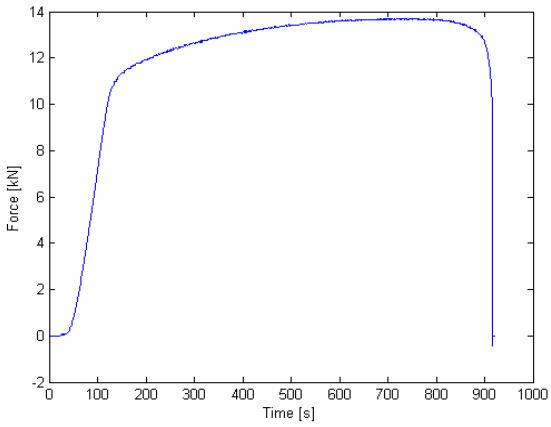


*Fig. 17: Force vs time*

The script firstly provides instructions to plot some graphs, Figs. 16÷19, that can be useful to check the quality of collected datas, detect problems and make subsequent considerations.

Fig. 16 Force vs extensometer and encoder signals. The datas collected for the extensometer do not start precisely from zero: the signal is plotted zero-adjusted, just subtracting or adding the same quantity to all values. The encoder signal should start from zero, anyway it is zero-adjusted before being plotted.

Fig. 17 Force vs time. The beginning of this curve is non-linear cause little time must pass before exerting force on the specimen. The elastic range is reached gradually: this occurs because the specimen and the grip have to align their axes with the axis of tension before the system machine + specimen behaves as

elastic. When preload is performed, this first portion should be reduced or not existing. The graph can be helpful to check if the machine acquires force values correctly during the test.

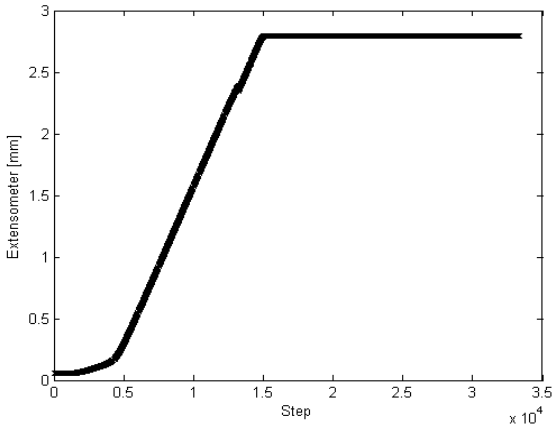


*Fig. 18: Extensometer signal vs sampling steps*

Fig. 18 Extensometer signal vs sampling steps. The initial part of this curve is non-linear and then it joints gradually to the elastic part: this is due to same reasons as explained for Fig. 17. When the extensometer reaches the maximum opening range, its blades start slipping on the specimen surface, giving constant signal. This graph is helpful to check if the extensometer is subjected to problems, i.e. slippages, during the test.

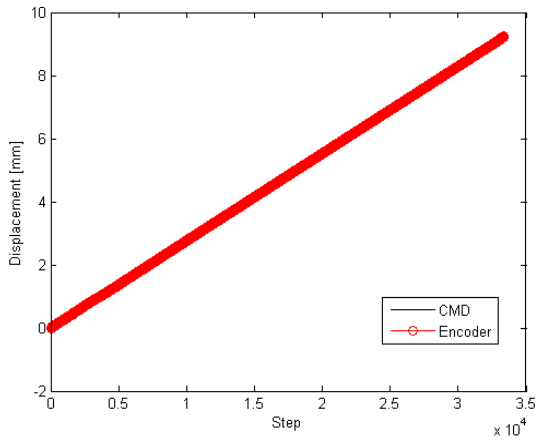


*Fig. 19: Encoder and axial command signals vs sampling steps*

Fig. 19 Encoder and axial command signals vs sampling steps. This figure is helpful to check if the crosshead works at the set constant rate. In the reported figure, since the encoder follows very closely the axial command and it is plotted with big red markers, the only visible line is its.

The magnification of the first part of Fig. 16 is shown in Fig. 20. The encoder curve is stretched to the right because the machine has its own elastic behavior, and partecipates to the elongation. Watching the extensometer signal, black curve in Fig. 20, two load values within which the behavior of the specimen appears linear are chosen. The progressive indexes of the points are named *iTare* and *iEnd*. Extensometer, force and encoder values before *iTare* are removed. Values before half kN force are usually cut out. The extensometer signal can be used to draw tensile curves only before the device reaches its maximum opening: after that moment, the signal is not meaningful anymore, see Fig. 18. In order to draw tensile curves until the failure of the

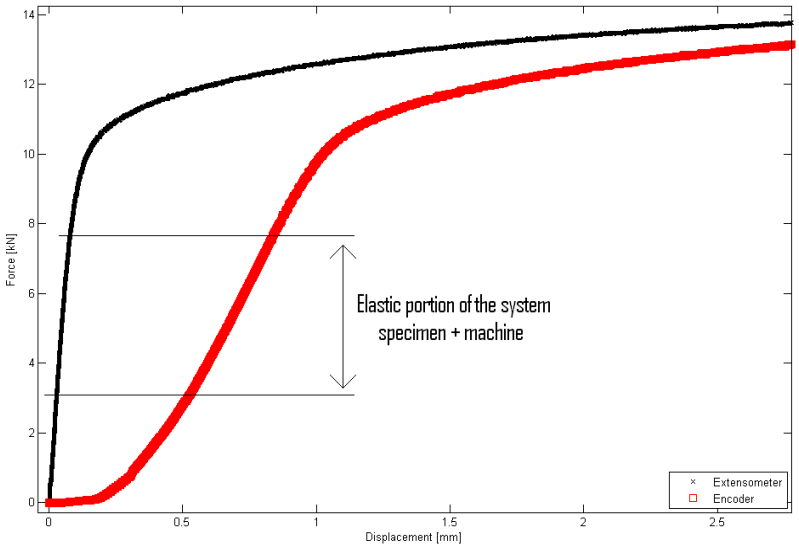


*Fig. 20: Force plotted vs extensometer and encoder signals, in black and red respectively*

specimen, the encoder curve, i.e. the red curve in Fig. 20, must be adjusted deleting the elastic contribution of the machine.

A linear stretch within the encoder curve must be eye detected. The progressive indexes of the delimiting two points are named *iStartComp* and *iEndComp*. These values are not the same as *iTare* and *iEnd*. For every encoder value $D$ in the decided range, Eq. (19) is valid:

$$D = ext + C * P \tag{19}$$

where *ext* and $P$ are extensometer and force values relative to $D$. The compliance of the system specimen + machine, $C$, is calculable by Eq. (20).

$$C = \frac{\Delta enc - \Delta ext}{\Delta P} \tag{20}$$

The script calculates slope and foot of the elastic interpolating line of the encoder curve. The foot is called *moffset* and it is used to obtain all the adjusted encoder values from the non-adjusted ones as in Eq. (21).

$$Adjusted\ encoder = D - C * P - moffset \tag{21}$$

where $D$ is any encoder value and $P$ is the relative force value, see scheme in Fig. 21. The assumption at the base of this operation is that the machine never deforms plastically: it gives only elastic contribution to the displacement, while the whole plastic deformation is stood by the specimen. It is now be possible superimposing the extensometer curve to the encoder curve adjusted knowing the compliance, see Fig. 22.

The adjusted encoder curve should match well the extensometer signal until the point in

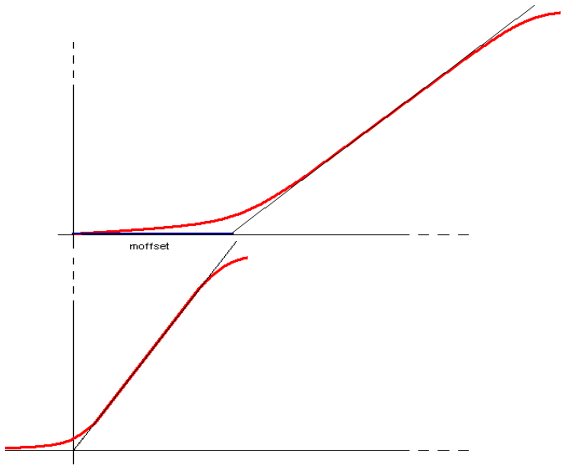


*Fig. 21: Scheme of non-adjusted and adjusted encoder*

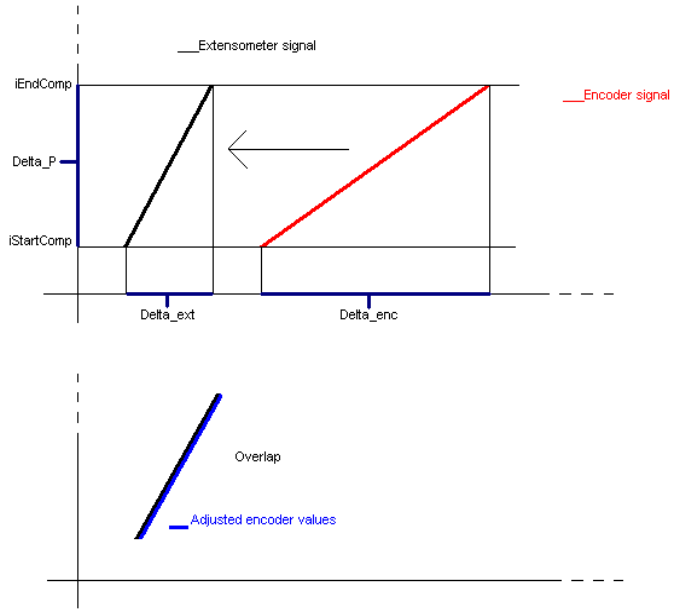


*Fig. 22: Removal of machine elastic contribution*

which the extensometer stops working and should prosecute from that point on as a prolongement.

The script calculates the engineering stress values dividing the force values by the initial area. The engineering strain values are obtained separately for the extensometer and the encoder dividing those values by the gauge lengths of extensometer (*GL*) and specimen (*GL2*) respectively. Then, the script calculates the slopes of the elastic lines in the engineering extensometer and adjusted encoder curves, i.e. the elastic moduleses of the curves. Stress values between *iTare* and *iEnd* are connected to get the elastic line in the former curve, *iStartComp* and *iEndComp* in the latter. The elastic modulus from the engineering extensometer curve is more meaningful because directly linked to the behavior of the specimen.

The total elongation to fracture of the specimen is calculated with Eq. (14), where $L$ is represented by *FL* and $L_0$ by *GL2*. For the yield strength, a straight line is drawn parallel to the elastic line in the engineering extensometer curve, starting from the abscissa value 0,002. Extensometer values are directly connected to the strain of the specimen: since the yield point is always reached within the opening range of the extensometer, the yield stress is calculated from the engineering extensometer curve. The intersection with the curve gives the desired value of yield strength. Due to the extensometer signal, the stress curve is not actually

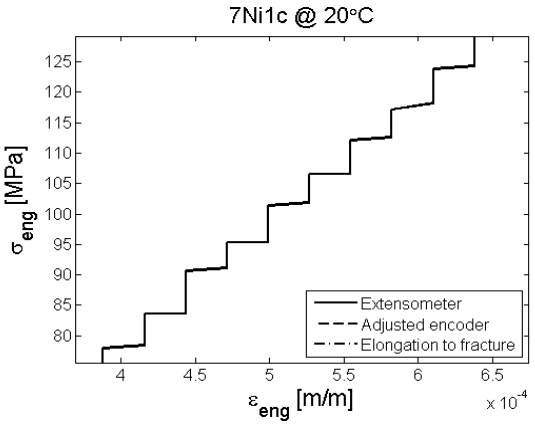


*Fig. 23: Zoom of zig-zag in engineering curve*

smooth: zooming, zig-zag can be noticed, see Fig. 23. There can be microvariations of nearly 2 MPa and so finding more than one value of yield strength is possible: if it happens, they are averaged. Rp0,2 is also calculated using a 200 GPa slope line, which is the expectable elastic modulus for weld and non-weld duplex steels. The latter Rp0,2 value is taken in consideration when the extensometer signal is markedly disturbed and so not reliable. For completeness, the script also calculates the yield stength considering the adjusted encoder curve, with the same procedure.

For Rm, the script detects the maximum value in the engineering encoder curve: the extensometer signal stops much before reaching such stress value. Rm is calculated as average of 40 stress values around mentioned maximum.

Fig. 24 shows the first parts of engineering extensometer and adjusted encoder curves. The elastic moduli from the two curves are reported. Elastic lines and relative parallels passing through abscissa 0,002 are displayed, as well as the 200 GPa slope passing through abscissa 0,002 (in red).

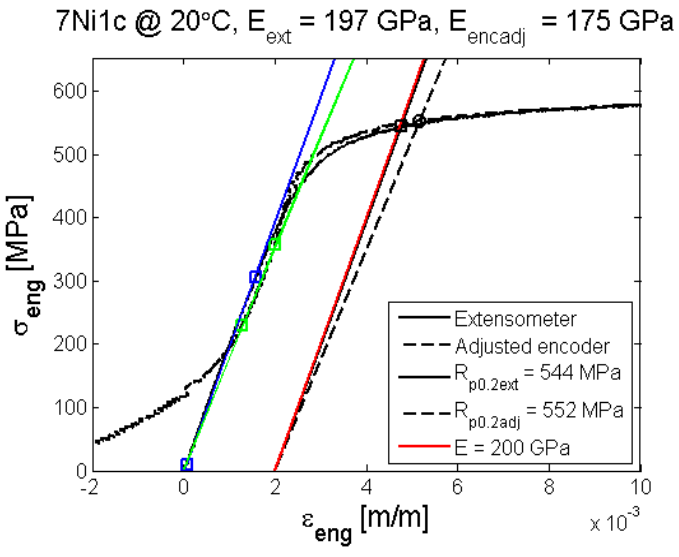


*Fig. 24: First part of engineering stress vs extensometer strain and adjusted encoder strain*

Fig. 26 shows the engineering extensometer and adjusted encoder curves superimposed, i.e. the complete engineering curve. A vertical line due to the slipping of the extensometer that has reached the maximum gap range can be noticed. The total elongation to fracture is traced as a vertical dashed line.

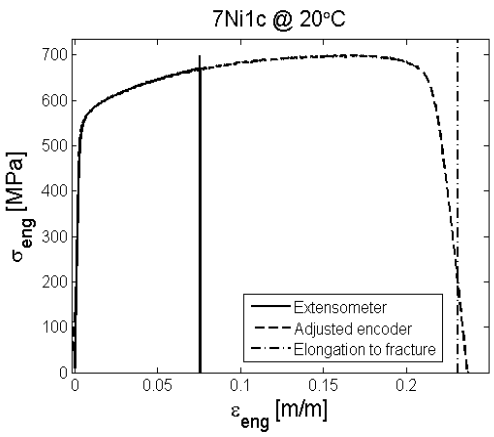


*Fig. 26: Engineering stress vs strain curve*

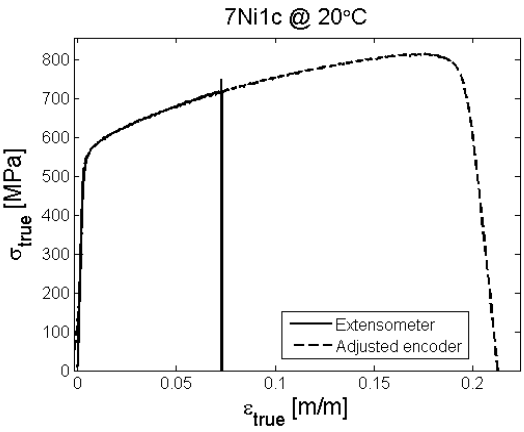


*Fig. 25: True stress vs strain curve*

Fig. 25 shows the true extensometer and adjusted encoder curves superimposed: this should provide the complete true curve. In order to get the true curve, the program calculates values of true extensometer strain, true adjusted encoder strain and relative true stress values with Eqs. (10) and (11). After the necking, the curve is still drawn using those equations instead of the more correct Eqs. (12) and (13). Anyway, the actually interesting graph for the aim of this work is Fig. 26.

Fig. 27 shows the fitting between engineering extensometer and adjusted encoder curves at the point where the extensometer stops working having reached its maximum range. This graph can be used as feedback to evaluate the reliability of the points *iStartComp* and *iEndComp* chosen: if the curves are not well superimposed, other points delimiting the elastic portion of the encoder signal can be chosen from Fig. 16 and the script be made run again. This is repeated until the superimposition is good, i.e. a meaningful encoder elastic range to evaluate the system compliance has been chosen. The matching is not so good if the extensometer gauge length differs significantly from the specimen gauge length, see 5.3. In 12.2, some meaningful graphs are reported for each tested specimen.

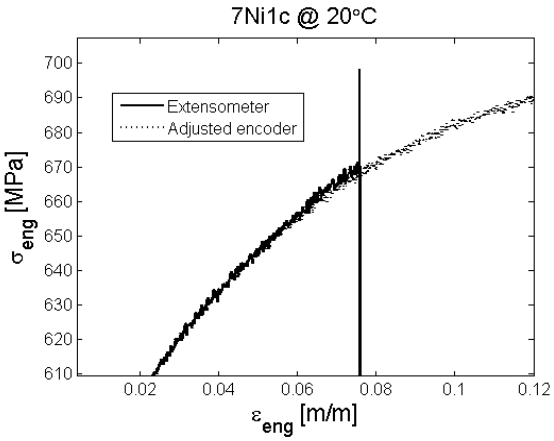


*Fig. 27: Fitting between engineering and adjusted encoder values*

*Specimens analysis*

The light optical microscope (LOM) is used to photograph the microstructure of deformed and undeformed materials and to check if failures of some specimens occured in the base or in the weld metal: see 6.1 for the description of tested tensile specimens. Portions of broken specimens are cut nearly 2 cm long. Portions of undeformed weld material are extracted from bigger specimens for toughness tests, with faces parallel to the welding direction. The samples are encapsulated in bakelite, grinded with four progressively finer grained disks, polished and then etched. Beraha II solution is used for deformed specimens and Beraha for undeformed ones. The magnifications used are 5x, 10x and 20x.

The scanning electron microscope (SEM) is used to photograph some fracture surfaces and their details, like inclusions, dimples, cleavage facets and so on. Portions of broken specimens nearly 1 cm long from the fracture surface are cut and subjected to a 15 minutes ultrasonic bath to be cleaned. The magnifications used range from 20x to 1200x.

The SEM apparatus is also used to perform energy dispersive X-ray spectroscopies. The EDS technique provides the elementary composition of a sample stimulated by an electron beam thanks to X-rays emission. Main problems of EDS are the difficulty to detect smalle size elements, the big volume involved by the X-ray emission and the possible unreliability if the sample surface is irregular.

## 5.3 Experimental issues

*Clip-on extensometer*

Experimental problems for this device can be:

1. The blades can slip during the test, because of bad positioning, collisions with the infusers or turbolences in the alcohol. Since specimens are limited in number, pc elaboration helps to get properties in case these problems occur: a proper instruction to align the parts of the extensometer signal before and after the drop is provided in the script. The procedure is schematized in Fig. 28. In 12.2, specimens which test has this

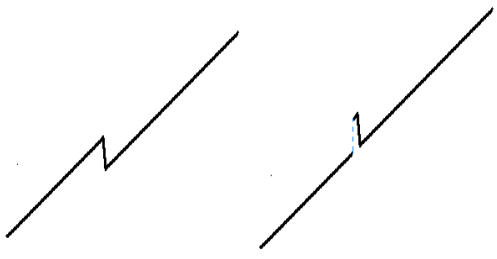

*Fig. 28: Scheme of slippage correction*

problem are signalled with a comment below their graphs.

2. The blades, if strictly fastened, can damage the specimen giving starting points for fracture. Anyway, this should not be a problem with duplex steel.

3. The working range is usually small and so it cannot be used to draw the entire tensile curves. After having reached the maximum opening, the extensometer blades start sliding on the surface of the specimen: this can both damage the specimen scratching its superficially and wear the blades themselves. The extensometer must work without problems during its operative range in order to draw tensile curves, see 5.2-*Data elaboration*. Rounded blades can affect the adherence to the specimen and if a slip occurs during the opening all the values subsequently registered are shifted from the real ones. So, blades are periodically substituted.

4. The extensometer datas received from the software are length variation from the "zero-point", that should correspond to the actual gauge length of the extensometer. The latter is provided by the manufacturer and checked with a caliber. So, before testing, the actual gauge length should be measured and the software should be set to recognize it as zero-point. This operation is performed periodically. After having positioned the extensometer on the specimen, it is normal that the distance between the blades is not equal to the nominal gauge length: the extensometer does not have to be zero-adjusted.

5. The gauge length of the extensometer must be the same or similar as that of the specimen, because the entire deformation of the specimen must be monitored. Since specimens usually show differently strained zones along their gauge lengths, extensometer values relative to limited part of length would not be representative of total deformations. Ultimate tensile strengths of specimens tested with improper extensometer gauge length are affected by error. If the strain was uniform along the whole length of specimens, the problem would not occur.

6. At subzero temperatures, the extensometer signal can be much disturbed, on particular at -20°C. This problem is likely due to the influence of temperature on the electronic circuit and cannot be solved. Moreover, at -20°C, the displacement values from the extensometer tend to lower during time. A good idea to monitor this trend would be

introducing in the bucket during tests an extensometer with stuck blades having same circuitry than the testing one, without connecting it to the specimen. From that extensometer, the signal lowering rate could be evaluated and the values of the testing extensometer could be adjusted. Unfortunately, an extensometer for the comparison is not available. At -40°C the extensometer works without significant disturbance.

*Encoder zero-adjustments*

As mentioned in 5.2-*Data elaboration*, the encoder must be zero-adjust before testing: otherwise, its collected values can be clearly zig-zag and lead to large imprecisions on the final measurements. This is an issue strictly connected to the circumstantial apparatus used. In 12.2, notes indicate which tests are involved in this systematic error.

*Cooling*

Pouring liquid nitrogen on the surface of the alcohol is not efficient because of the exaggerated wasting of nitrogen and the smoke covering the surface of the alcohol makes impossible to monitor what happens under it during the test.

With the adopted solution of the “infusers”, see 5.1, care must be taken during substitution. Clumsy movements can cause bumps against the extensometer and excessive swirls in the alcohol that can in turn affect extensometer measures.

Reaching the low desired temperature value is tricky. One way is slowing the stirrer, removing one or both the infusers and putting a new one some minutes later: in this way the temperature does not usually vary for several minutes. The stirrer must be slowed in order to make the cooling less effective, otherwise the temperature would decrease if there were any infuser or increase if there were not. Another way is reaching 1° or 2°C lower then desired, then removing both the infusers and keeping the stirrer at high rates. This would lead to raise the temperature to the desired level in little time; then the stirrer should be slowed or switched off when the test is started to not disturb the extensometer signal.

The temperature, of course, must be kept stationary also during the test: the infusers are substituted when the temperature raises of 1°C. During tests at -40°C, the raise of temperature tends to be fast. Since the stirrer cannot be accelerated, the only way to keep the right temperature is keep subsituting the infusers every minute. This is not so effective anyway: the

temperature usually stays at -40°C during the very first part of the test, i.e. during the elastic behavior, but then it raises up to -38°C. It is possible to cool back to -40°C accelerating the stirrer when the extensometer has reached its maximum opening and so it has stopped to send useful signals. The stirrer can always be accelerated when the extensometer stops working.

It is necessary to not run out of liquid nitrogen during a test: the nitrogen level in the pot must be checked before starting each test. Testing at -40°C, for example, requires a nitrogen pot refilling before each test.

*Total elongation*

A problem encountered about elongation measurements is finding a method to mark specimens in stirred alcohol permanently. Waterproof-ink and marking-ink pentips do not work: instead, pencil marks resist well. Marks are manually drawn on the specimens at the ends of their gauge length measured with a ruler. The lengths after fracture are also measured with the ruler accosting the broken fragments. Thickness and non-perfect linearity of the marks affect measures, as well as the sensibility of the ruler (half millimiter) and the alignment of the fragments.

Moreover, the measure of total elongation as in Eq. (14) is questionable. Tested specimens can have different lengths and if the strain was uniform along the whole gauge length for a certain material, the total elongation would be the same for all the different lengths. Actually, specimens usually show one or more necked zone. Then, tested specimens contain both weld and base metal most times and so tend to have different elongation behaviors along their length.

A logical way to solve this problem would be measuring separately the strains in different zones of a specimen and calculating the local elongations with Eq. (14). Then, the total elongation would result as the weighted average of those values on the different zone lengths. This method is unfortunately difficult to perform and it is usually avoided: transitions between differently strained zones are gradual and very sensible measuring tools would be necessary.

To synthesize, total elongations calculated in this work are just useful for comparisons.

# 6 MATERIALS PRESENTATION

LDX2101® (UNS S32101) is a duplex steel for general purpose use. LDX2101 contains more nitrogen and less nickel than 2205: the former element is an effective austenite stabilizer, so it should compensate the lower content of the latter. The increased nitrogen content raises the allowed quantity of manganese that can be added to the alloy. Mn reaches in turn a significant austenite stabilization effect and improves the pitting resistance in cooperation with N, see 3.2. The reduced Ni content lowers the cost of production and is the reason why LDX2101 is classified as "lean" duplex. The mechanical properties of LDX2101 are slightly lower than those of 2205. Regarding the corrosion resistance, LDX2101 is equivalent or slightly superior to 304L.

Here follows the element composition in weight% for LDX2101, [18]:

*Table 1: weight% composition of LDX2101*

| **Cr** | **Ni** | **Mn** | |
|---|---|---|---|
| 21,0 min. - 22,0 max. | 1,35 min. - 1,70 max. | 4,00 min. - 6,00 max. | |
| **Mo** | **N** | **Si** | **C** |
| 0,10 min. - 0,80 max. | 0,20 min. - 0,25 max. | 1,00 max. | 0,040 max. |
| **P** | **Cu** | **Fe** | |
| 0,040 max. | 0,10 min. - 0,80 max. | Balance | |

The comparison with an average alloying composition of 2205 grade is worthy, see Table. 2, [19].

*Table 2: weight% composition of main alloying elements in 2205*

| **Cr** | **Ni** | **Mo** | **C** | **N** |
|---|---|---|---|---|
| 22 | 5.7 | 3.1 | 0.02 | 0.17 |

## 6.1 Presentation of specimens

The procedure to obtain welded plates from which specimens are extracted is the following. Base metal is hot-rolled to obtain plates and subsequently subjected to solution treatment. The latter has multiple aims. Keeping the material at the right temperature for enough time (30 minutes is usually enough, [12]), its microstructure relaxes and spheroidizes, becoming less anisotropic. Secondary undesired phases possibly present in the metal are solubilized and, with a proper quench, they do not reform. Water is the common cooling medium and is used in the current case, too. The solubilization temperature should be as near as possible to that studied for the specific steel: if lower, secondary phases would nucleate and grow; if excessive, ferrite would form in too large amount. The choice of temperature must keep in consideration the chemical composition. For the base metal plates 1050°÷1100°C are used. Pieces thicker than 80 mm are difficult to quench cause their heart may cool down too slowly and hence being subjected to precipitations, [12], but it is not the current case. Eventually, two plates at a time are welded to obtain "type 4" or "X" joints, as in Fig. 29. Welding with "X" arrangement is advantageous because the root pass (the first pass that connects the edges in the center of the X) does not have to ensure optimum penetration, being continued later by welding on the other side. This is particularly important for welds thicker than 15 mm, [1]. The root pass should provide sufficient material to connect completely the edges and avoid pores, notches or lack of fusion. Each weld is realized with 18 subsequent depositions of filler material. The bulk temperature never exceeds 150°C during welding.

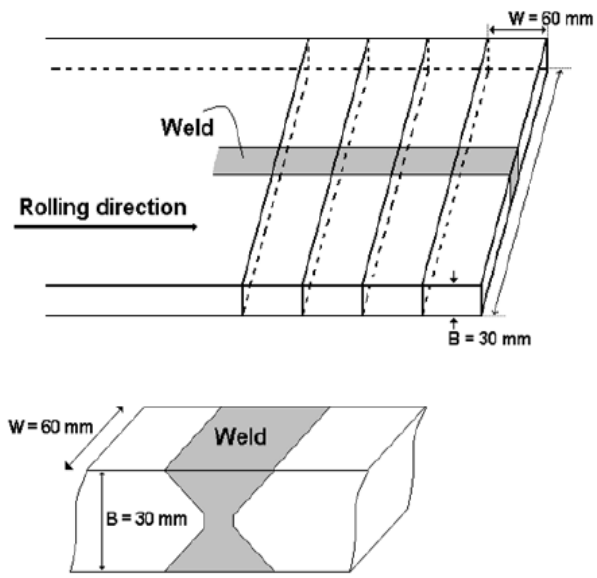


*Fig. 29: Weld geometry*

Welds differ for chemical composition mainly and then for welding method used. The names chosen to distinguish the welds are:

- *1,5 Ni*. Filler metal with the same Ni content as the base metal (nearly 1,5% in weight)

is used. The weld method is SAW (submerged arc welding, or UP with swedish acronym).

- *5 Ni*. The weld root is obtained with two passes of filler containing nearly 5% Ni; then, same filler material as for *1,5Ni* is used with the addition of Ni powder to adjust the composition (between 2,5 g and 4,9 g for each pass). SAW is used for every pass.
- *7 Ni*. Filler material containing nearly 7% Ni is used. The first 7 strings are deposited with MIG. The other ones with SAW. MIG method should be more controllable and should give less defects in a delicate area as that of the root.

There are no indications about the shielding gas used with MIG.

Mechanical strengths of solution treated base metal plates from plate certifications are listed in Table. 3. The differences are due to the different solubization temperatures: 1100°C for plates destined to *1,5Ni* and *5Ni* weldings, 1050°C for *7Ni* welding.

*Table 3: Strengths of base metal plates [MPa]*

| | **Rp0,2** | **Rm** |
|---|---|---|
| *Plates for 1,5% and 5%Ni welding* | 474 | 684 |
| *Plates for 7%Ni welding* | 478 | 694 |

The main constituents of the flux used for SAW is showed in Table. 4. This flux is neutral since it contains Cr.

*Table 4: Main compounds %w in the flux material*

| **$SiO_2$** | **MgO** | **$CaF_2$** | **$Al_2O_3$** | **Cr** |
|---|---|---|---|---|
| 7 | 0 | 50 | 36 | 3 |

The composition of the filler material used for *7Ni* welds is shown in Table. 5. The compositions of the other fillers are not available. However, the main difference is a gradually lower Ni content compensated by a gradually higher Mn one.

*Table 5: Precise composition %w of the filler material used for 7% Ni welding*

| C | Si | Mn | P | S |
|---|---|---|---|---|
| 0.02 | 0.5 | 0.71 | 0.02 | 0 |
| **Cr** | **Ni** | **Mo** | **Cu** | **Co** |
| 23.13 | 7.3 | 0.25 | 0.15 | 0.04 |
| **N** | **Sn** | **V** | **Al** | **W** |
| 0.12 | 0.01 | 0.05 | 0.01 | 0.01 |

The chemical compositions of the 3 types of weld are reported in Table. 6, [20].

*Table 6: Compositions of welds*

| | | Si | Cr | Mn | Fe | Ni |
|---|---|---|---|---|---|---|
| | Min, w% | 0.60 | 21.33 | 3.53 | 67.84 | 1.01 |
| ***1,5Ni*** | Max, w% | 1.71 | 23.04 | 4.55 | 71.94 | 1.71 |
| | Mean, w% | 0.82 | 22.01 | 4.01 | 69.56 | 1.34 |
| | Min, w% | 0.54 | 21.27 | 2.00 | 68.27 | 3.87 |
| ***5Ni*** | Max, w% | 0.96 | 22.84 | 3.73 | 70.17 | 5.92 |
| | Mean, w% | 0.76 | 22.06 | 3.04 | 69.20 | 4.93 |
| | Min, w% | 0.37 | 21.76 | 0.78 | 64.78 | 5.30 |
| ***7Ni*** | Max, w% | 0.63 | 24.14 | 2.31 | 69.35 | 6.63 |
| | Mean, w% | 0.50 | 22.93 | 1.47 | 66.89 | 6.02 |

Ni and Mn contents are indirectly proportional, as expected from the fillers used.

The ferrite content of welds and solution treated base metal plates is available in Table. 7, [21]. The analysis was performed on surfaces transverse to the direction of welding. Ferrite content actually varies within the weld, [11], so these values are just indicative, see 6.2.

*Table 7: Ferrite content of base and weld metal*

| | Base metal | Weld |
|---|---|---|
| *1,5%Ni* | 56.80% | 79.60% |
| *5%Ni* | 56.80% | 57.40% |
| *7%Ni* | 55.00% | 59.30% |

It is evident that ferrite content is particularly high in *1,5Ni* welds. Next to the chemical denomination, each specimen is classified depending on how it is extracted from the weld, see Fig. 30.

- *Surface cross weld* specimens (*a*) are cut out transversely, near a surface and contain some base metal on both ends.
- *Root cross weld* specimens (*b*) are cut transversely in the root region, so they contain more base metal than *a* specimens. Root regions have usually slightly different microstructure and properties than the rest of the weld.
- *Weld* specimens specimens (*c*) are cut along the direction of welding, superficially.

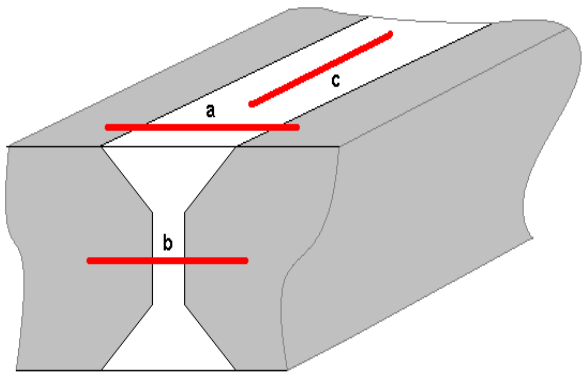


*Fig. 30: Scheme of specimens cutting*

In order to study weld properties, only *c* specimens would be reliable since *a* and *b* specimens also contain base metal. Anyway, in real conditions a weld always works connected to base metal so it is also important to study the behavior of *a* and *b* specimens.

So, there are 9 kinds of specimen and each of them is described by the chemical composition of the weld and the position from which it is extracted, e.g. *5Ni_weld* (or *5Ni_c*).

*a* specimens are tested at 20°, 0°, -20° and -40°C, as well as the *c* specimens. *b* specimens are tested only at room temperature and -20°C.

### 6.2 Analysis of materials

The microstructure of *1,5Ni* welds, showed in Figs. 31 and 33, depends on the position from which specimens are extracted, as well as the microstructures of *5Ni* and *7Ni*. In the figures, the ferrite is black and the austenite white. The direction of passes is indicated by the direction of austenite strips. Factors that mainly influence austenite content and morphology are the Ni and N contents as well as the heat input. These factors are introduced in 3.1, 3.2 and 4.3.

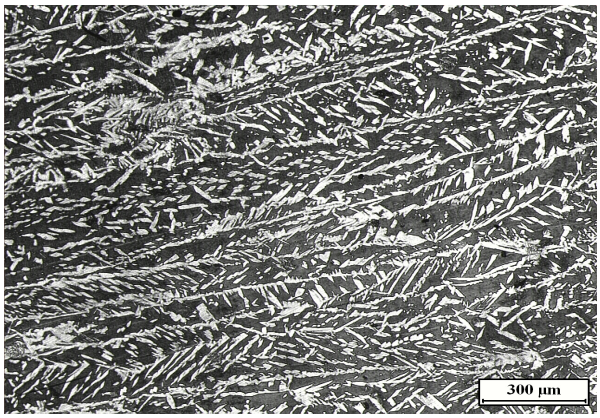


*Fig. 31: zone in 1,5Ni rich in austenite*

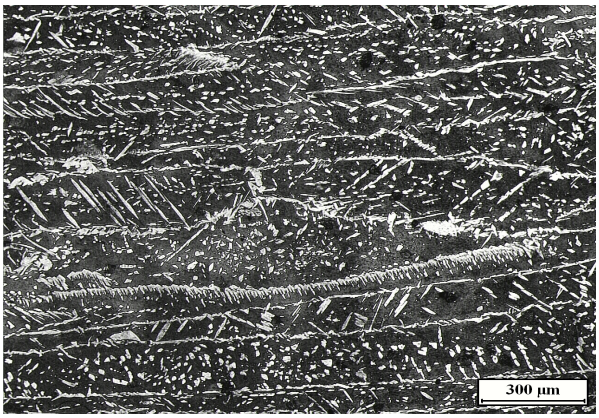


*Fig. 32: microstructure of 1,5Ni*

In the case of *1,5Ni* only SAW method is used, as said in 6.1. Its great heat input should compensate the lack of Ni regarding austenite formation. Anyway, some zones of the weld are rich in intragranular austenite, see Fig. 32 and 33, while other zones are rich in grain boundary and Widmanstätten austenite, see Fig. 31. The former case means that locally heat input or Ni content are low. In Fig. 33, it is possible to notice the absence of Widmanstätten austenite, even if some austenite grains may be Widmanstätten austenite intercepted transverse to long axis, as suggested in [22]. The microstructure in Figs. 32 and 33 is similar at some extents to that noticed in the electron beam welding (low heat input, fast cooling) of duplex steels with pre-placed nickel foils, while the microstructure in Fig. 31 is more similar to that obtained in 2205 duplex steel with GTAW, another high-heat input method, [22].


*Fig. 33: intragranular austenite in 1,5Ni*

The secondary phases that could be detected with a LOM are σ and χ, but little dark spots in the micrographs should be etching defects or dirt. Those two phases should not form, since the materials undergo to cooling rates faster than critical. This consideration comes from the comparison between the $\Delta_{12/8}$ suggested in literature (basing on which welding parameters are designed, see 4.3) and the critical cooling rate for σ phase, see 3.3. The latter determines that the transition time between 1200° and 800°C should not exceed 140 s, while the former is right between 4÷15 s. The critical cooling rate for χ formation is slower than for σ, so it is not problematic. Smaller precipitations cannot be detected with LOM. Metal strings deposited with multipass technique are thin and so the cooling rate is as high as expected in the whole deposited metal: all kinds of precipitation listed in 3.3 should be avoided. However, a problematic precipitation in duplex welding could be that of chromium nitrides, because the solubility of N in ferrite drops rapidly with a decrease in temperature. This precipitation is likely ot occur when the composition is greatly unbalanced towards the ferrite. TEM analysis conducted in [22] find that nitrides are present in case of electronic beam autogenous welds, but not when a higher heat input method like GTAW with Ni addition is used. So, the welds are assumed to be free of secondary phases.

Same considerations about secondary phases and heat inputs are valid for *5Ni* and *7Ni*. In Figs. 34 and 37, microstructures from a *5Ni* weld are showed. In *5Ni*, all three kinds of

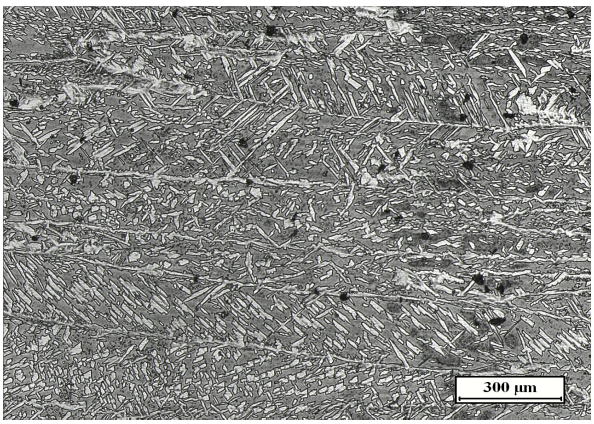


*Fig. 34: microstructure in 5Ni*

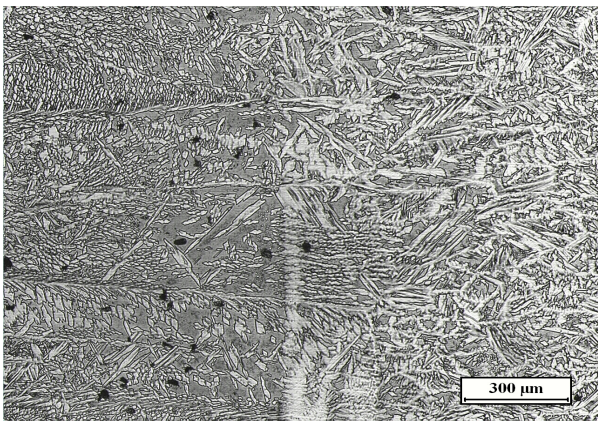


*Fig. 35: transition between passes in 5Ni*

austenite are present and their relative amount varies from pass to pass, as well as the austenite content, as evident in Fig. 35. Comparing for example Fig. 32 with Fig. 34, an increase in austenite content is observed, as expected. However some zones lack of austenite, as that in Fig. 37. Other zones can be instead rich in intragranular austenite, meaning that they undergo to faster cooling or they are locally poor in nickel. Indeed, a major problem in welding is dilution, as explained in 4.3: the amount of Ni cannot be the same in every point of the weld and can vary from pass to pass, even if multipass technique should encourage re-melting and mixing.

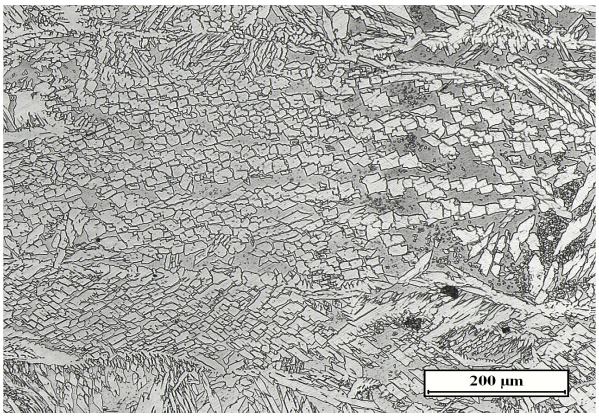


*Fig. 36: intragranular austenite in 5Ni*

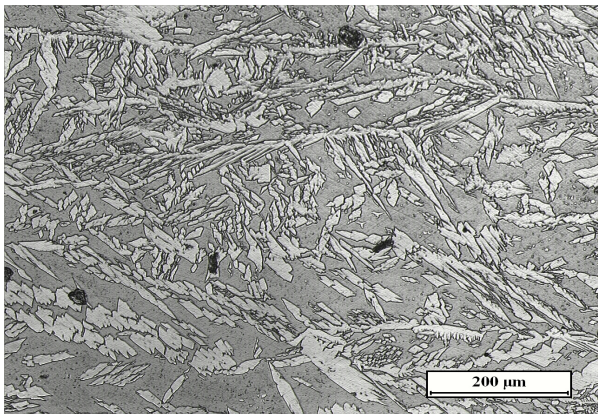


*Fig. 37: zone poorer in austenite in 5Ni*

A study conducted on power beam welded duplex steels shows that chemical composition can have larger effect than heat input on the final austenite content, [7]. Different welding methods than power beam have been used for the tested materials, but the study confirms that local differences in nickel content influence greatly the local microstructure. Differences in phase balance lead of course to inhomogeneous mechanical properties within welds.

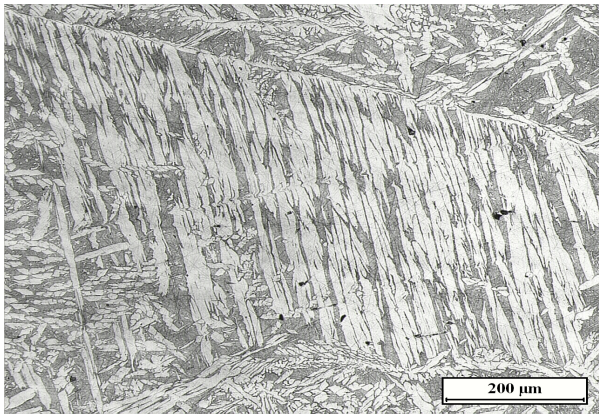


*Fig. 38: Widmanstätten austenite in 7Ni*

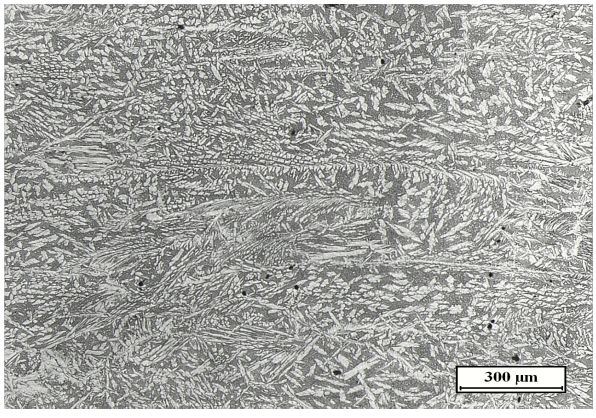


*Fig. 39: microstructure of 7Ni*

Figs. 38÷41 show morphologies of *7Ni* welds. The first figure shows the presence of a very

coarse formation of Widmanstätten side plates while the second one shows all three kinds of austenite. Being the Ni content high, higher temperature morphologies of austenite are stabilized. Yet, intragranular austenite is present in large amount. In *7Ni*, the use of MIG together with SAW is a factor that can lead to difference in heat input between subsequent passes.

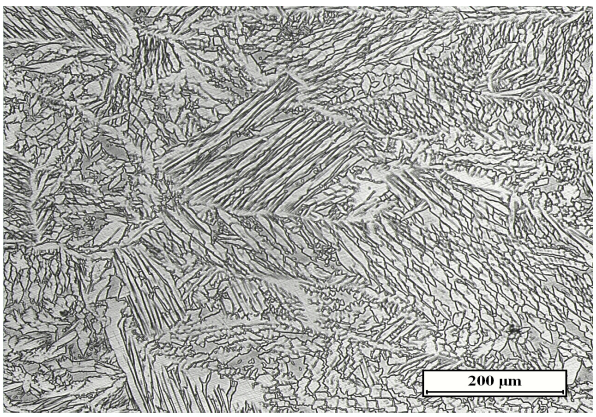


*Fig. 40: zone rich in austenite in 5Ni*

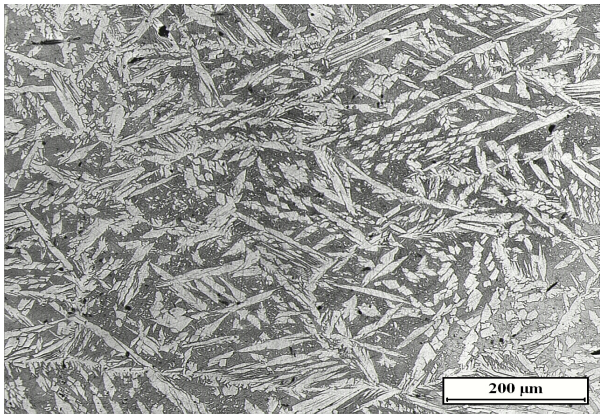


*Fig. 41: detail of 7Ni*

Due to local Ni content and heat input, the local austenite content can be even lower than in *5Ni* welds, see Figs. 40÷41.

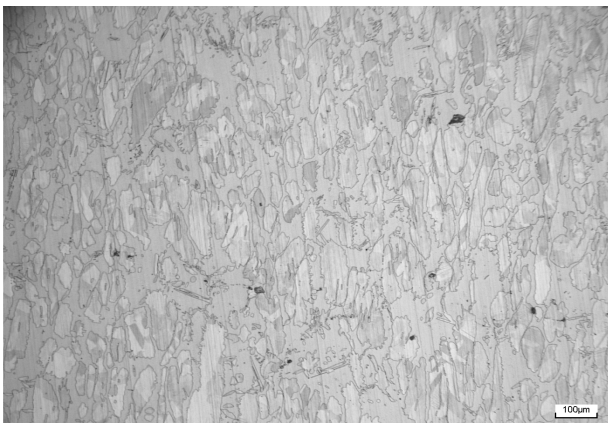


*Fig. 42: base metal from deformed specimen*

Fig. 42 is a photo of base metal taken from a deformed specimen. Before welding, the base metal is assumed to be free of secondary phases, as mentioned before. The welding process however produces HAZ, see 4.3. It is common to distinguishing high temperature heat affected zone (HTHAZ), close to the weld, and low temperature one (LTHAZ). The former undergoes to almost total ferritization during welding and it ranges from the molten pool to the metal that reaches nearly 1000°C during welding; the latter remains duplex and it occupies the zone subjected to 950°÷650°C during welding, [23]. Most studies concentrate on HTHAZ, since LTHAZ is not recognized for having great effect on properties of duplex steels. During cooling, austenite reforms in the HTHAZ. The final quantity of austenite can be 50%÷70% if appropriate welding conditions are provided, [24].

N must be present in the HTHAZ in right quantity to provide sufficient austenite formation: the increased solvus line delays the ferritization during heating and makes the austenite nucleating and growing earlier during cooling, as seen in 3.2. N can easily diffuse away during welding and if the cooling is too rapid, there is no time for it to diffuse back, [25], but this should not be the current case: LDX2101 contains more N than other duplex steels and the set heat input is high. Rather, slow cooling rates that can derive from high heat input could lead to excessive coarsening of ferrite that could in turn hinder the subsequent austenite formation. However, this seems not to occur in LDX2101 because of its high N content, [26]. The HTHAZ in duplex steels is so narrow that austenite formed in the weld during cooling "conceals" it, [27]. So, the HTHAZ cannot be well distinguish from the weld metal, see Fig. 43 on the left. Since the narrow HTHAZ is also in contact with the weld metal and has similar chemical composition, it is a matter of common sense considering their cooling rates similar. So, secondary phases relatively slow to precipitate as σ and χ should not be present in the HTHAZ. $Cr_2N$ and $Cr_{23}C_6$ were found in the HTHAZ of welded LDX2101, [28]. Anyway, the former precipitate when ferrite is in excess and in fact it was found dense only in rapidly cooled HTHAZ. The latter was found in grain boundaries, but in very low quantity due to low C content. Titanium nitrides were also found in HTHAZ of duplex steels. Titanium can be present in small quantity (it is not even mentioned in Table. 1) and compete with Cr to form nitrides. $\gamma_2$ was found to have formed in already solidified weld metal after new passes and re-heating; its effect on mechanical properties was found to be irrelevant, [29].

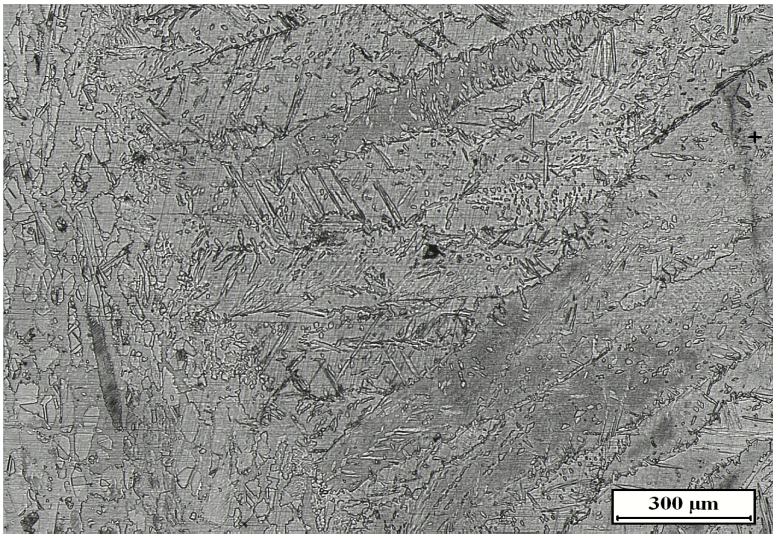


*Fig. 43: base-weld transition on a deformed specimen*

# 7 RESULTS

## 7.1 Fractures

*Table 8: Table of fractures*

| Spec type | T | Fracture loc. | Position | Fracture type | Rp0.2error% | Necking | |
|---|---|---|---|---|---|---|---|
| * 1p5Ni_a | 20 | w | 2 cm thr | Cleavage | 0.53 | ✓ | |
| * 5Ni_a | 20 | b | 1,5 cm thr | Dimples | 0.17 | ✓ | |
| * 7Ni_a | 20 | w | In the middle | Dimples | 0.17 | ✓ | # |
| 1p5Ni_b | 20 | b | 1 cm thr | Dimples | 0,00 | ✓ | # |
| 5Ni_b | 20 | b | 0,5 cm thr | Dimples | 0.93 | ✓ | |
| * 7Ni_b | 20 | b | 1,5 cm thr | Dimples | 0,00 | ✓ | # |
| 1p5Ni_c | 20 | w | 1 cm thr | Cleavage | 0.19 | ✓ | |
| 5Ni_c | 20 | w | 1,5 cm thr | Dimples | 0.16 | ✓ | |
| 7Ni_c | 20 | w | In the middle | Dimples | 0.18 | ✓ | |
| 1p5Ni_a | 0 | w | In the middle | Cleavage | 1.32 | ✓ | # |
| 5Ni_a | 0 | b | 0,5 cm thr | Dimples | 1.59 | | |
| 7Ni_a | 0 | w | In the middle | Dimples | 2.92 | ✓ | # |
| 1p5Ni_c | 0 | w | 1 cm thr | Cleavage | 1.82 | | |
| 5Ni_c | 0 | w | 2 cm thr | Dimples | 1.30 | | |
| 7Ni_c | 0 | w | In the middle | Dimples | 2.29 | | |
| 1p5Ni_a | -20 | w | In the middle | Cleavage | 3.79 | | |
| 5Ni_a | -20 | w | In the middle | Dimples | | ✓ | |
| 7Ni_a | -20 | w | 1,5 cm thr | Dimples | 0.50 | ✓ | # |
| 1p5Ni_b | -20 | b | 1 cm thr | Dimples | 0.87 | ✓ | |
| 5Ni_b | -20 | w | In the middle | Dimples | 1.55 | ✓ | # |
| 7Ni_b | -20 | b | <1 cm thr | Dimples | 3.20 | ✓ | # |
| 1p5Ni_c | -20 | w | 1 cm thr | Cleavage | 1.03 | | |
| 5Ni_c | -20 | w | In the middle | Dimples | 1.12 | ✓ | |
| 7Ni_c | -20 | w | In the middle | Dimples | 0.50 | ✓ | |
| 1p5Ni_a | -40 | w | In the middle | Cleavage | 0.76 | | |
| 5Ni_a | -40 | w | 1,5 cm thr | Dimples | 1.38 | | |
| 7Ni_a | -40 | w | In the middle | Dimples | 0.00 | ✓ | |
| 1p5Ni_c | -40 | w | In the middle | Cleavage | 0.96 | | |
| 5Ni_c | -40 | w | In the middle | Dimples | 0.61 | | |
| 7Ni_c | -40 | w | 1,5 cm thr | Dimples | 1.12 | ✓ | |

*Legend*

* *Extensometer with a 25 mm gauge length instead than 36 mm*

*Rp0.2 taken from standard elastic modulus of 200 GPa*

*Rp0.2 taken from the experimental elastic modulus*

*Specimen with no extensometer signal*

The localization and approximate position of all fractures are showed in Table. 8. The letters "w" and "b" stand for fracture in the weld and in the base metal respectively. "*c*" specimens are completely made of weld metal, so for them the fracture localization "w" is obvious. Regarding the type of fracture, specimens that show mostly cleavage facets or dimples are marked as "cleavage" and "dimples" respectively. Coherently, the former show a fracture at 90°, the latter at 45° or a cup-and-cone one. Specimens that break after having reached the maximum engineering stress are marked with ✓ under the voice Necking. The extensometer does not work during the test of *5Ni_weld* at 0°C, red colored in Table. 8. Its engineering adjusted encoder curve is obtained using the average compliance of *weld* specimens tested at 20°C and its Rp0,2 is extracted from that curve. This is an arbitrary procedure and the yield strength value of that specimen is just indicative.Yield strengths of specimens with bad extensometer signal (color orange) are obtained with a line of slope 200 GPa. Reporting the calculated elastic moduli for each specimen is not interesting since they are similar to 200 GPa at all temperatures, too. The percent error between Rp0,2 evaluated with the experimental elastic modulus and with the reference 200 GPa modulus is also reported for each specimen. In order to better understand mentioned issues, refer to 5.2-*Data elaboration*. The symbol # means that the specimen breks at a distance from a thread less than 25% of the final length: staying at ASTM, [3], the mechanical properties obtained for these specimens should not be taken as reliable. However, common sense says that at least the yield strength should be considered valid, since it is not connected to the position of the fracture. Moreover, it is desirable to check when and how fractures actually occur in the specimens, so all tests are considered as "valid".

### 7.2 Total elongations and strengths

In the following pages, total elongations and mechanical strengths of all tested materials are reported. The specimens are classified by position from which they are extracted from welds (*weld*, *root cross weld* and *surface cross weld*). At each temperature it is possible comparing the properties of *1,5Ni*, *5Ni* and *7Ni*.

Total elongations to fracture measured with the ruler are gross measurements as explained in 5.3. In order to check the reliability of those elongations, "fictive" total elongations are plotted in the same Figs. 44, 45 and 46. Fictive elongations are obtained considering as final length the last strain value in each engineering curve (see 12.1). These elongations are not the actual

ones, since they do not take in consideration the elastic unloading to which specimens are subjected once failed. Anyway, they should provide the correct relative ranking of elongation of *1,5Ni*, *5Ni* and *7Ni* at each temperature, so it is meaningful comparing them with the hand-measured ones. Fortunately, they show that hand-measured elongations are reliable, since the ranking of elongations is the same as their at each temperature.

Weld specimens

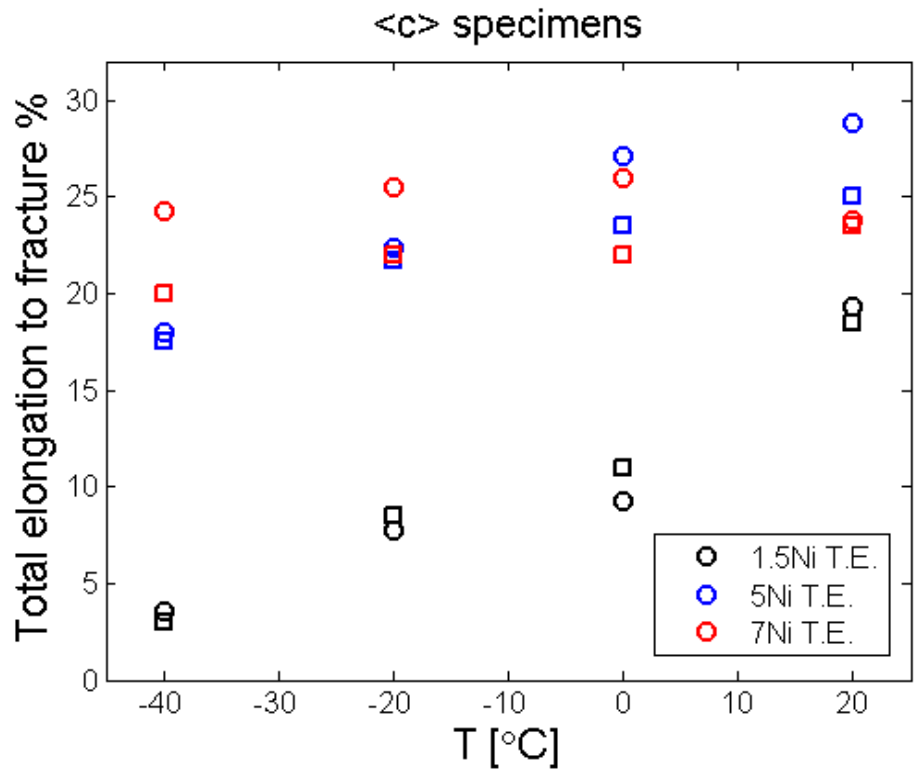


*Fig. 44: Total elongations of weld specimens. Squares represent the elongations measured with ruler and circles the fictive ones*

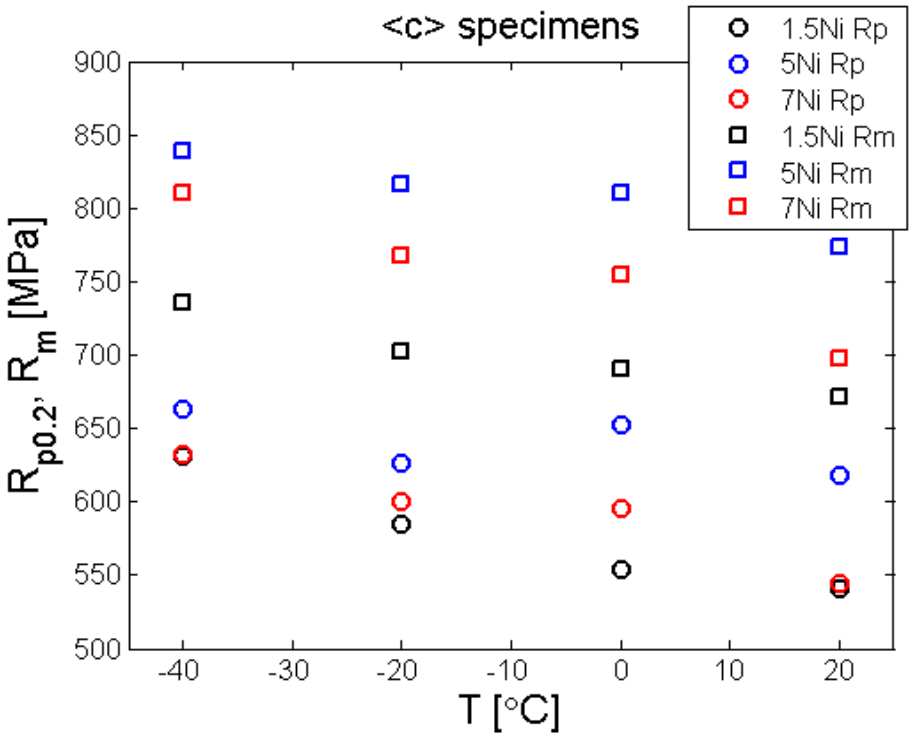


*Fig. 45: Tensile strengths of weld specimens. N.B. 5Ni at 0°C has not reliable values due to absence of extensometer signal*

Root cross weld specimens

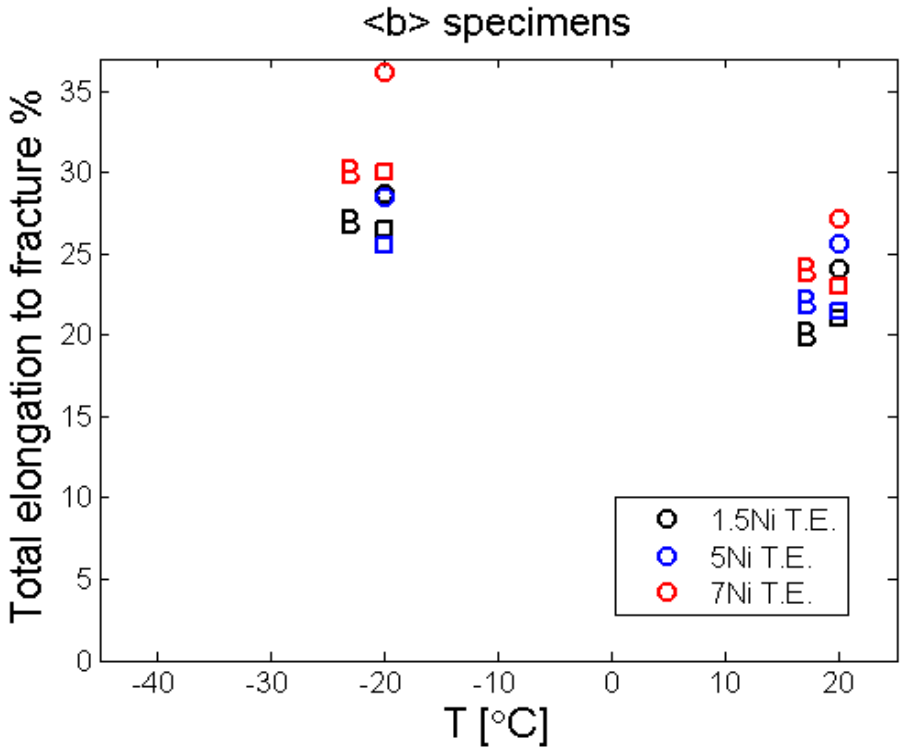


*Fig. 46: Total elongations of root cross weld specimens. Squares represent the elongations measured with ruler and circles the fictive ones. B means failure in the base metal*

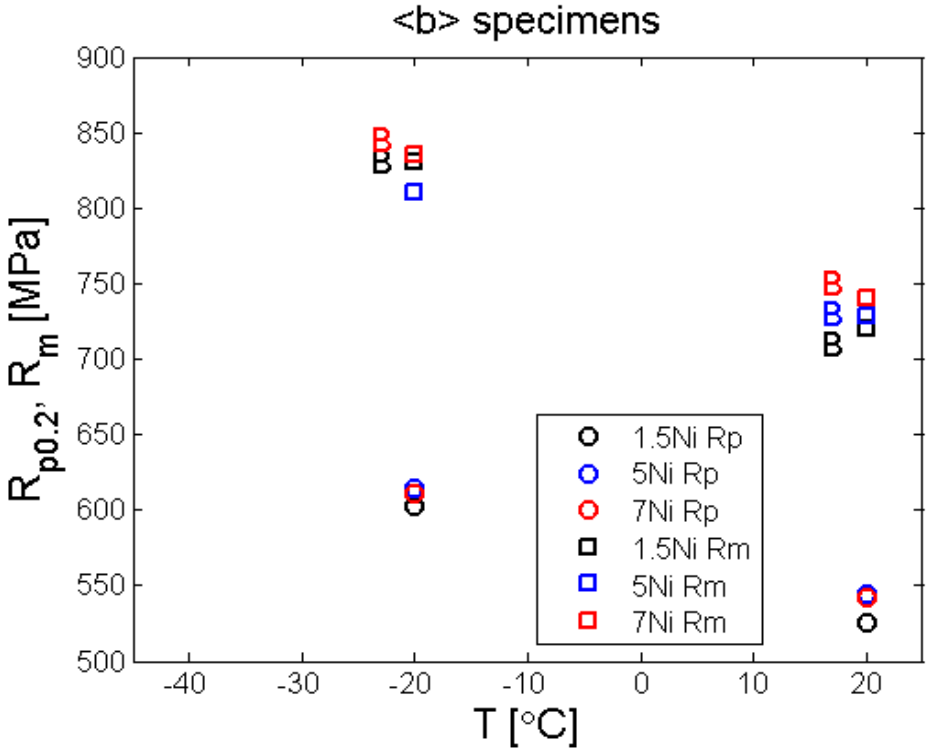


*Fig. 47: Tensile strengths of root cross weld specimens. B means failure in the base metal*

Surface cross weld specimens

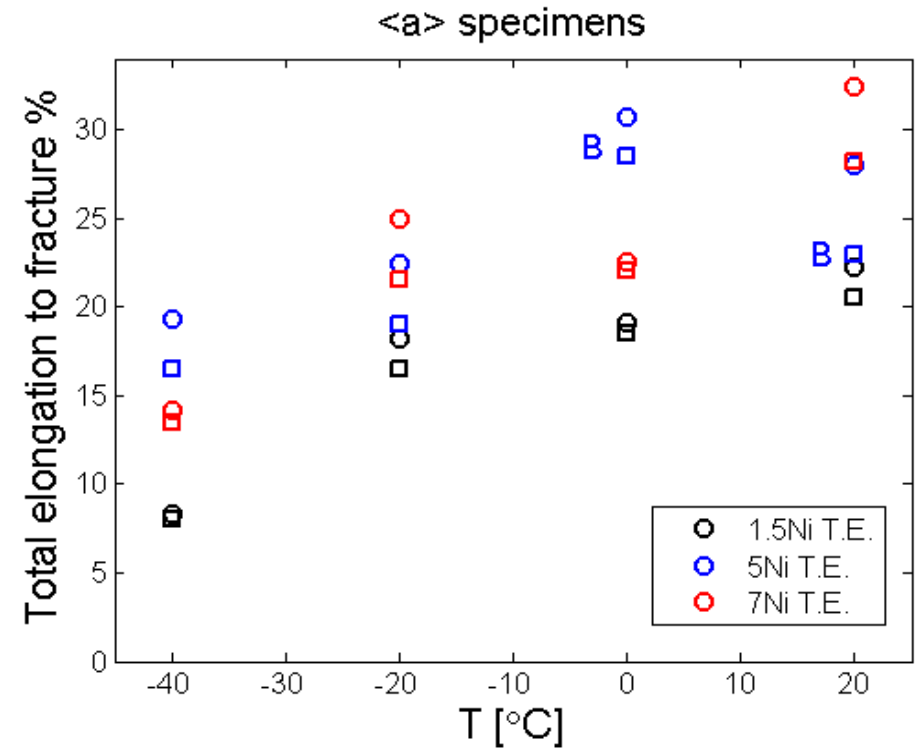


*Fig. 48: Total elongations of surface cross weld specimens. Squares represent the elongations measured with ruler and circles the fictive ones. B means failure in the base metal*

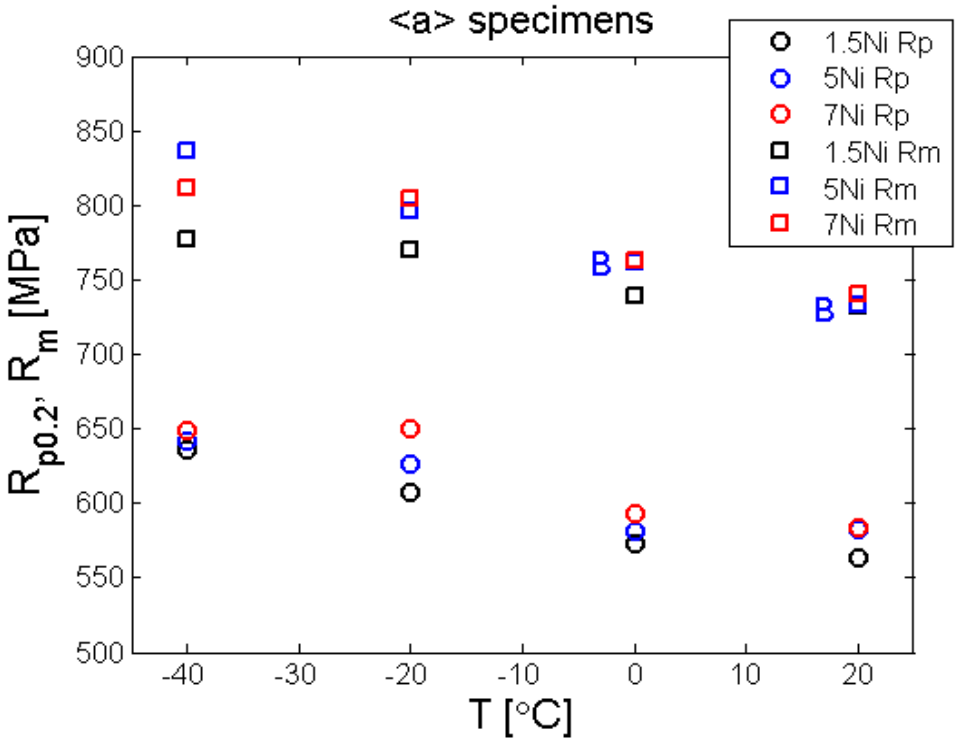


*Fig. 49: Tensile strengths of surface cross weld specimens. B means failure in the base metal*

*Observations about weld specimens*

- *1,5 Ni* specimens have the lowest elongations
- *5 Ni* and *7 Ni* specimens elongate nearly the same, even if *5 Ni* tend to decrease their ductility at low temperatures while *7 Ni* ductility tends to remain constant
- *1,5 Ni* have the lowest strengths and *5Ni* have the highest
- At fixed temperatures, strengths differ markedly between specimens

*Observations about root cross weld specimens*

- These specimens tend to fail in the base metal
- Specimens at -20° show more elongation than at 20°
- *7 Ni* specimens elongate more than the others
- *1,5 Ni* specimens tend to have the lowest properties; anyway, all properties do not vary much between specimens at the same temperature
- The *5 Ni* specimen at -20° is the only one that does not fail in the base metal and its tensile strength is lower than the others

*Observations about surface cross weld specimens*

- *1,5 Ni* specimens have the lowest elongation to fracture at all temperatures
- *5 Ni* specimens fail in the base metal at 20° and 0°C; in the latter case the elongation is higher
- *1,5 Ni* specimens tend to have the lowest strengths and *7Ni* the highest

### 7.3 Reference datas

Minimum measured strength values for worked base metal LDX2101 and typical values for the weld metal taken from literature, [1], are shown in Table. 9.

*Table 9: Strengths for LDX2101 [MPa]*

| | **Minimum values for base metal** | | | **Typical values for pure weld metal** | |
|---|---|---|---|---|---|
| | *P* | *H* | *C* | *MIG* | *SAW** |
| **Rp0.2** | 450 | 480 | 530 | 520 | 570 |
| **Rm** | 650 | 680 | 700 | 710 | 750 |

*P* Hot-rolled plate *H* Hot -rolled coil

*C* Cold-rolled coil * welded with Avesta Flux 805

Room temperature strengths of base metal LDX2101, [30], are shown in Table. 10. They can be compared with those measured for the solution treated base metal plates in Table. 3: the difference is quite small.

*Table 10: Strengths at various temperatures for base metal LDX2101 [MPa]*

| | *20°C* | *0°C* | *-40°C* |
|---|---|---|---|
| **Rp0.2** | 488 | 529 | 585 |
| **Rm** | 694 | 724 | 762 |

Reference datas for weld LDX2101 which root bead is performed with SMAW (shielded metal arc welding) and subsequent passes with FCAW (flux-cored arc welding) are Rp0,2 of 515 MPa and Rm of 697 MPa, [30].

304 and 316 austenitic grades, for which LDX2101 can be a substitute, have both Rp0,2 of 290 MPa. Rm is 621 MPa for the former and 579 MPa for the latter, [31]. 304 and 316 "L" grades contain less carbon in order to avoid carbides precipitation and have even lower strengths, not reported here.

Reference engineering strengths for as-welded (without post-treatment) 2205 duplex grade can be found in [32]: yield and ultimate tensile strengths of 559 MPa and 729 MPa

respectively. It must be remembered that LDX2101 is a less alloyed duplex grade and its properties are slightly lower.

Regarding the total elongation to fracture, A5 datas (see 2.2) found in literature are 30% for base and MIG-welded metal and 25% for the SAW-welded, [1]. Comparisons with experimental datas are in this case tricky: most of the specimens contain both base and weld metal. Moreover, their diameter is 5 mm: from Eq. (15), in order to compare their total elongations with A5 datas, their gauge length should be 25 mm instead of 36.

### 7.4 Comparisons with references

Comparing datas in 7.3 with measured properties, reported in Table. 15 (see 12.1) it can be observed that:

- All weld specimens (*c*) at 20°C have at least higher Rp0,2 than that specified for MIG welds in Table. 9, but only the *5Ni* specimen exceeds those reported for SAW welds.
- Specimens at 20°, 0°C and -40°C have higher strengths than reference base metal at the respective temperatures. The only exceptions are the Rm of the *1,5 Ni* specimen at 20° and -40°C, that are slightly lower.
- The increase in strengths as temperature decreases is significant: for example, specimens at -40°C have even Rp0,2 similar to Rm of base metal at 20°C.
- Rp0,2 of specimens at room temperature, and also at lower temperatures, are greater or comparable to the minimum Rp0,2 value for cold-rolled base metal coils. The latter is the higher value among the ones indicated for rolled pieces.
- Rm of specimens at room temperature, and a fortiori at lower temperatures, are greater than the minimum Rm value for cold-rolled base metal coils. An exception is again a 1,5 Ni specimen (*weld* at 20°C) which Rm is however more than the minimum for hot-rolled base metal plates.
- Rp0,2 and Rm of all specimens at room temperature, and a fortiori at lower temperatures, are higher than those of the austenitic grade 304.

### 7.5 Presence of inclusions

All fractures surfaces of specimens that fail in the weld metal show the presence of at least

one round inclusion nearly 100 µm large, see SEM Figs. 50 and 51. These inclusions are often surrounded by flat circular areas, surrounded in turn by dimples on the remaining surface. Moreover, all magnified final parts of tensile curves show more or less sudden drops in tension. These facts indicate that these inclusions always initiate the failure when the latter occurs in the weld metal, see 8.2.

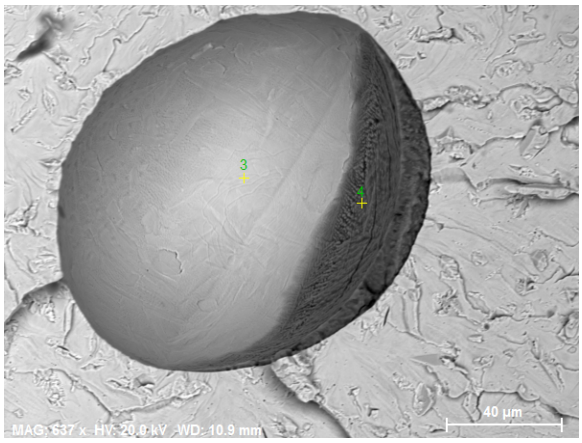


*Fig. 50: Inclusion in a 1,5Ni specimen*

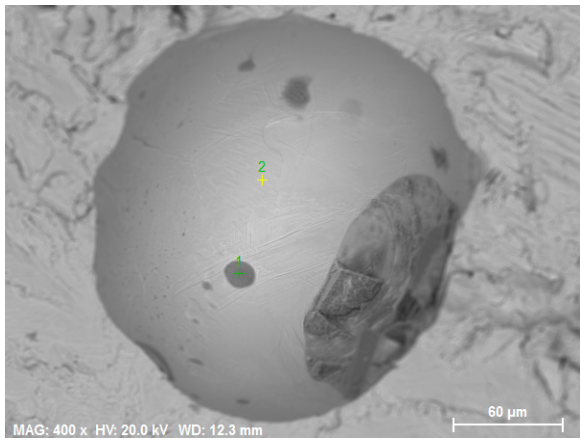


*Fig. 51: Inclusion in a 7Ni specimen*

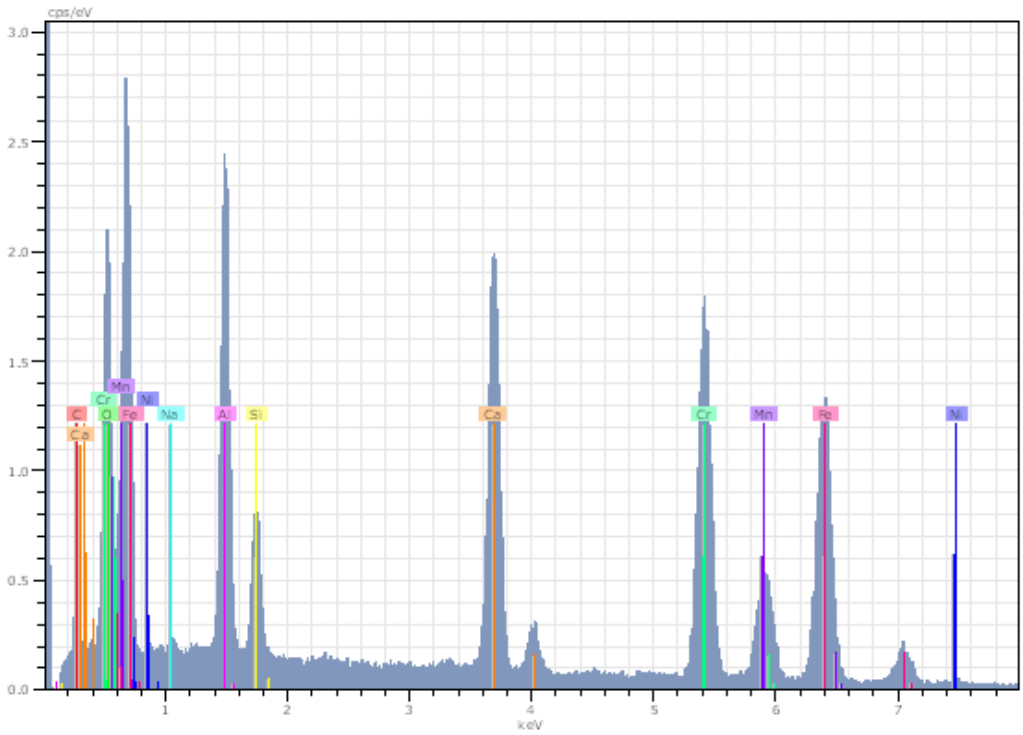


*Fig. 52: Element spectrum of point 3 in Fig. 50*

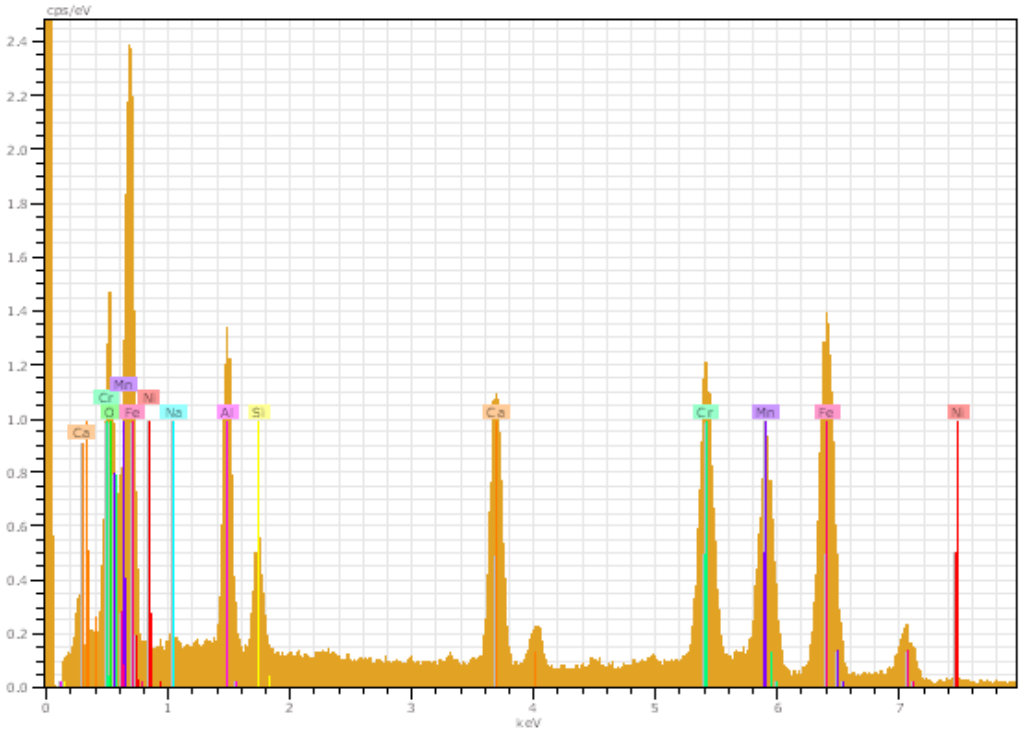


*Fig. 53: Element spectrum of point 4 in Fig. 50*

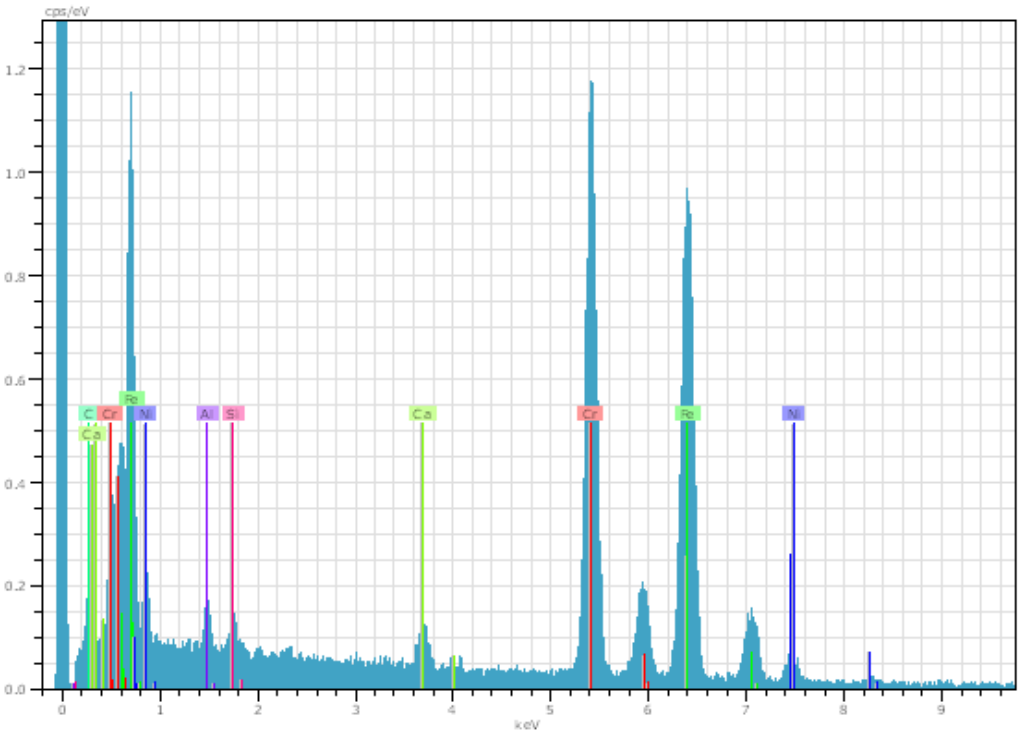


*Fig. 54: Element spectrum of point 1 in Fig. 51*

In Figs. 52÷54 the elementary analysis of green points in Figs. 50 and 51 give remarkable peaks for the same elements: Si, Ca, Al and O. Comparing these results to the composition of the flux used for SAW welding in Table. 4, the result is quite univocal: the inclusions are flux granules that remain in the molten pool during solidification. Afterall, this is a common problem in SAW welds, as said in 4.2. Fluorine is difficult to identify with EDS, so its absence in spectrums is normal.

Flux granules are for sure the inclusions that affect more the tensile behavior and their effects on the fracture surfaces is even evident to the naked eye. The EDS analysis also finds other inclusions. Their influence on the tensile behavior is anyway difficult to clear and they are found just on few fracture surfaces. Figs. 55 and 56 show these inclusions and Tables. 11 and 12 their chemical analysis. The inclusions turn out to be granules of calcium oxide, coming in turn from the flux, and probably sulfides.

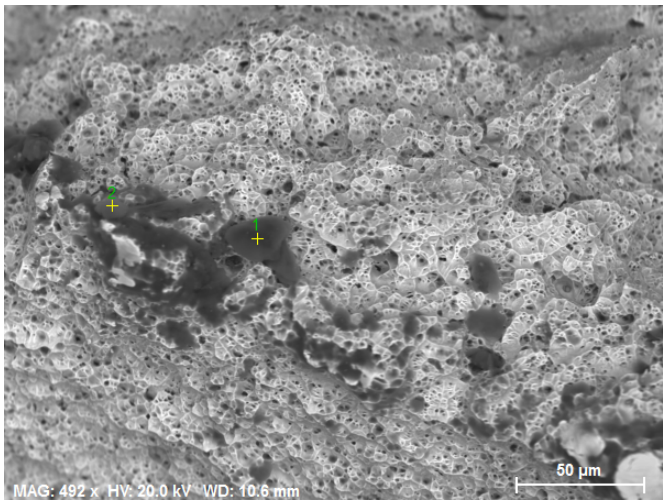


*Fig. 55: Inclusions of CaO in a 7Ni specimen*

*Table 11: Element analysis of point 1 in Fig. 55*

Spectrum: 1

| Element | Series | norm. C [wt.%] | Atom. C [at.%] |
|---|---|---|---|
| Oxygen | K-series | 53.00 | 74.38 |
| Silicon | K-series | 0.68 | 0.54 |
| Sulfur | K-series | 0.39 | 0.27 |
| Chlorine | K-series | 0.17 | 0.11 |
| Calcium | K-series | 37.12 | 20.80 |
| Chromium | K-series | 2.56 | 1.10 |
| Iron | K-series | 4.94 | 1.99 |
| Nickel | K-series | 0.52 | 0.20 |
| Sodium | K-series | 0.62 | 0.61 |
| Total: | | 100.00 | 100.00 |

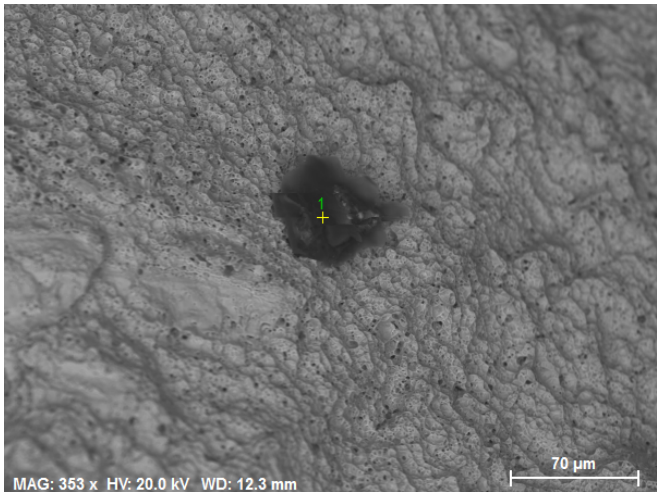


*Fig. 56: Sulfide in a 7Ni specimen*

*Tabella 12: Element analysis of point 1 in Fig. 56*

Spectrum: 1

| Element | Series | norm. C [wt.%] | Atom. C [at.%] |
|---|---|---|---|
| Oxygen | K-series | 15.45 | 35.17 |
| Sodium | K-series | 3.00 | 4.75 |
| Magnesium | K-series | 1.27 | 1.90 |
| Aluminium | K-series | 1.01 | 1.36 |
| Silicon | K-series | 1.17 | 1.52 |
| Phosphorus | K-series | 0.55 | 0.65 |
| Sulfur | K-series | 4.17 | 4.73 |
| Chlorine | K-series | 2.61 | 2.68 |
| Potassium | K-series | 0.27 | 0.25 |
| Calcium | K-series | 1.14 | 1.04 |
| Chromium | K-series | 17.55 | 12.29 |
| Iron | K-series | 47.10 | 30.71 |
| Nickel | K-series | 4.01 | 2.49 |
| Manganese | K-series | 0.70 | 0.46 |
| Total: | | 100.00 | 100.00 |

# 8 DISCUSSION

## 8.1 General points

*Types of fracture*

Steels can show ductile, brittle or mixed failures. It is not aim of this work describing them in detail, but a brief introduction is useful to understand the behavior of the tested materials.

Metal alloys under progressive load discharge stresses with plastic deformation. This occurs thanks to the slipping of atoms on precise directions and planes depending on the type of lattice. Atoms do not displace together, but subsequently. This can be seen as the “walking” of local defects in the lattice, i.e. dislocations. Deformation is a complicated process since dislocations can interfere between each others. In polycristalline materials, as all commercial steels, the deformation occurs differently in every grain because of different orientations or types of lattice. Moreover, every grain is hindered in its deformation by the adjacent ones.

Impurities, in the broadest sense of the term, tend to block dislocations reducing the local possibility to deform. These discontinuities, which nature and dimensions can vary a lot, are always present in real metal alloys. They can be seen as solid particles occupying holes within the metal bulk. As the metal undergoes to plastic deformation, these holes elongate in the direction of tension while the metal bridges between them shrink. When the latter become too thin to sustain load, the micro-voids coalesce and the material fails. The resulting fracture surface consists of craters separated by ridges. Depth of dimples is connected to the ability of the specimen to plasticize. Failures that occur with formation of dimples are typically transcrystalline and they involve the whole section of the material at the same time [33]. It must be noticed that only ductile failure processes are considered, as they are the usual case in the tests. They are characterized by significant energy absorption, connected to plastic deformation. Brittle failures occur instead within or soon after the elastic behavior of a material, with little or no plastic deformation.

Actually, even if the process that brings to failure is ductile, the fracture surface may not show dimples but cleavage. The latter consists of smooth surfaces and is due to uncontrolled propagation of a crack on determined crystallographic planes. Cleavage cannot occur in austenite, but is possible in ferrite on planes (100), [33]. Since lattices of different grains have

different orientations, a crack can subdivide into more cracks crossing a grain bounday in order to proceed on the favored crystallographic planes. Grains which favored propagation planes are too inclined to be followed by the crack may break with formation of dimples. Cleavage occurs at the speed of sound of the material and is connected to sudden failure before the material exhausts its ability to plasticize. It cannot be predicted with much accuracy, so it is particularly dangerous. Even if before the final failure a large amount of energy can be absorbed, cleavage in itself does not consume energy to occur. So, cleavage facets are connected to more brittle failure. Cleavage is typically intra-cristalline.

Fracture surfaces can show both dimples and cleavage facets. Actually, this is the most common situation, see 8.2.

*General factors influencing tensile behavior*

As mentioned, plastic deformation occurs in metals with dislocations motion. During the deformation, new dislocations form and interact with each other causing progressive strengthening of the material, i.e. work-hardening. The accumulation of dislocations, however, reduces the path for their motion itself, making the metal more prone to fail. In a general way, factors that enhance the ability of dislocations to move increase elongation and absorbed energy before fracture, while reducing the strength of metals; viceversa for factors that hinder the dislocations motion.

Microstructure in welds is more irregular and can contain a lot of defects, e.g. inclusions, or undesired precipitations that can hinder dislocations. Welds usually contain residual stresses, which are connected to hardening, too. Inclusions in weld metal act as stress-risers promoting crack formation and catastrophic propagation. Low temperatures reduce the ability of dislocations to move. These facts explain some general trends in experimental results: weld metal has higher strengths than base metal but lower elongations. Strengths tend to increase as temperature decreases, oppositely to elongations.

Other factors can influence the tensile behavior of materials, e.g. the strainrate, but only discriminating factors in this work have been described.

## 8.2 Discussion of single specimens

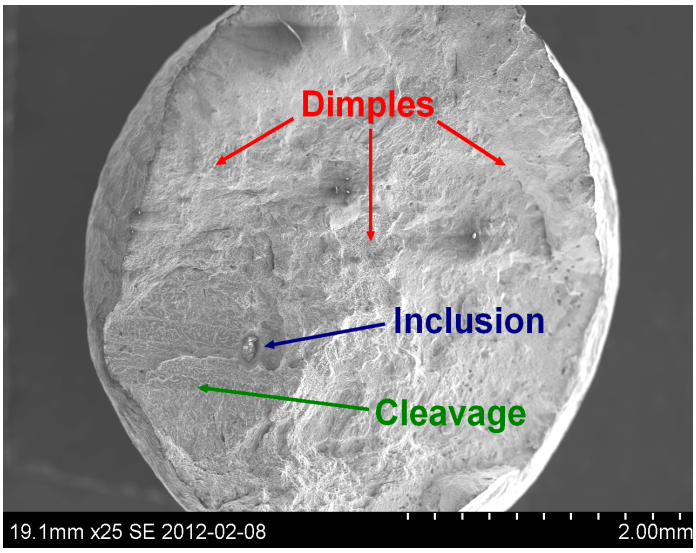


*Fig. 57: Fracture section of 5Ni_weld at 20°C*

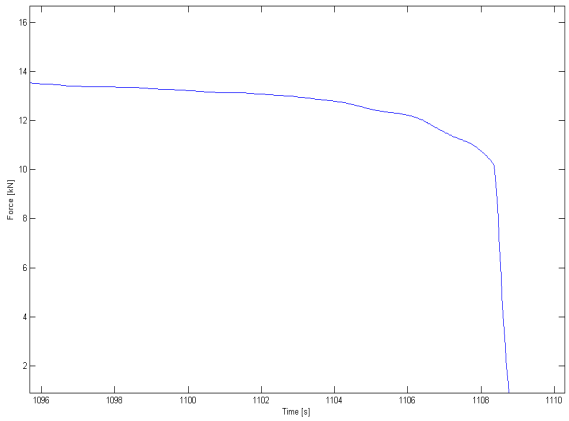


*Fig. 58: Final part of force curve, 5Ni_weld at 20°C*

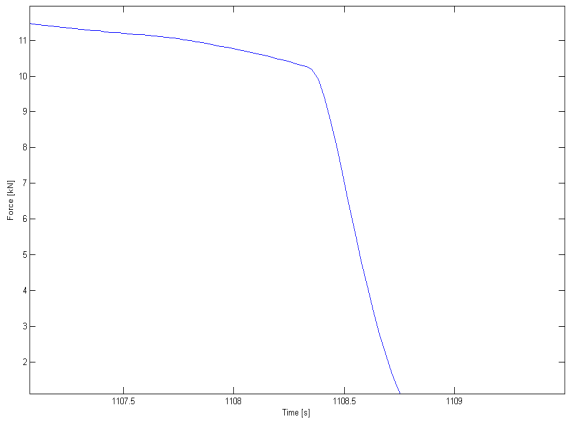


*Fig. 59: Final drop of force in 5Ni_weld at 20°C*

Here follows an inquiry about some single specimens that aims to analyze differences in tensile behavior among materials in greater detail. Firstly, *weld* specimens will be investigated as they consist of weld metal only and so they are more meaningful in order to depict the behavior of welds. Some *root cross weld* and *surface cross weld* specimens are discussed just after.

It must be remembered that each kind of specimen (determined by orientation and chemical composition) is tested only once at each temperature: a larger inquiry could produce slightly different results on single specimens.

*Weld specimens ("c")*

These specimens, as well as *surface cross weld* ones, do not contain MIG-welded metal, but just SAW-welded. *5Ni_weld* tested at room temperature gives an example of the failure that occurs in most specimens at all temperatures, although sometimes with little variations.

In Fig. 57, the site of a flux inclusion (see 7.5), a cleavage zone around it and dimples in the remaining section

can be viewed. Actually in the image there is not the inclusion, but a pore observable in other fracture surfaces, too: the inclusion was removed by the ultra-sonic bath or remained in the facing fracture surface. Fig. 58 shows instead the final part of the graph force vs. time of testing. A gradual decrease in force means that necking occurs, and this is coherent with the oval section in Fig. 57. Fig. 59 is a magnification of the very final part of the curve (the axis have different scale than in Fig. 58). Just after second 1108, the force drops in less than a second. This drop means that an event causing quick failure occurs before the specimen exhausts its capacity to deformate plastically: in the latter case, the decrease in force would be more gradually until final rupture. This is coherent with the fracture surface and can only be connected with the effect of the inclusion: this starts a cleavage fracture, reducing the resisting section suddenly and leading to rupture.

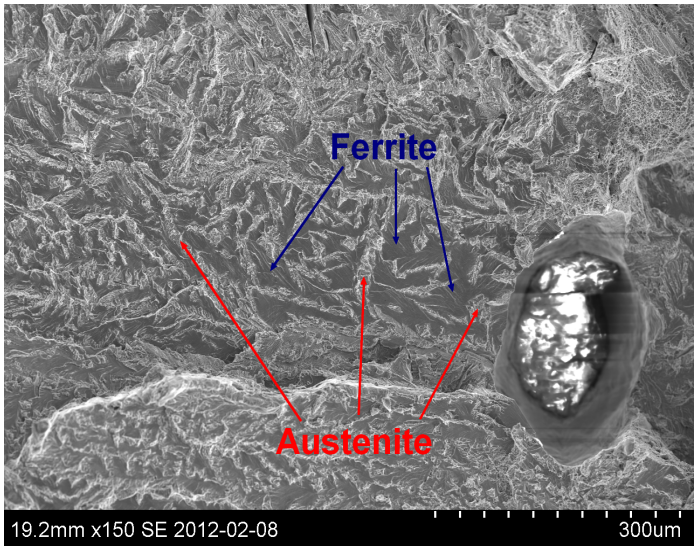


*Fig. 60: Cleavage zone in 5Ni_weld at 20°C*

Actually, cleavage cannot occur in austenite for normal DSS alloys, as mentioned in 8.1. The microstructure of duplex welds consists of fine and irregularly shaped austenite grains separating ferrite, as mentioned in 3.1. So, a crack cannot propagate undisturbed in the section, but has to bypass the austenite grains or "waiting" for their plastic failure before propagating again in an adjacent ferrite grain with cleavage. The magnification of the zone around the inclusion, in Fig. 60, shows clearly smooth dark surfaces (ferrite) and brighter profiles in relief (austenite). Therefore, this kind of fracture pattern is not totally cleavage but a mix of patterns that depends on quantity and dimension of austenite grains. This can explain why the force drop is never perfectly vertical. The presence of dimples around the mentioned zone confirms that the crack is not totally undisturbed because otherwise it would propagate in the entire section. So, after initial propagation of a crack, the remaining section fails breaking metal bridges between micro-voids with formation of dimples, see 8.1. Anyway, this does not provide additional strength because the bridges are subjected to great and quick stress raise in nearly half second and they fail suddenly. So,

inclusions represent a detrimental factor in all failures, since they start cracks and anticipate the failure due to coalescence of micro-voids. The correlated effect is the reduction of the energy absorption. Flux inclusions are not present in MIG welds and this can explain why in literature the average total elongation for MIG welded duplex steels is 5% higher than for SAW welds.

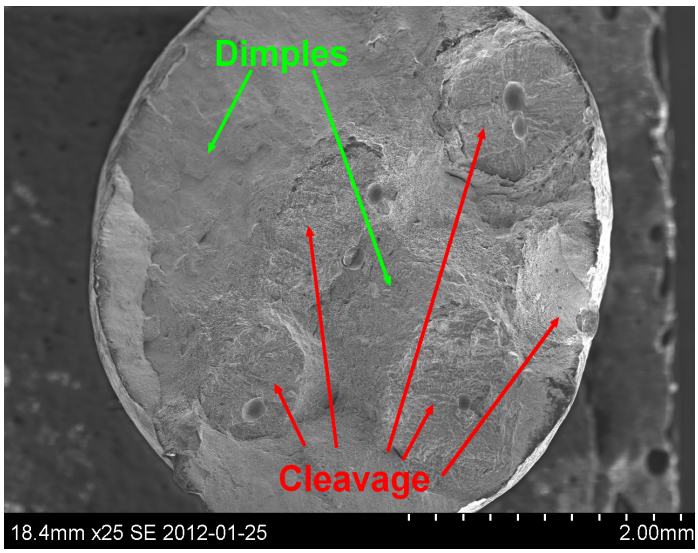


*Fig. 61: Fracture section of 5Ni_weld at 0°C*

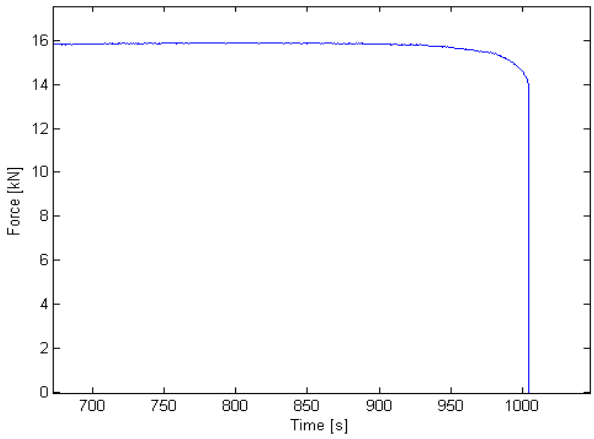


*Fig. 62: Final drop of force in 5Ni_weld at 20°C*

*5Ni_weld* specimen tested at 0°C has an unusual fracture surface: many inclusions with their relative propagation zones can be noticed amid the dimples, Fig. 61. They are at different heigths, even if this detail cannot be noticed in the photo. The final part of the force curve, in Fig. 62, is similar to Fig. 58. The difference is the much reduced necking before the final drop: during a stress plateau, the force starts decreasing and the failure is reached soon after. The maximum achievable engineering stress seems however to have been reached.

The number of inclusions that propagate cracks turns out to be negligible for the total elongation of the specimen, see also Fig. 44. The logical deduction is that once a crack starts propagating from an inclusion, the increased stress within the remaining section leads to crack initation and propagation from other inclusions, too. Anyway, it is the onset of the first propagation that controls failure and total elongation.

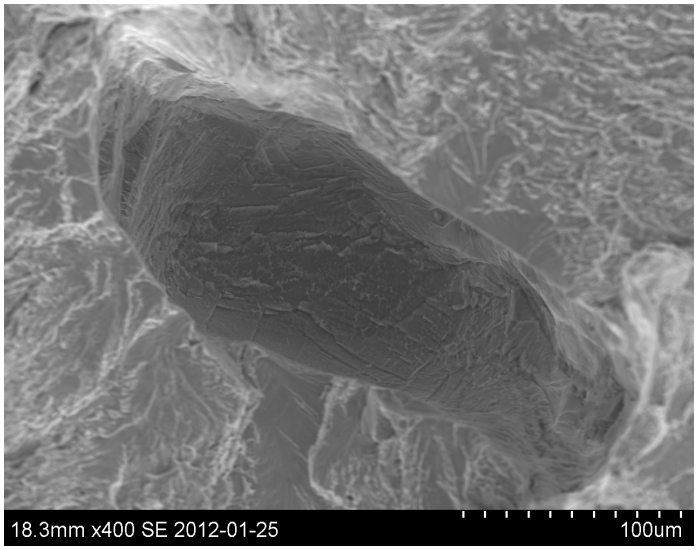


*Fig. 63: Inclusion in 7Ni_weld at 20°C*

Since inclusions start cracks that lead to failure, their distribution, size and shape play for sure a role in the process. Unfortunately, these factors are not controllable. At room temperature, *7Ni_weld* fails before *5Ni_weld* and this is almost for sure due to the irregular shape of the inclusion starting a crack, which acts as strong stress-concentrator, Fig. 63.

*5Ni* and *7Ni* show dimpled areas at all temperatures, even if the zones involved by crack propagation around the inclusions are progressively larger as temperature decreases. This is connected to the already mentioned reduced ability of the material to plasticize at lower temperatures.

Table. 13 shows engineering and true ultimate tensile strength and elongation for each *weld* specimen. Necking is not emphatic in most of the tests, so true Rm should be similar to the actual stress that the material experiences right before failing. *7Ni* specimens fail after nearly the same elongation at all temperatures, within a range of 4%. Their Rm values increase nearly 17% from 20° to -40°C. Oppositely, *5Ni* specimens fail at nearly the same stress at all temperatures, within a 2%, while their elongations decrease of nearly 30% from 20° to -40°C. *5Ni_weld* tested at 0°C must not be considered, since its strength values were obtained in arbitrary way and are not reliable, see 7.1. These observations lead to say that failure in *5Ni_weld* specimens is stress-controlled, while in *7Ni* is strain-controlled. This can be explained as higher average ductility of *7Ni* at low temperatures, that would delay the crack propagation from inclusions. Reaching same elongation at low temperature means reaching higher stress levels before rupture, because of the previously explained effect of temperature. *5Ni* specimens would instead fail when the stress field right around an inclusion becomes critical and at lower temperatures this occurs after less elongation.

Staying at Table. 13, *5Ni* specimens have always higher strength than *7Ni*, as already observed in 7.2. *5Ni* and *7Ni* specimens have similar austenite content, as seen in Table. 7, and they both consist of SAW-welded metal. So, the reason for the higher properties of *5Ni*

must be the chemical composition. In order to compensate the lack of Ni for the austenite stabilization, *5Ni* welds are additioned with Mn in respect of *7Ni*. As said in 3.2, Mn addition can increase strength without lowering the total elongation if σ phase precipitation is avoided, as in the welds tested. Mn must be the reason for the higher performances of *5Ni* in respect of *7Ni*. However, it is not clear from literature if the element affects or not the total elongation at low temperatures. Probably, Mn is less effective than Ni in ensuring ductility at low temperatures and this would explain the stress-controlled behavior of *5Ni*.

*Table. 13: Engineering Rm, True Rm and T.E. of weld specimens*

| | | Rm_eng [MPa] | Rm_true [MPa] | T.E. |
|---|---|---|---|---|
| | 1p5Ni1c | 541 | 745 | 18,46 |
| *20°C* | 5Ni1c | 618 | 930 | 25 |
| | 7Ni1c | 544 | 813 | 23,12 |
| | 1p5Ni2c | 554 | 735 | 11,11 |
| *0°C* | 5Ni2c | 652 | 982 | 23,60 |
| | 7Ni2c | 595 | 883 | 22,09 |
| | 1p5Ni3c | 585 | 738 | 8,64 |
| *-20°C* | 5Ni3c | 626 | 945 | 22,05 |
| | 7Ni3c | 600 | 907 | 21,88 |
| | 1p5Ni4c | 631 | 760 | 3,16 |
| *-40°C* | 5Ni4c | 663 | 949 | 17,47 |
| | 7Ni4c | 631 | 953 | 19,83 |

*5Ni* seems to be preferable to *7Ni* for use at room temperature since similarly ductile, more resistant and even cheaper (due to lower Ni content). Due to compensating effects, at -40°C *5Ni* and *7Ni* have similar strengths and elongations.

*1,5Ni* specimens need a separate discussion. Their total elongations are by far the worst among all specimens, see Fig. 44. *1,5Ni* welds contain more Mn and less Ni than the other welds, and Table. 13 shows that their failure is stress-controlled as that of *5Ni*. This is coherent to what already discussed, but *1,5Ni* specimens also have the lowest mechanical strengths (only their Rp0,2 are sometimes comparable to those of *7Ni*, see Fig. 45). This is not

coherent with the higher Mn content.

The main difference between *1,5Ni* on one side and *5-7Ni* on the other is the much higher ferrite content of the former, see Table. 7. The microstructures are also different, as explained in 6.2. *1,5Ni* welds contain mostly intragranular austenite, while *5Ni* and *7Ni* mostly grain boundary and Widmanstätten austenite. Intragranular austenite forms at lower temperatures during cooling, giving more time to ferrite grains for growing. Viceversa, when at higher temperature the other two types of austenite form, the growth of ferrite is hindered: the resulting microstructure is finer and shows a more even ferrite/austenite balance. Moreover, in *1,5Ni* welds the ferrite is more connected and this is like having larger ferrite grains. Hall-Petch relates mechanical properties with the reciprocal of the square root of the grain size. For example, Eq. (22) shows the Hall-Petch relation for the yield strength.

$$\sigma = \sigma_0 + \frac{K_y}{\sqrt{d}} \tag{22}$$

$\sigma$ is the yield strength, $\sigma_0$ is the resistance of the lattice to dislocations motion, $K_y$ is a hardening constant and $d$ is the average grain size. So, the smaller the average grain, the bigger the yield strength.

The results of a line intercept counting analysis conducted on micrographs of *1,5Ni*, *5Ni* and *7Ni* are showed in Table. 14. *5Ni* and *7Ni* have similar ferrite grain sizes, much smaller than *1,5Ni*. This confirms what above discussed about the lower properties of *1,5Ni*. Regarding the ferrite, it must be noticed that the method leads to calculate the average distance between austenite grains, not the real ferrite grain size. Even if improper, anyway, the denomination "grain size" is kept because larger distance between austenite grains has comparable effect as having larger ferrite grain size.

*Table. 14: Average ferrite and austenite grain size, median ferrite and austenite grain size [µm] and number of measurements.*

| | Ferr. | Aust. | Med.F. | Med.A. | N° ferrite | N° austenite |
|---|---|---|---|---|---|---|
| *1,5%Ni* | 28.98 | 12.58 | 26.03 | 12.33 | 46 | 43 |
| *5%Ni* | 13.00 | 13.98 | 10.27 | 12.33 | 68 | 65 |
| *7%Ni* | 12.29 | 11.20 | 9.59 | 9.59 | 50 | 48 |

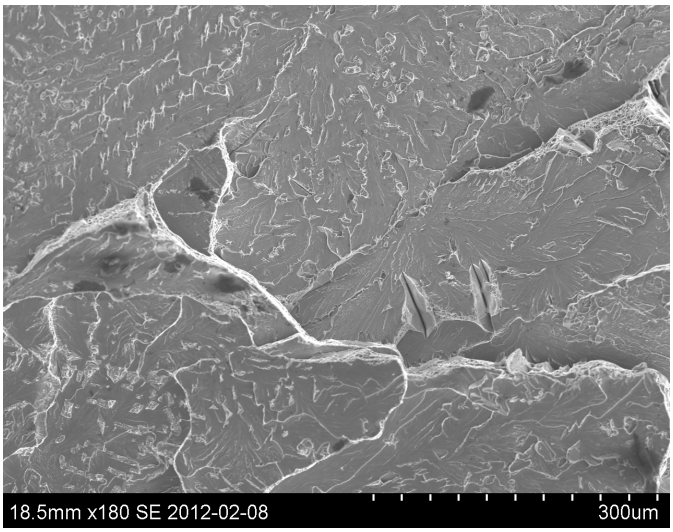


*Fig. 64: 1,5Ni_weld at 0°C, detail of fracture surface*

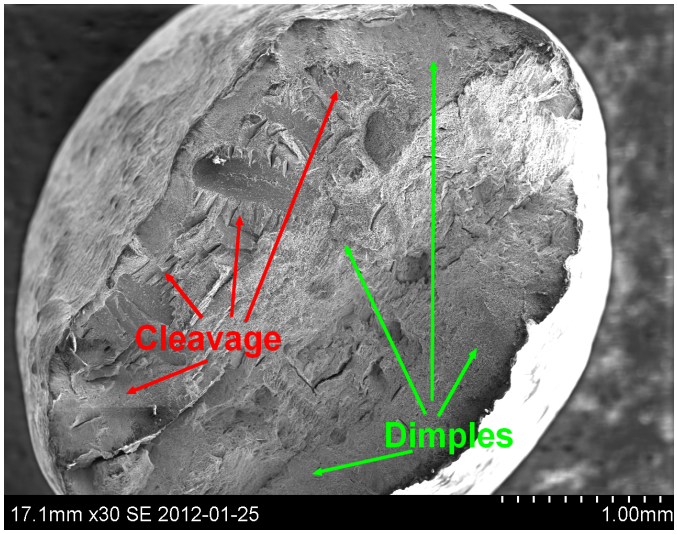


*Fig. 65: Fracture section of 1,5Ni_weld at 20°C*

The continuity and large amount of ferrite in *1,5Ni* welds provides longer mean free path for cracks. This is for sure another factor that undermines total elongations of *1,5Ni*.

The combination of detrimental factors causes their final failures to occur while the stress is still rising (i.e. before reaching the plastic instability, i.e. necking) at 0°, -20° and -40°C: thise fractures are brittle, see relative curves in 12.2. Cleavage occupies most of their fracture surfaces and starts for sure from inclusions since at least one is always noticeable. Profiles of austenite grains can barely be noticed in Fig. 64, that shows an example of *1,5Ni_weld* tested at low temperature, 0°C. The river-like profile is probably due to a coarse austenite grain boundary.

The *1,5Ni_weld* specimen at room temperature represents an exception, since it fails after elongating similarly to *5Ni* and *7Ni* and with more marked necking, see Fig. 65 and final part of the force curve in Fig. 66. The cleavage area is broader and more irregular

than those of *5Ni* and *7Ni* at the same temperature, and this confirms that *1,5Ni* is more subjected to cleavage.

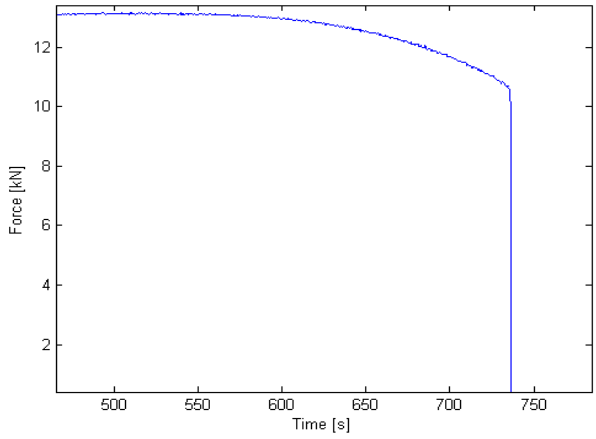


*Fig. 66: Final part of force curve, 1,5Ni_weld, 20°C*

The behavior of this specimen confirms that total elongations really depend on uncontrollable characteristics of the inclusions, that can truncate the plastic deformation before or after the necking occurs. The tendency to fail before reaching the necking and so the maximum achievable engineering stress increases as temperature decreases, see Table. 8. The engineering tensile curves of *weld* specimens sorted by testing temperature are showed in 12.1.

*Root cross weld specimens ("b")*

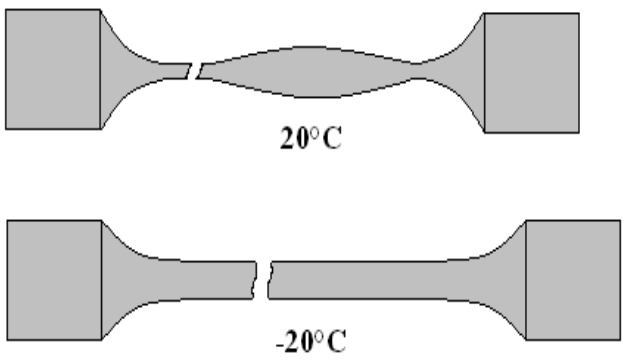


*Fig. 67: qualitative final shape of root cross weld specimens at 20° and -20°C*

At -20°C, all *root cross weld* specimens elongate more than at room temperature, as seen in 7.2. Base metal occupies nearly half of their length and at room temperature the plastic deformation before failure occurs mostly in it, see Fig. 67. The same figure also shows the simplified profile of broken specimens at -20°C: the reduction in section is more uniform along the whole length. This means that as temperature lowers to -20°C, the strength of the base metal increases more than that of the weld metal and becomes comparable to it: the weld metal is forced to deform more than at room temperature. Figs. 68 and 69 show the microstructures of base and weld metal in *1,5Ni_root cross weld* failed at -20°C: the degree of deformation is in fact not so different.

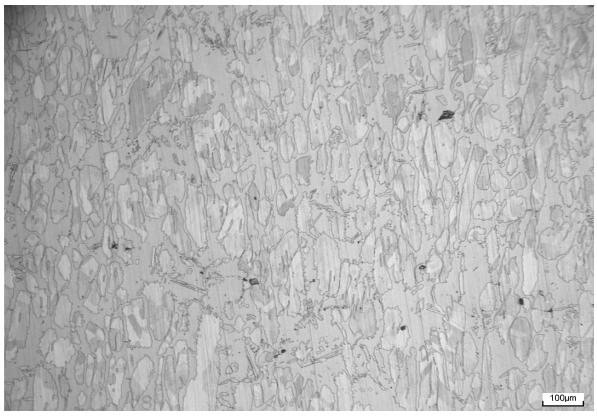


*Fig. 68: Base metal in deformed 1,5Ni_root cross weld at -20°C*


*Fig. 69: Weld metal in deformed 1,5Ni_root cross weld at -20°C*

However, specimens tend to fail in the base metal both at room temperature and at -20°C. So, measured mechanical strengths should be connected to the base metal and not depending much on the chemical composition of welds. This is coherent to what observed in Fig. 47. This also means that a higher quantity of base metal along the axis of tension tends to make the failure process "safer" than expected: the rupture is not caused by the sudden propagation of a crack in the weld but it occurs after progressive plasticization of the base metal.

As mentioned in chapter 6.2, the HTHAZ in duplex welds is very narrow: it should affect the tensile behavior of the specimens only in case the fracture would occur in it, but this never happens. No precise informations are found in literature about the size of LTHAZ and its influence on properties: since the zone could be large, when speaking of base metal one may be actually talking about LTHAZ. This goes for all specimens.

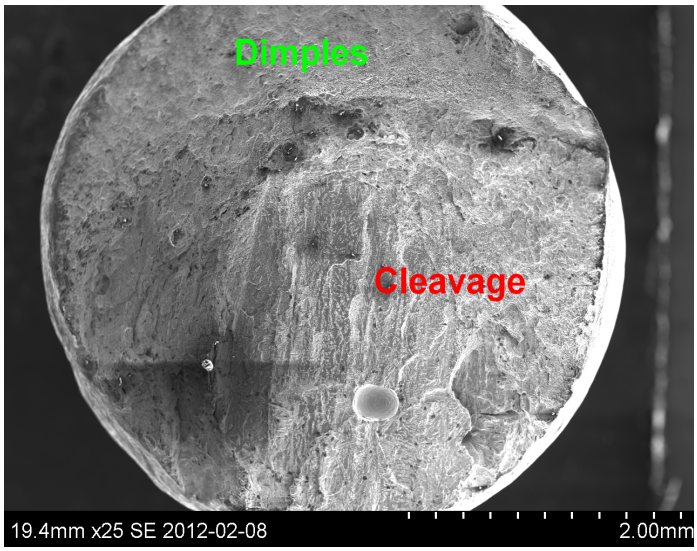


*Fig. 70: Fracture section of 5Ni_root cross weld at -20°C*

*5Ni* at -20°C is the only specimen that breaks in the weld metal and shows an elongation similar to *1,5Ni*, a 5% lower than *7Ni*. As viewable in Fig. 70, this is due to the presence of an inclusion nearly 200 µm large that interrupts the plastic deformation with formation of

cleavage, as commonly happens in *weld* specimens. A peculiarity of this specimen, however, is observable from the end of its force curve in Fig. 71: after the cleavage has been set, the failure does not occur instantly.

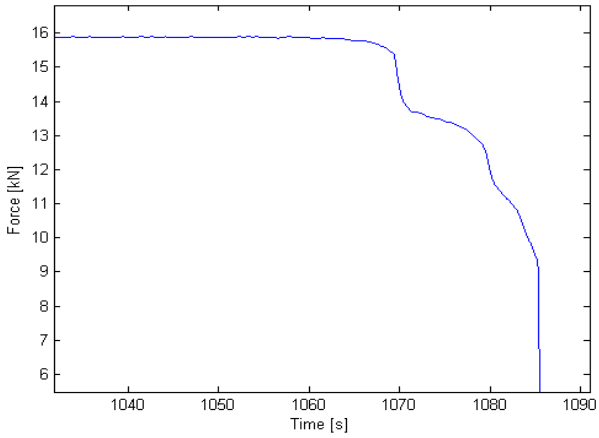


*Fig. 71: Final part of force curve for 5Ni root cross weld at -20°C*

The load has a 2 kN drop, but then its decrease is stabilized and the final rupture is reached through subsequent steps after 15 seconds. This means that the cleavage stops and resume: an effective mechanism inhibiting the crack propagation intervenes. *Root cross weld* specimens are extracted from the weld root as seen in Fig. 30. The origin of the inhibiting mechanism should be connected to this fact, since it occurs in the only *root cross weld* specimen that breaks in the weld, not in other tested specimens. In particular, it could be due to the transition of the crack from a root pass to another one with different microstructure. This depends on how the single specimen was cut and is difficult to check. It must be noticed that *7Ni_root cross weld* specimens should not contain flux inclusions because their weld metal is deposited with MIG. Moreover, root passes are usually performed with higher quality standards than others, so they are less prone to fail.

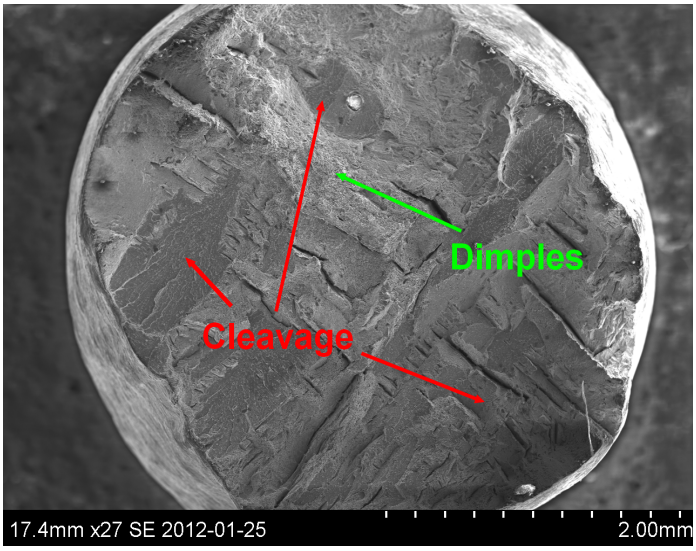


*Fig. 72: Fracture section of 1,5Ni_surface cross weld at 20°C*

*Surface cross weld specimens ("a")*

The fracture surface of *1,5Ni_surface cross weld* at 20°C in Fig. 72 consists of a cleavage zone around a flux inclusion, a circular dimpled zone just around and a broad cleavage area with parallel deep cracks that lie on planes parallel to the axis of tension. Fig. 73 shows that the force drops after a

gradual decrease, confirmed by a slight necking in Fig. 72.

It is not possible that the failure process consists of cleavage formation around the inclusion, dimples and cleavage again in progressive order: in that case, the first cleavage would be blocked and then resumed, so Fig. 73 would likely report a step.

The probable process of failure is the following. The cracks aligned with the axis of tension form during plastic deformation, showing tendency of the specimen to brittleness. They do not affect significantly the load trend because of their orientation. Their parallelity can be connected to the welding direction which is transverse to the length of *surface cross weld* specimens, but the precise mechanism of their formation is not clear. When necking has reduced the resistant section enough, the nearly 100 μm large inclusion initiates crack propagation. As soon as the resistant section is reduced, another crack starts propagating quickly across the remaining area due to sudden increase of load in it. The crack probably originates in the outer surface of the specimen and propagates first in the region pointed by the left red arrow in Fig. 72, which is very smooth. The two propagation zones are at different heights and they are connected by thin metal ridges that fail without considerable resistance as soon as the second propagation occurs, giving dimples. Beyond the precise chronology of events during the final failure, it must be observed that the latter is started by an inclusion and it occurs in less than one second, so it is uncontrollable as usual.

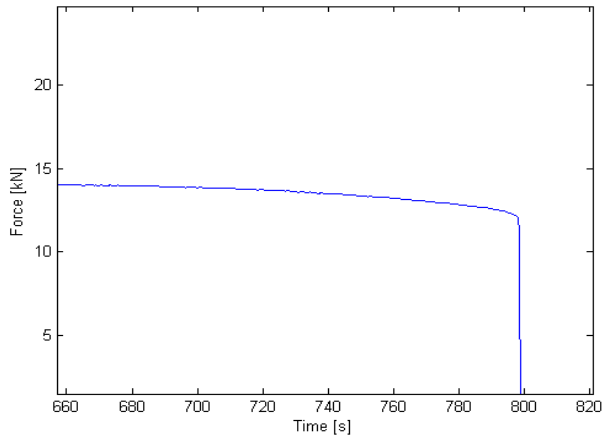


*Fig. 73: Final part of force curve for 1,5Ni_surface cross weld at 20°C*

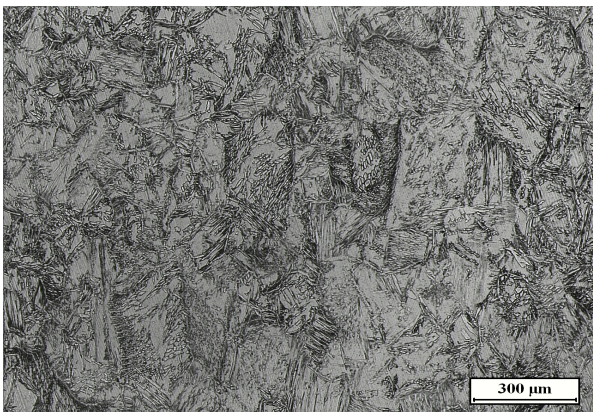


*Fig. 74: Micrograph of 7Ni_surface cross weld at 20°C*

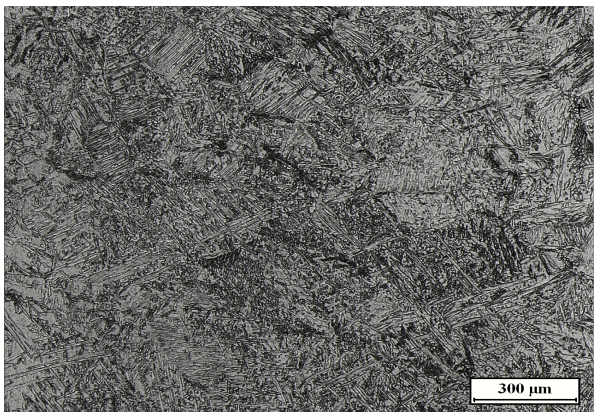


*Fig. 75: Micrograph of 5Ni_surface cross weld at 20°C*

For *1,5Ni* specimens, same discussion as for *weld* specimens is valid.

*5Ni_surface cross weld* specimens fail in the base metal at 20° and at 0°C, while at the same temperatures *7Ni* fail in weld. The base metal does not contain flux inclusions that shorten the elongation. A failure in the base, so, should be connected to larger elongation to fracture. This is coherent with the test at 0°C, but at 20°C *7Ni* elongates more than *5Ni*. As said discussing *weld* specimens, *5Ni* welds have higher strength due to higher Mn content. In *surface cross weld* specimens, strengths of *5* and *7Ni* are quite similar but are influenced by the presence of base metal. As said above discussing *weld* specimens, *5Ni* welds in themselves have higher strength due to higher Mn content. In *5Ni_surface cross weld* at room temperature, so, the deformation occurs almost completely in the base metal, while the weld does not deform. The less performing weld of *7Ni*, instead, partecipates more to the deformation. At 0°C, *5Ni_surface cross weld* undergoes to the same mechanisms showed for *root cross weld* specimens and its total elongation is much higher. Figs. 74 and 75 show the microstructure of deformed *7* and 5*Ni* at room temperature. If the phase balance was the same, the austenite in *7Ni* shoud look more packed since higher deformation is reached. The phase balance can vary a lot within the same weld, as explained in 6.2. However, these micrographs suggest that *5Ni* at 20°C could be more resistant than *7Ni* also because of finer grain size.

At -40°C, *1,5Ni_surface cross weld* shows a completely cleavage fracture surface, while *7Ni* still shows dimples, despite of large areas involved by cleavage around a flux inclusion. Smaller impurities can also be detected on its surface. They are sulfides or other impurities coming from the flux, as in Figs. 55 and 56.

The tensile properties plotted for chemical composition in 12.1 show that *1,5Ni_weld* specimens have lower properties than *1,5Ni_surface cross weld* specimens. For the other compositions, *weld* specimens behave similarly to *surface cross weld* specimens or even better. This means that *1,5Ni* welds in themselves are not performing, but, when working with base metal, the overall properties are improved by the latter. The higher Ni content improves the behavior of the weld in itself and makes it similar to that of weld + base metal.

Generally, properties of *surface cross weld* and *root cross weld* specimens also depend on how the particular specimens are cut: they do not always contain the same amount of base metal for example. Since they are cut transversely to the direction of welding, they should also contain more heterogeneities than *weld* specimens, due for example to segregations and dilution mentioned in 4.3. This heterogeneities are both chemical and microstructural. So, properties of *surface cross weld* and *root cross weld* specimens should be taken as indicative.

# 9 CONCLUSIONS

In the present work, tensile properties of welded LDX2101 duplex stainless steel are studied at 20°, 0°, -20° and -40°C. The tested specimens are composed of base and weld metal or just the latter. They are extracted from welded plates, transversely and along the direction of welding. Three types of weld are analyzed and the main difference between them is the Ni content: nearly 7%, 5% and 1,5% in weight. The decrease in Ni is compensated by addition of Mn that is in turn an austenite stabilizer. Each type of weld is realized with a slightly different welding method: combinations of SAW and MIG are used with multipass. No post-weld treatments are performed. Before drawing some conclusions, it must be remembered that one kind of specimen (characterized by extraction position on the weld and chemical composition) is tested only once at each temperature. So, it is not possible performing statistical analysis on a large population. Moreover, welds are not uniform nor isotropic and multiple experimental issues may affect measurements.

The results of the work say that:

- Total elongations to fracture of all specimens that fail in the weld metal are controlled by the presence of flux granules for SAW welding. These inclusions start the propagation of a crack before or after having reached the maximum achievable engineering stress, bringing quickly to failure before exhausting the possible plasticization. The failure process also depends on uncontrollable characteristics of inclusions like size, shape and distribution.

- Specimens that fail in the base metal tend to show higher elongations since the base metal can deformate and neck more than the weld.

- Both yield and ultimate tensile strengths tend to increase with the decrease of temperature while total elongations to fracture tend to decrease, as expected. Exceptions are the specimens cut transversely to the welding direction that contain base metal for nearly half of their length: they elongate more as temperature decreases. This is due to the hardening of the base metal, that at -20°C forces the weld metal to partecipate more in the elongation.

- Considering just weld metal, *5Ni* specimens have higher strengths than *7Ni* at all temperatures. The average grain sizes of the two types of weld are comparable, as are their austenite morphologies: so, the superiority of *5Ni* must be due to the enhanced Mn content.
- *1,5Ni* specimens generally elongate less and are more prone to brittle failures than others.
- *1,5Ni* welds have lower strengths than *5Ni* and *7Ni* even if containing more Mn. The reason is the double average ferrite grain size. This is due to austenite lack and morphology.
- The total elongation of *7Ni* is strain-controlled, i.e. it occurs at similar strain values at all testing temperatures.
- The total elongation of *5Ni* is stress-controlled, i.e. it occurs at similar stress values at all testing temperatures. The same goes for *1,5Ni*. Excluding other reasons, this should be connected to the different influence of Mn and Ni on dislocations motion at low temperatures.

## 10 ACKNOWLEDGEMENTS

I desire to thank Johan Pilhagen for its tutoring activity and the patience carried in trying to solve with me multiple experimental issues. Besides, I wish to thank prof. Rolf Sandström and Irene Calliari for having given me the opportunity to perform my activity of thesis in Sweden and the company Outokumpu that has provided the materials. I also thank my family that has supported me during my stay in Stockholm.

## 11 REFERENCES

1: Avesta Welding, How to weld duplex stainless steels

2: Robert N Gunn, Duplex stainless steels, Abington Publishing, (2003), 1-21

3: ASTM, Standard Test Methods for Tension of Metallic Materials, (2009)

4: en.wikipedia.org

5: V. Muthupandi, P. Bala Srinivasan, S.K. Seshadri, S. Sundaresan, Materials Science Engineering A, Structural Materials: Properties, Microstructure and Processing (2003), 358

6: www.cartech.com

7: V. Muthupandi, P. Bala Srinivasan, V. Shankar, S.K. Seshadri, S. Sundaresan, Effect of nickel and nitrogen addition on the microstructure and mechanical properties of power beam processed duplex stainless steel (UNS 31803) weld metals, Materials Letters 59 (2005), 2305-2309

8: K.A. Johannson, Duplex stainleess steels '94, Conf proc (1994), paper KVII

9: R. Francis, Duplex stainless steels '94, Conf proc (1994), paper KIV

10: I. Calliari, M. Zanesco, E. Ramous, Precipitazione di fasi secondarie in un acciaio duplex 2205 trattato isotermicamente, La metallurgia italiana 10 (2004), 41-45

11: R. Badji, M. Bouabdallah, B. Bacroix, C. Kahloun, B. Belkessa, H. Maza, Phase transformation and mechanical behavior in annealed 2205 duplex stainless steel welds, Materials Characterization 59 (2008), 447-453

12: G. Melotti, R. Bertelli, I. Calliari, M. Zanesco, E. Ramous, Il trattamento di solubilizzazione degli acciai inossidabili duplex, La metallurgia italiana 4 (2005), 39-42

13: Robert N Gunn, Duplex stainless steels, Abington Publishing, (2003), 139-141

14: Robert N Gunn, Duplex stainless steels, Abington Publishing, (2003), 146-164

15: Robert N Gunn, Duplex stainless steels, Abington Publishing, (2003), 115

16: R.A. Walker, D.N. Noble, Proc. weldability of materials, Detroit (1990), 117-125

17: T. Børvik, H. Lange, L.A. Marken, M. Langseth, O.S. Hopperstad, M. Aursand, G. Rørvik, Pipe fittings in duplex stainless steel with deviation in quality caused by sigma phase precipitation, Materials Science and Engineering A 527 (2010), 6945-6955

18: Sandmeyer steel company, Product data sheets

19: Outokumpu, Product data sheets

20: R. Pilhagen, R. Sandström, Project meeting, Avesta

21: Mikael Johansson, LOM and image analysis software according to ASTM E1245

22: V. Muthupandi, P. Bala Srinivasan, S.K. Seshadri, S. Sundaresan, Effect of weld metal chemistry and heat input on the structure and properties of duplex stainless steel welds, Materials Science and Engineering A358 (2003), 9-16

23: S.D. Brandi, Materials Science Forum, 426-432 (2003), 4063-4068

24: T.Omura, T. Kushida, T. Kudo, T. Hayashi, Y. Matsuhiro, T. Hikida, Tetsu-To-Hagane (1997), 575-580

25: S. Hertzman, W. Roberts, M. Lindenmo, Proc. Duplex stainless steels '86, The Hague (1986), 257-263

26: E.M. Westin, B. Brolund, S. Hertzman, Steel Research Int. 79 (2008), 473-481

27: B.E.S. Lindblom, B. Lundqvist, N.E. hannerz, Scand. J. Metallurgy (1991), 305-315

28: Elin M. Westin, Welds in the lean duplex stainless steel LDX 2101, effect on microstructure and weld oxides on corrosion properties, (2008)

29: L. Karlsson, Proc. Duplex stainless steels '97, Maastricht, The Netherlands (1997), 43-58

30: H. Sieurin, R. Sandström, Fracture toughness of the lean duplex stainless steel LDX 2101, Metallurgical and materials transactions A (2006), 2975-2981

31: AK steel, Product data sheets

32: K. Chandra, R. Singhal, V. Kain, V.S. Raja, Low temperature embrittlement of duplex stainless steel: correlation between mechanical and electrochemical behavior, Materials science and Engineering A 527 (2010), 3904-3912

33: L. Engel, H. Klingele, An atlas of metal damage, Wolfe Publishing Ltd, (1981), 40-71

# 12 APPENDICES

## 12.1 Appendice A

Here follow some figures and tables relative to section 7 that are not reported before because they repeat datas already showed in other visual ways.

Total elongations to fracture and strengths are plotted for the specimens, now grouped depending on the chemical composition.

For each testing temperature, engineering curves of weld specimens are grouped and displayed.

Yield strength, ultimate tensile strength and elongation to fracture of all specimens are shown in Table. 15.

*1,5% Ni content in the welding filler*

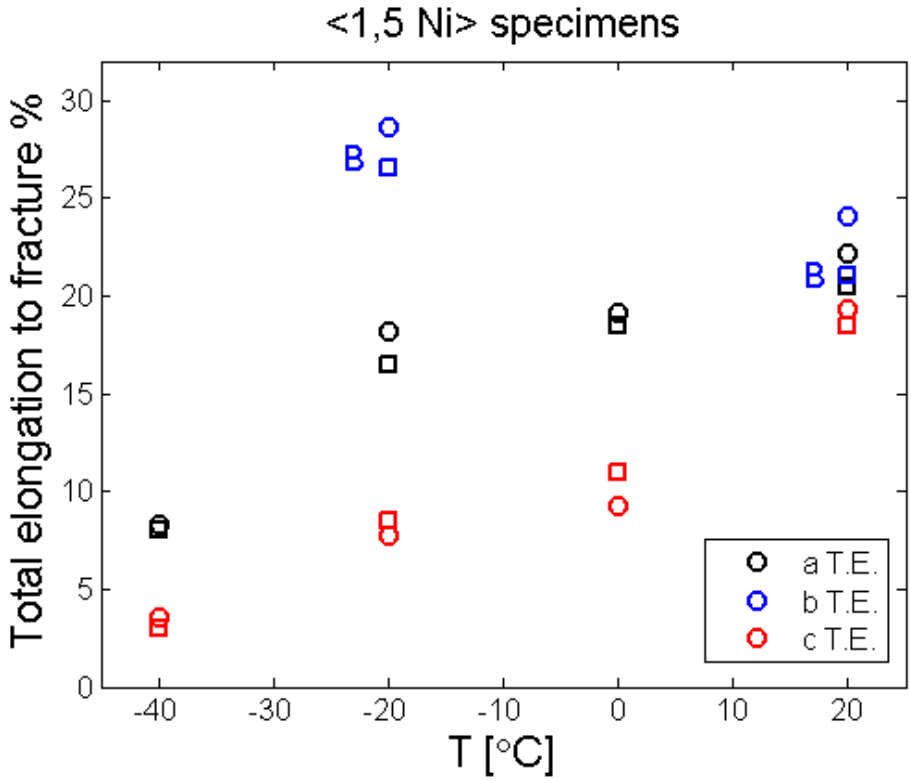


*Fig. 76: Total elongations of 1,5Ni specimens. Squares represent the elongations measured with ruler and circles the fictive ones.*

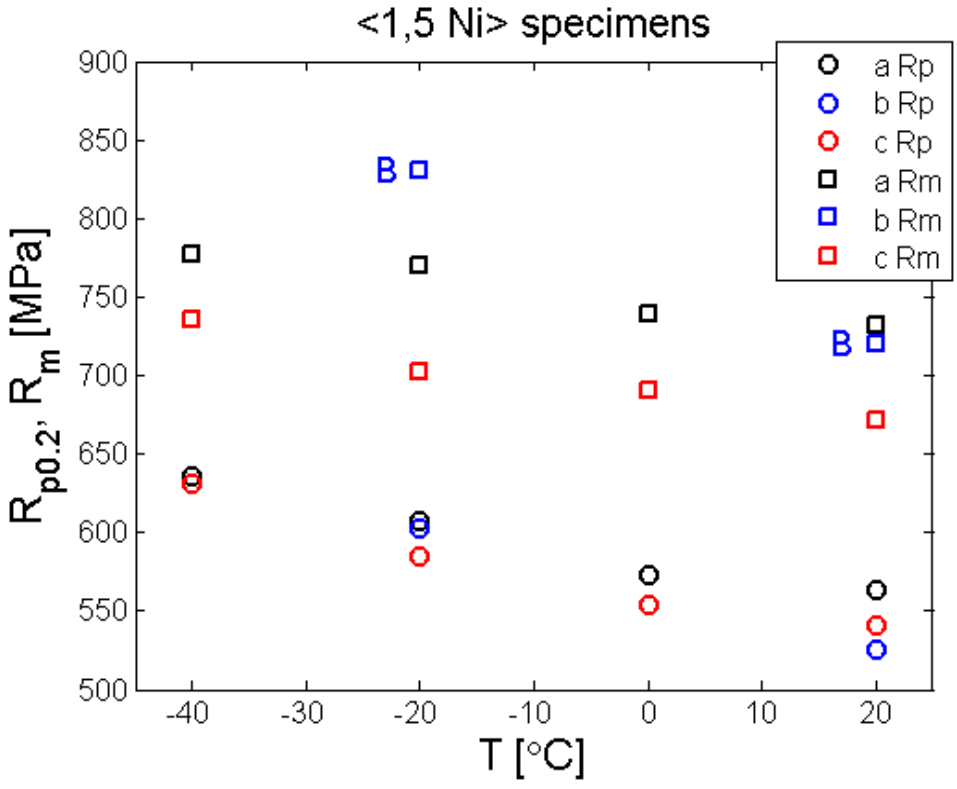


*Fig. 77: Tensile strengths of 1,5Ni specimens*

*5% Ni content in the welding filler*

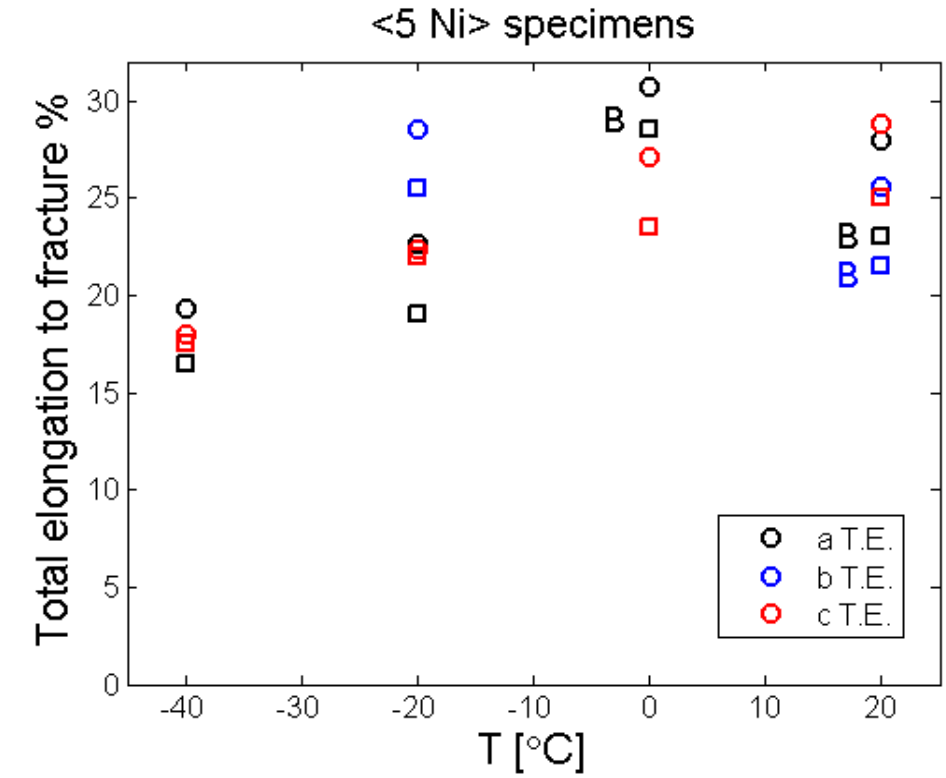


*Fig. 78: Total elongations of 5Ni specimens. Squares represent the elongations measured with ruler and circles the fictive ones*

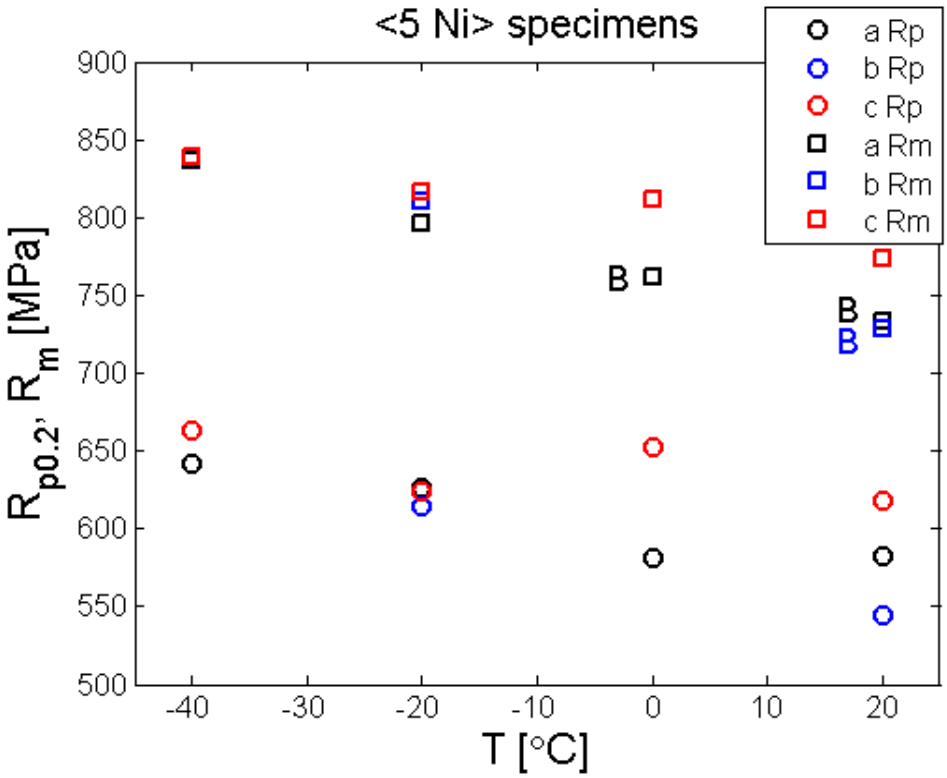


*Fig. 79: Tensile strengths of 5Ni specimens. N.B. 5Ni c at 0°C has not reliable values due to absence of extensometer signal*

*7% Ni content in the welding filler*

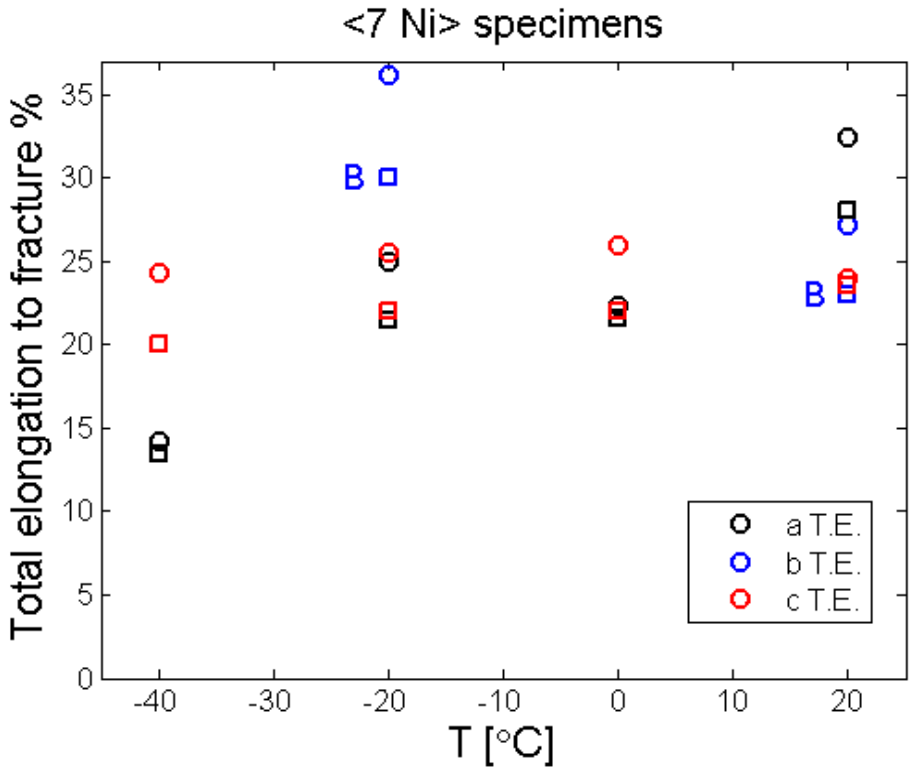


*Fig. 80: Total elongations of 7Ni specimens. Squares represent the elongations measured with ruler and circles the fictive ones*

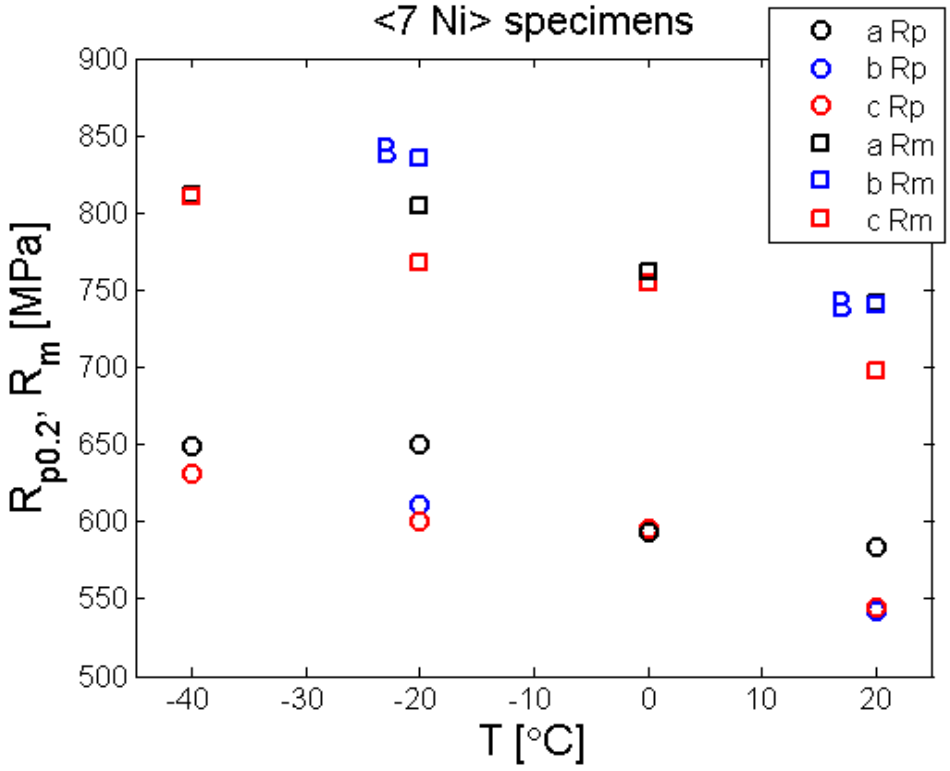


*Fig. 81: Tensile strengths of 7Ni specimens*

*Weld specimens at 20°C*

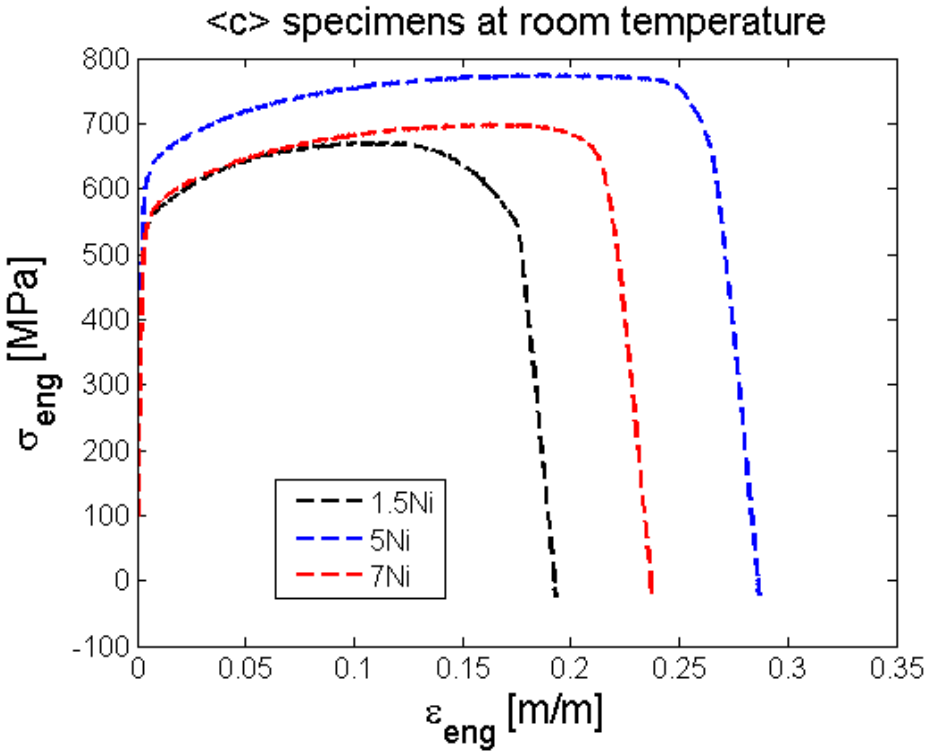


*Fig. 82*: *Engineering curves of weld specimens at 20°C*

*Weld specimens at 0°C*

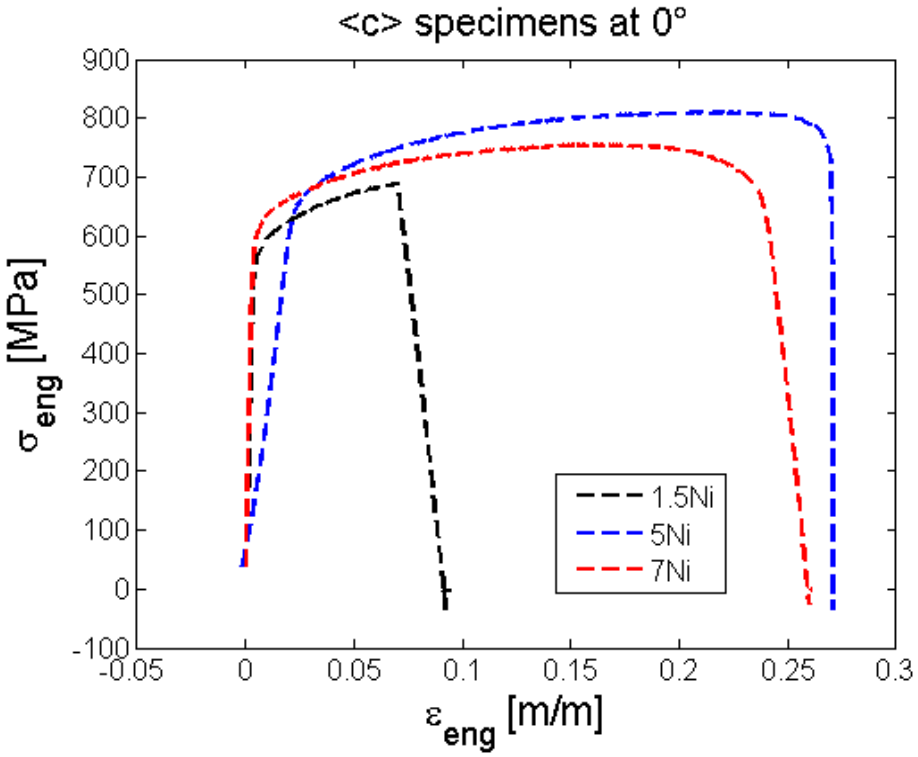


*Fig. 83*: *Engineering curves of weld specimens at 0°C. N.B. 5Ni has not reliable values due to absence of extensometer signal*

*Weld specimens at -20°C*

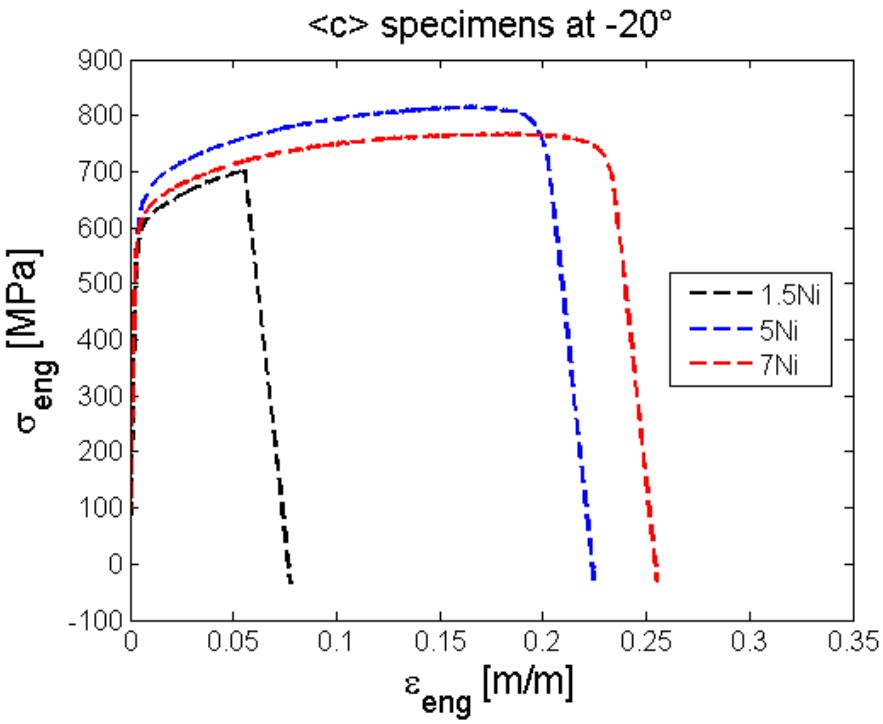


*Fig. 84*: *Engineering curves of weld specimens at -20°C*

*Weld specimens at -40°C*

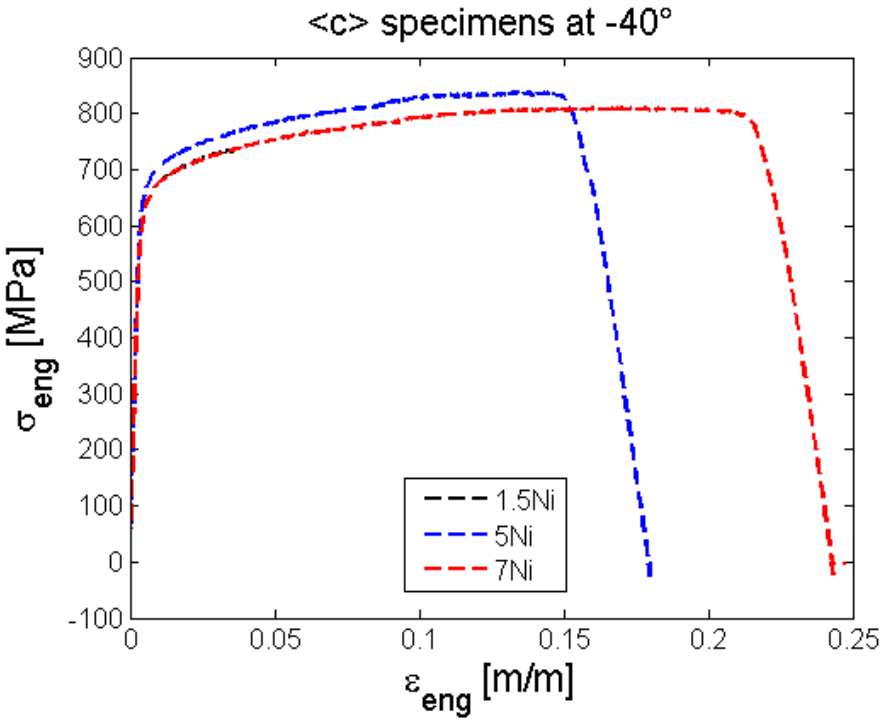


*Fig. 85*: *Engineering curves of weld specimens at -40°C. N.B. 1,5Ni is superimposed to 7Ni and its failure occurs after little strain*

*Table 15: Mechanical properties*

| Specimen | Temperature | Rp0.2 | Rm | T.E. |
|---|---|---|---|---|
| * 1p5Ni_a | 20 | 564 | 732 | 20.5 |
| * 5Ni_a | 20 | 583 | 733 | 23.0 |
| * 7Ni_a | 20 | 584 | 740 | 28.0 |
| 1p5Ni_b | 20 | 525 | 720 | 21.0 |
| 5Ni_b | 20 | 544 | 729 | 21.5 |
| * 7Ni_b | 20 | 542 | 740 | 23.0 |
| 1p5Ni_c | 20 | 541 | 671 | 18.5 |
| 5Ni_c | 20 | 618 | 774 | 25.0 |
| 7Ni_c | 20 | 544 | 698 | 23.5 |
| 1p5Ni_a | 0 | 573 | 739 | 18.5 |
| 5Ni_a | 0 | 581 | 762 | 28.5 |
| 7Ni_a | 0 | 593 | 762 | 22.0 |
| 1p5Ni_c | 0 | 554 | 690 | 11.0 |
| 5Ni_c | 0 | 652 | 810 | 23.5 |
| 7Ni_c | 0 | 595 | 755 | 22.0 |
| 1p5Ni_a | -20 | 608 | 770 | 16.5 |
| 5Ni_a | -20 | 627 | 796 | 19.0 |
| 7Ni_a | -20 | 650 | 804 | 21.5 |
| 1p5Ni_b | -20 | 603 | 830 | 26.5 |
| 5Ni_b | -20 | 614 | 810 | 25.5 |
| 7Ni_b | -20 | 611 | 835 | 30.0 |
| 1p5Ni_c | -20 | 585 | 702 | 8.5 |
| 5Ni_c | -20 | 626 | 816 | 22.0 |
| 7Ni_c | -20 | 600 | 768 | 22.0 |
| 1p5Ni_a | -40 | 636 | 777 | 8.0 |
| 5Ni_a | -40 | 642 | 836 | 16.5 |
| 7Ni_a | -40 | 649 | 812 | 13.5 |
| 1p5Ni_c | -40 | 631 | 736 | 3.0 |
| 5Ni_c | -40 | 663 | 839 | 17.5 |
| 7Ni_c | -40 | 631 | 810 | 20.0 |

*Legend*

* *Extensometer with a 25 mm gauge length instead than 36 mm was used*

*Rp0.2 taken from standard elastic modulus of 200 GPa*

*Rp0.2 taken from the experimental elastic modulus*

*Specimen with no extensometer signal*

## 12.2 Appendice B

In the following pages, engineering tensile curve, the first part of the engineering curve and the matching between extensometer and encoder curves relative to every tested specimen are showed. These graphs correspond to Figs. 26, 24 and 27 respectively (Fig. 24 is plotted without reporting elastic interpolating lines for more clarity of view).

Specimens tested with a 25 mm gauge length extensometer, rather than with a more proper 36 mm gauge length one, are marked with * and they can be recognized by the considerable mismatch in their third reported graph.

Specimens which extensometer signal does not turn out to be smooth are marked with ^: their yield strengths are calculated using the 200 GPa slope.

Tensile curves are the most important graphs and so they are displayed in greater size.

For completeness, remarkable experimental notes are reported for some specimens. In order to understand details about the curves, refer to section 5.

Specimens are sorted by decreasing temperature. For each temperature, they are first sorted by position from which they are extracted (in the order *surface cross weld*, *root cross weld* and *weld*, i.e. *a*, *b* and *c*) and by chemical composition of the weld (in the order *1,5Ni*, *5Ni* and *7Ni*). This order does not correspond to the chronological order of testing.

Numbers reported in specimen names above each graph (e.g. *1,5Ni **1** a*) are numbers used to indicate specimens univocally during the experimental practice, so they have no particular meaning.

*Specimens at 20° C*

*1,5 Ni surface cross weld at 20°C **

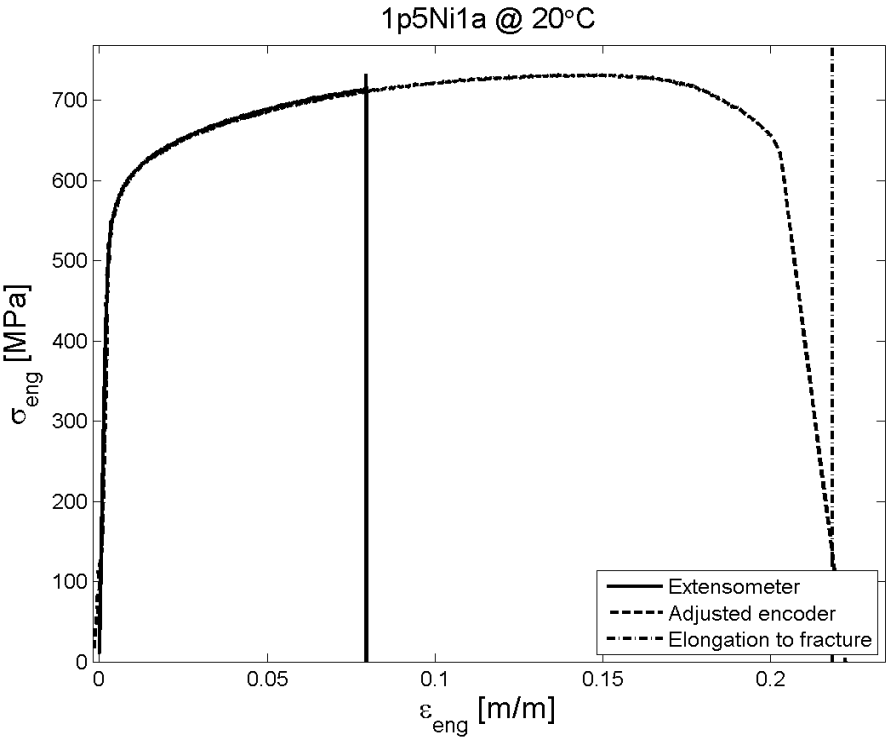


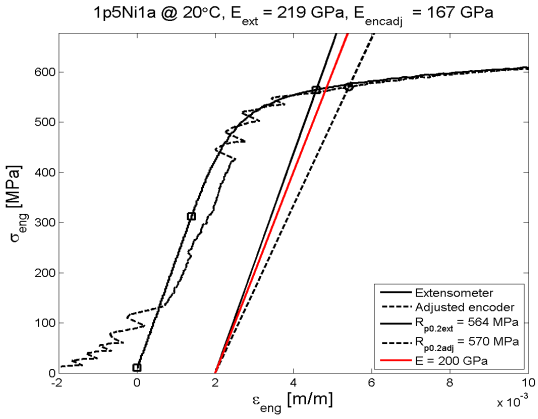


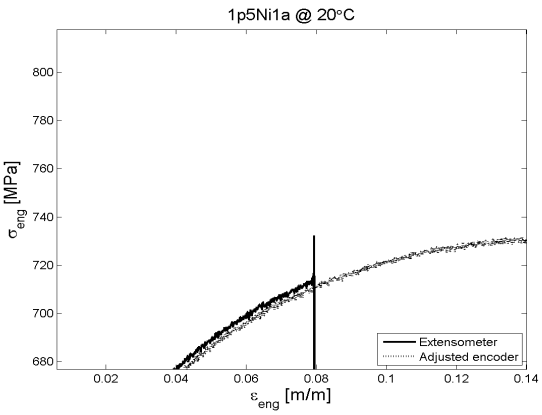


Before testing, a 6 kN pre-load is performed without registering it. Anyway, after preload, the load value is not zero-adjusted. The encoder signal is not zero-adjusted before testing, as clear from its zig-zag, see 5.3.

*5 Ni surface cross weld at 20°C **

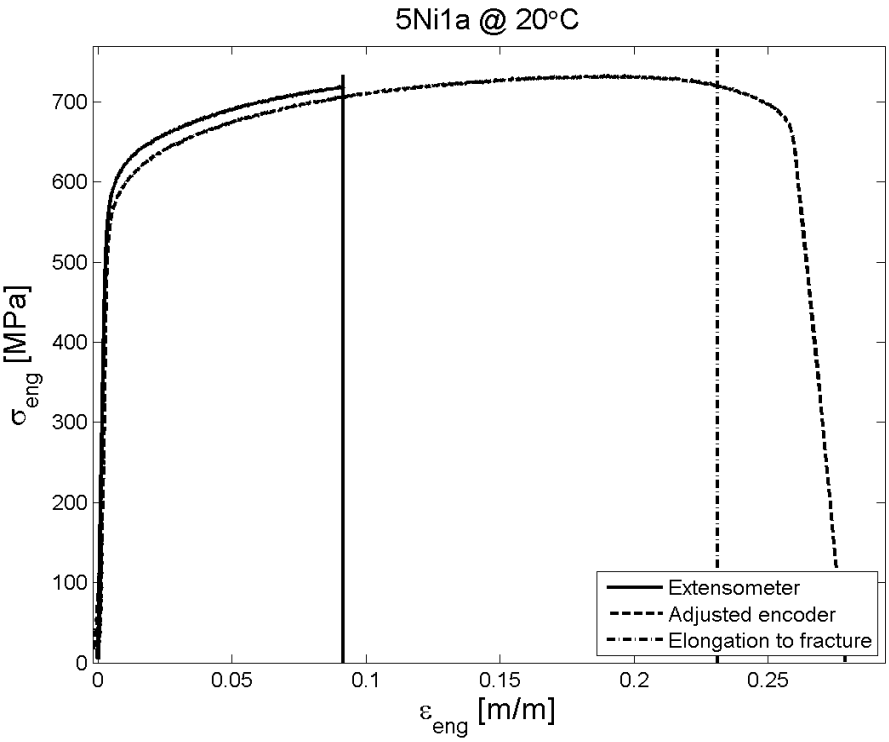


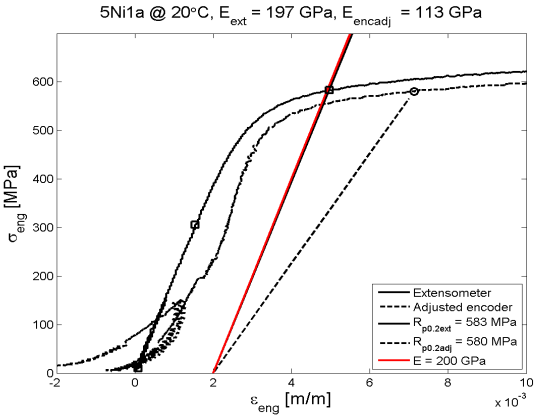


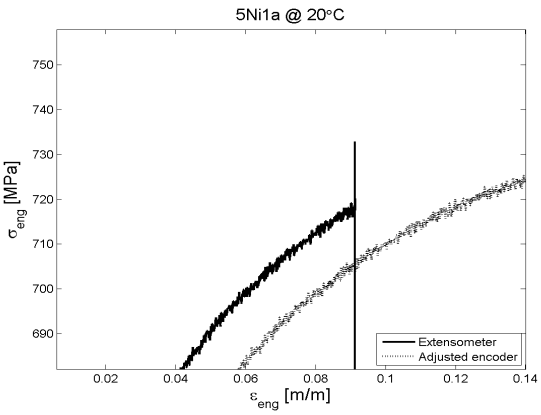


Before testing, the extensometer gauge length is zero-adjusted. This is an incorrect procedure. However, most of the imprecisions come from the improper extensometer gauge length, see 5.3.

*7 Ni surface cross weld at 20°C **

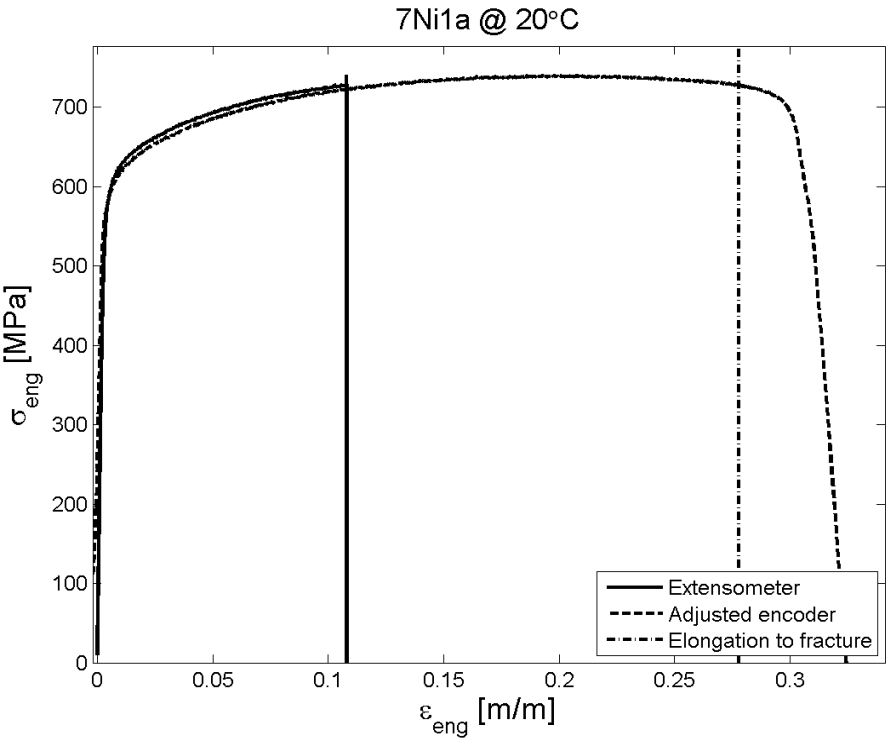


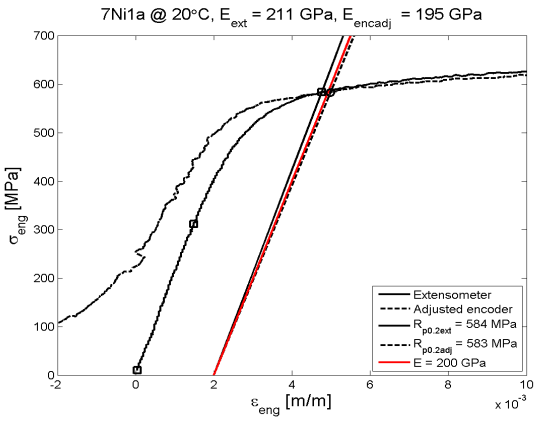


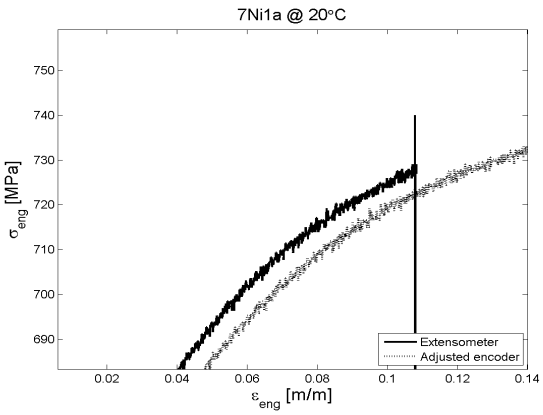

*1,5 Ni root cross weld at 20°C*

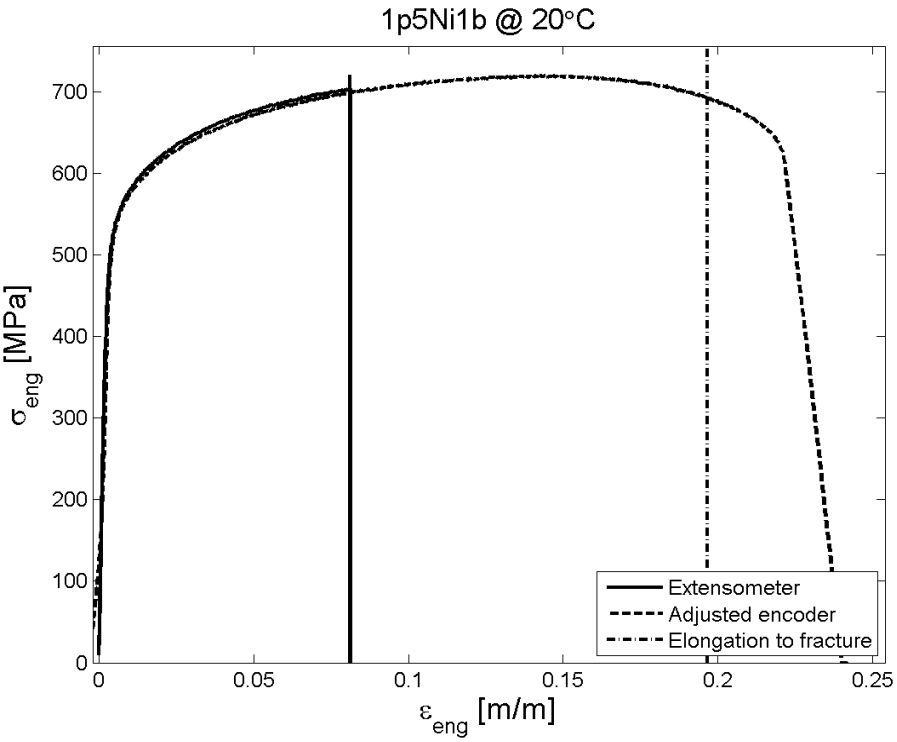


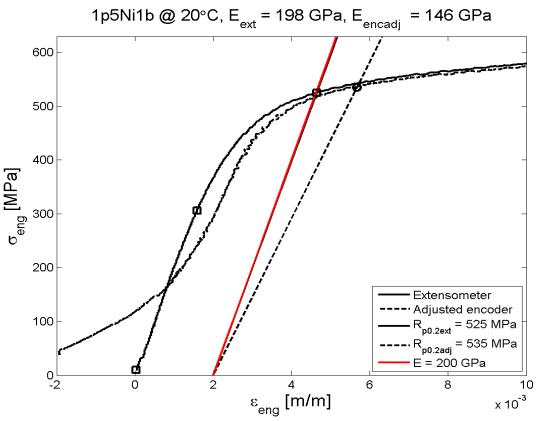


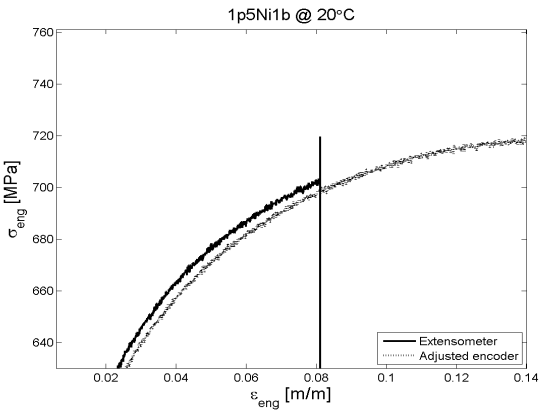

*5 Ni root cross weld  at 20°C*

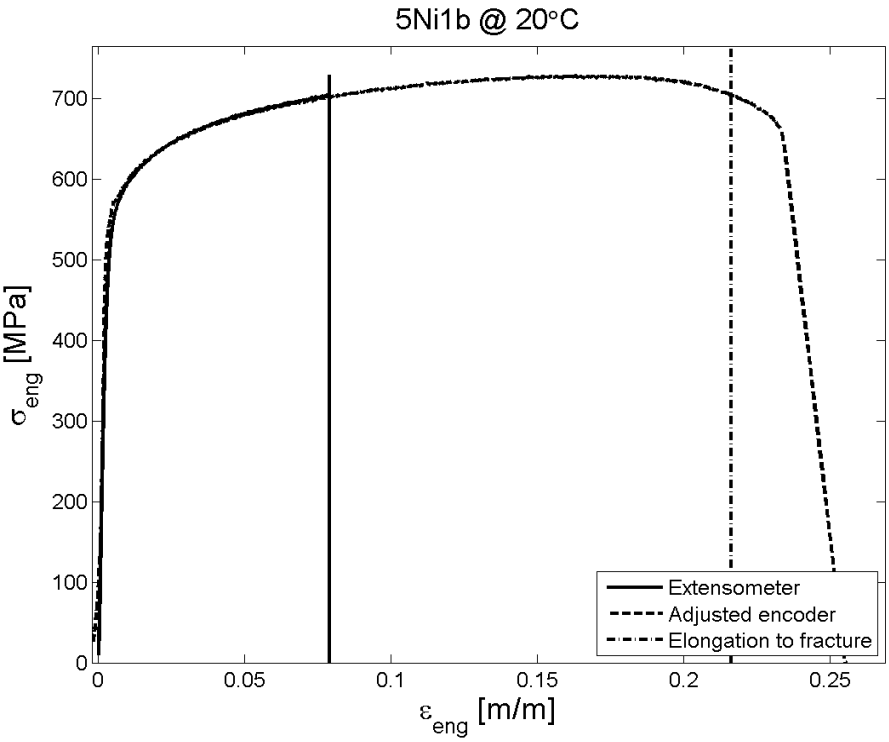


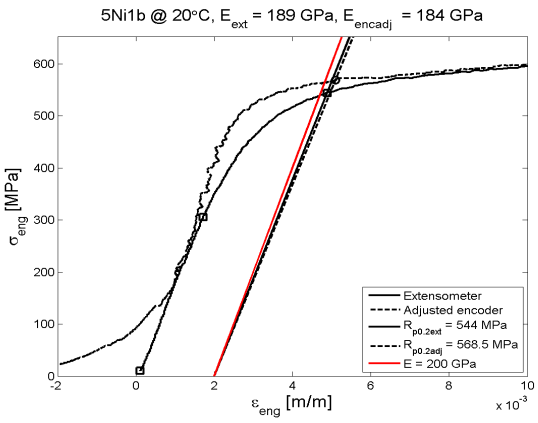


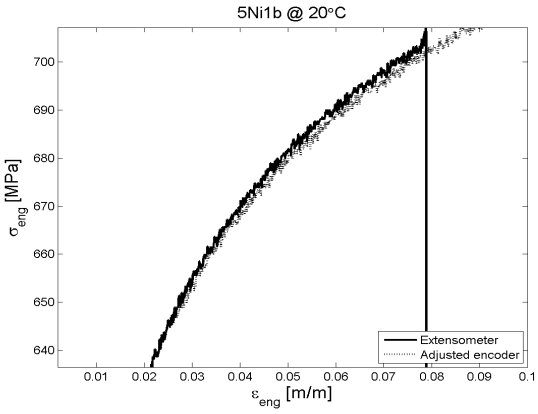

*7 Ni root cross weld at 20°C * ^*

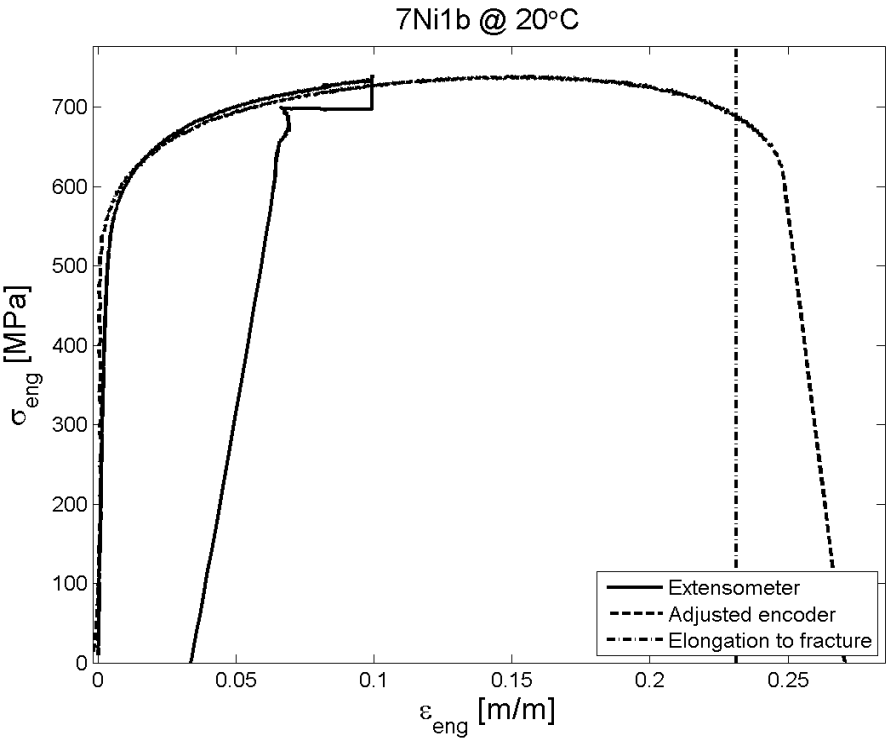


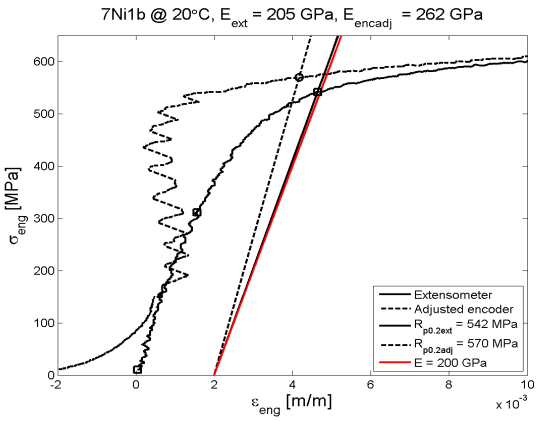


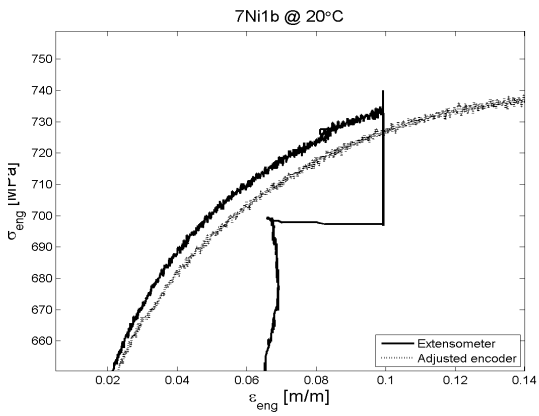


After having reached the extensometer maximum opening, one blade disconnects from the specimen springing back, see the low-right graph. The first part of the encoder signal is clearly bad due to missed zero-adjustment before testing (see 5.3). The matching between extensometer and encoder, coming from trial and error, is however acceptable if compared with that of other specimens marked with *.

*1,5 Ni weld  at 20°C*

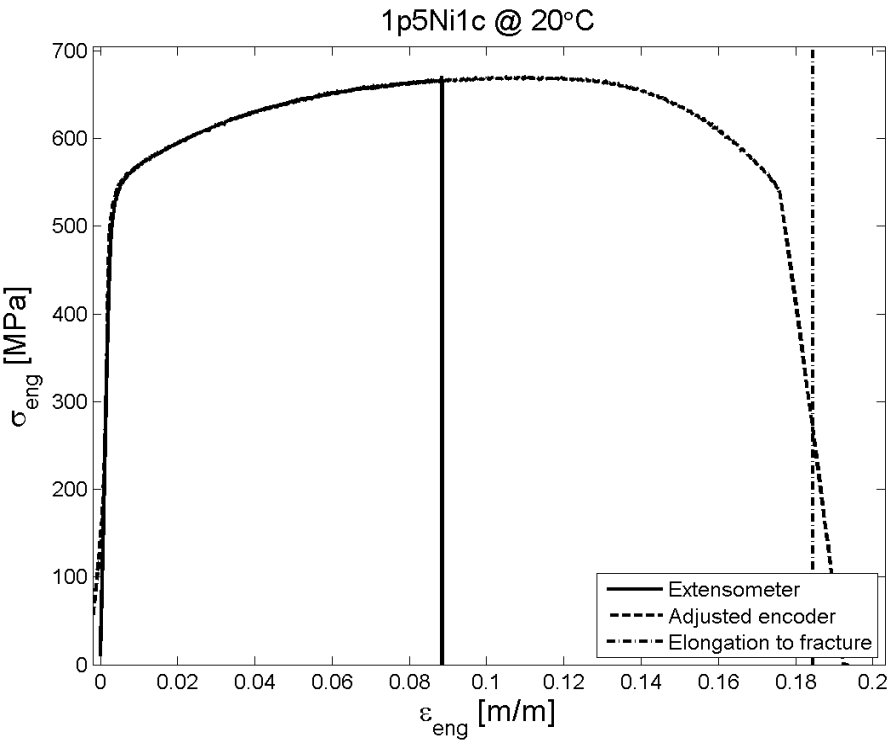


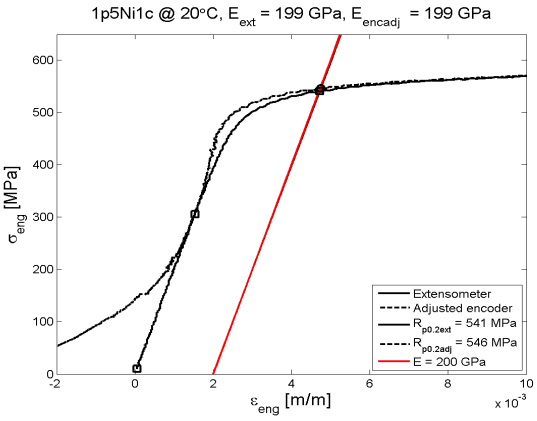


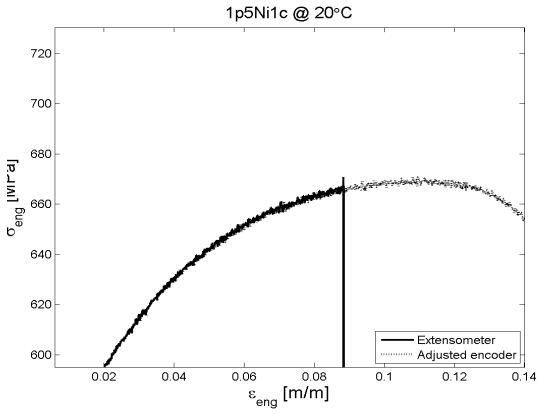

*5Ni weld at 20°C*

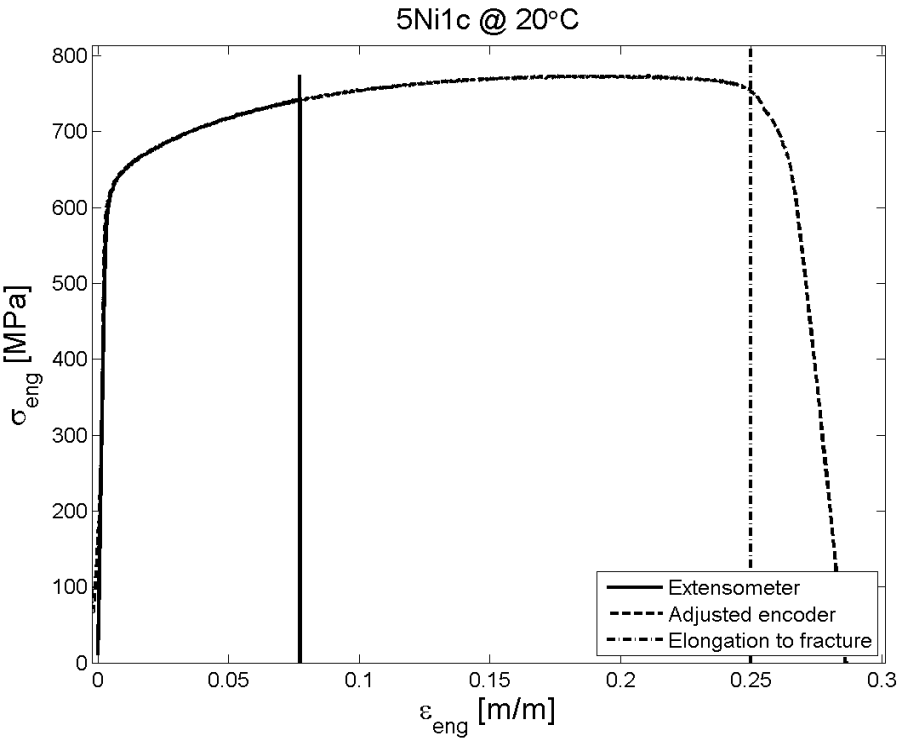


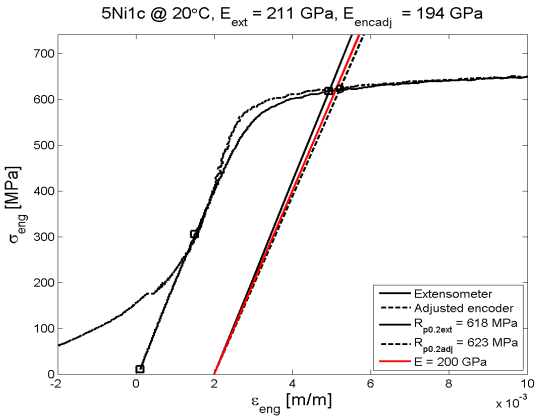


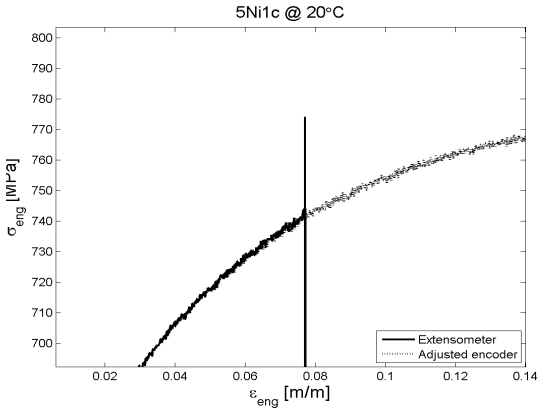


The extensometer is zero-adjusted at 25 mm before testing.

*7 Ni weld at 20°C*

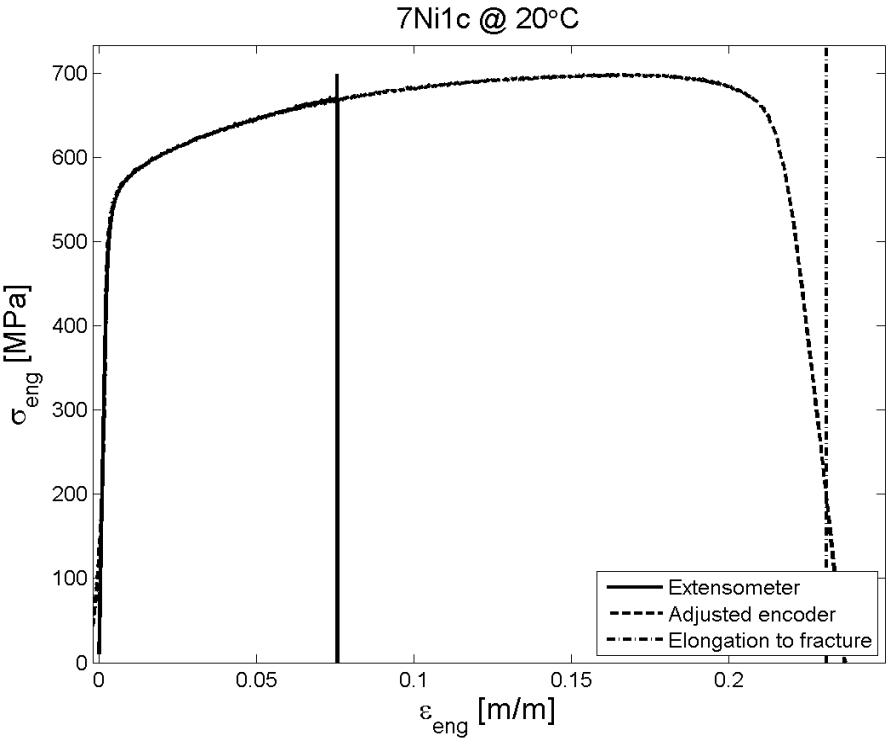


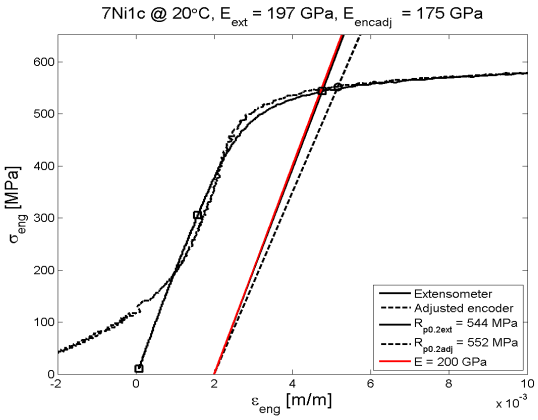


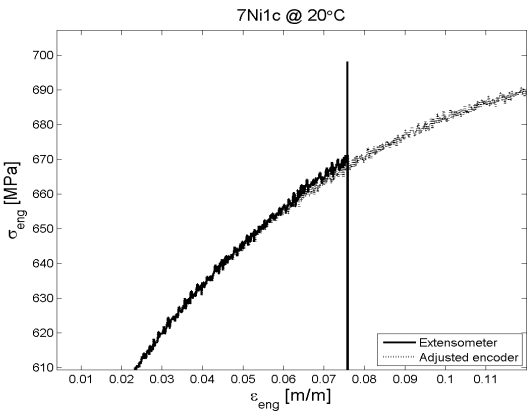

*Specimens at 0° C*

*1,5Ni surface cross weld at 0°C ^*

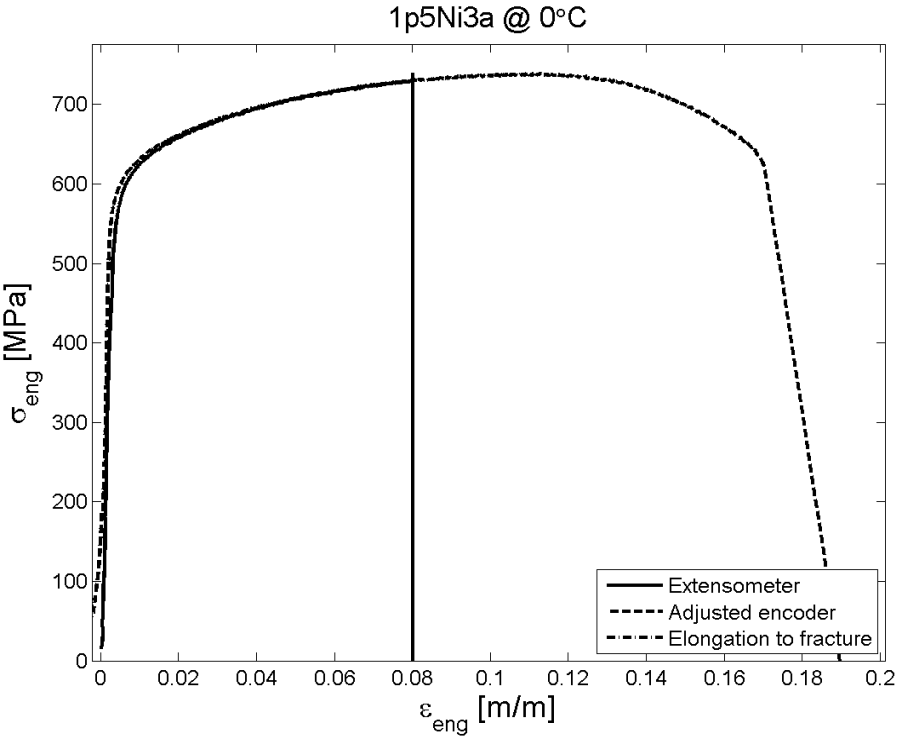


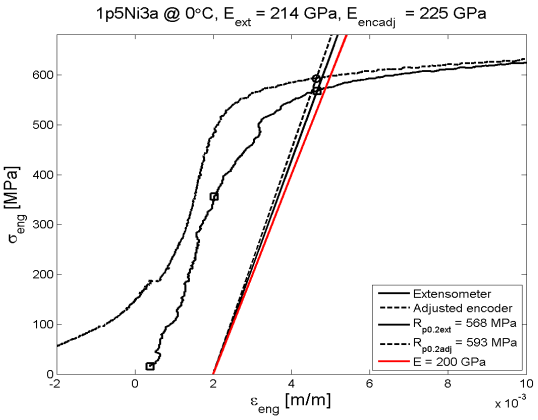


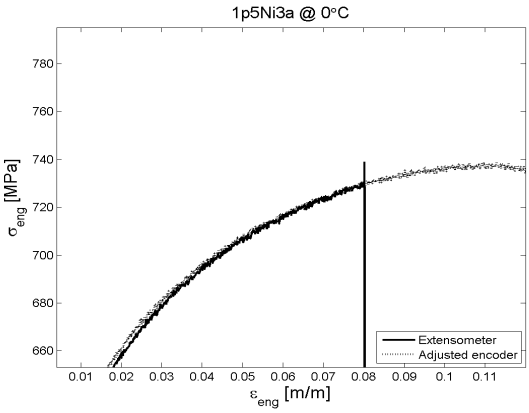


The extensometer signal is quite stable before testing. The cooling procedure is: going to -2° C, then slowing the stirrer and waiting for the temperature to rise. -1° C is kept during nearly the whole test.

*5Ni surface cross weld at 0°C ^*

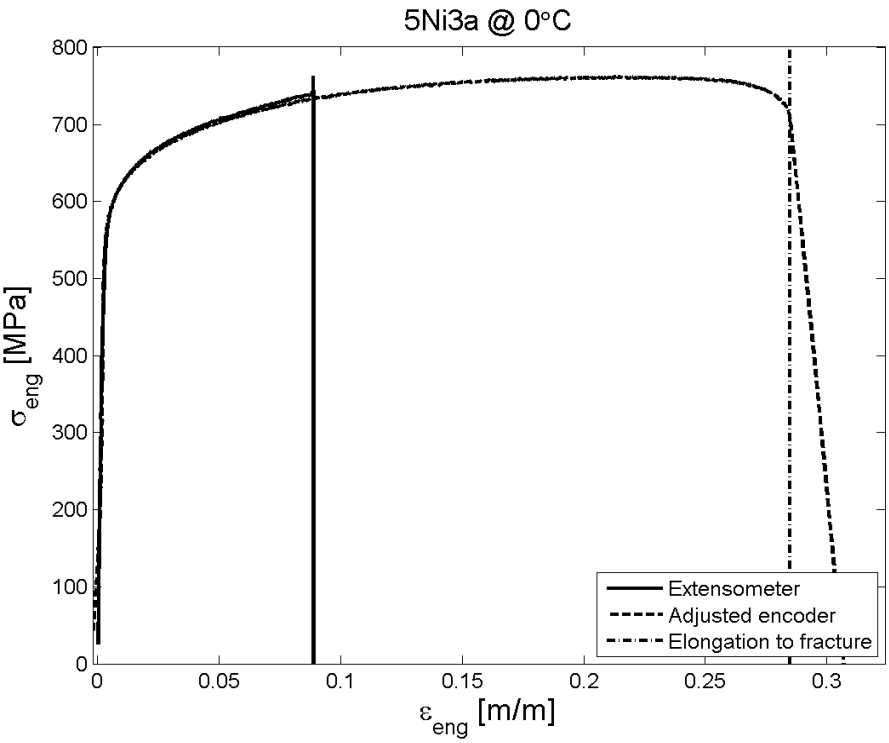


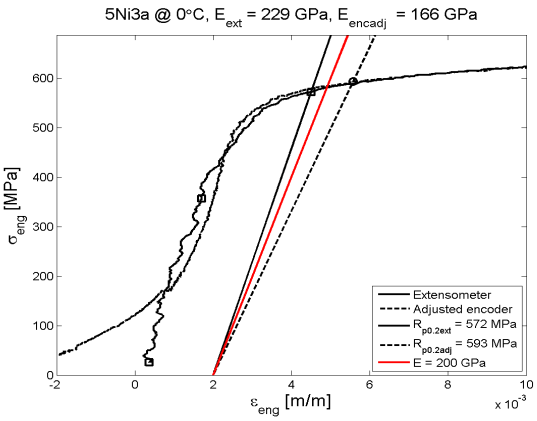


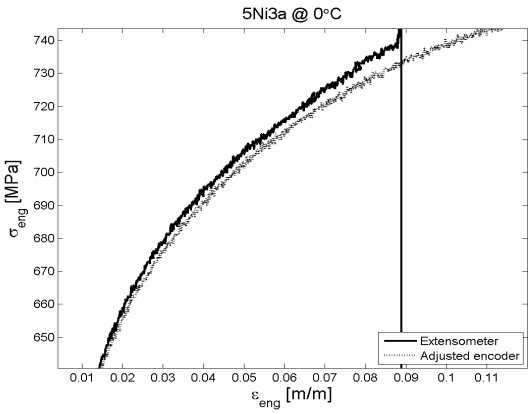


The oscillation of the extensometer before testing is +/- 0,01 mm, so quite much. The whole test is performed at 0°C. The extensometer signal is not good during the test and there are some slippages, too.

*7Ni surface cross weld at 0°C ^*

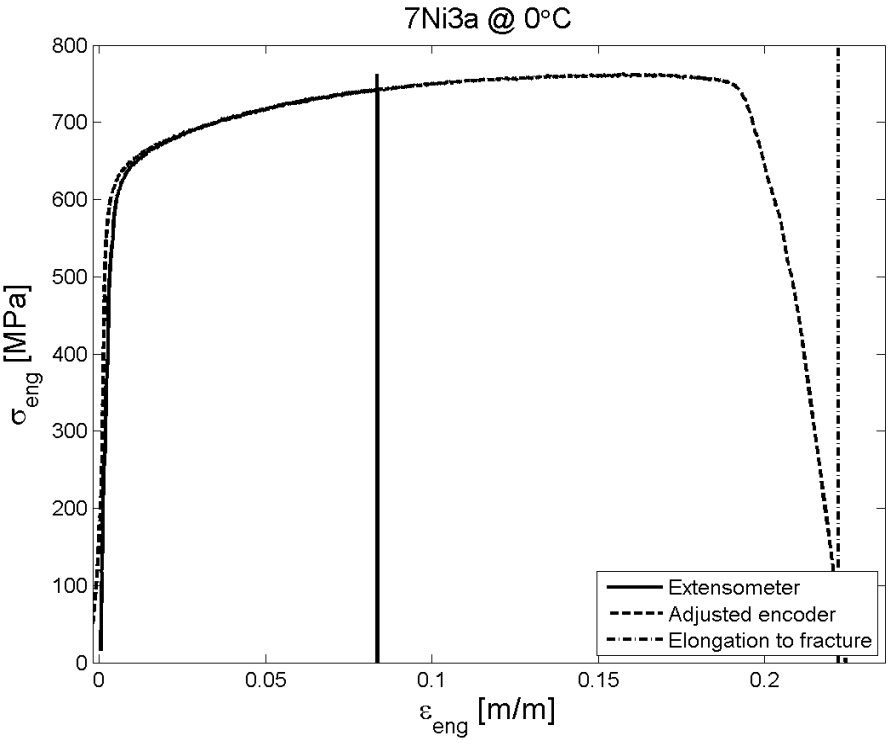


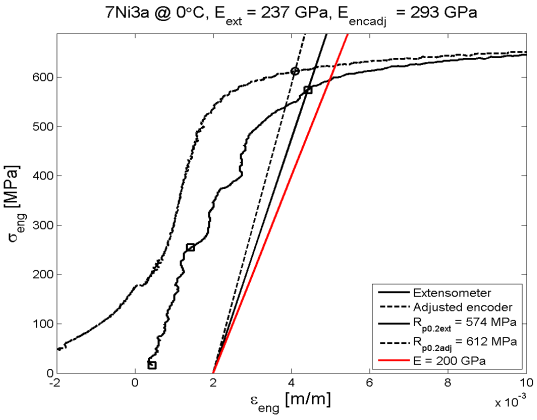


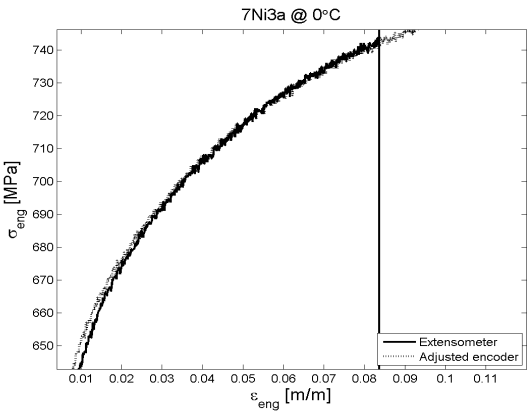


The extensometer signal tends to lower before the test and is not good during it. Most of the test is performed at -1°C.

*1,5Ni weld at 0°C ^*

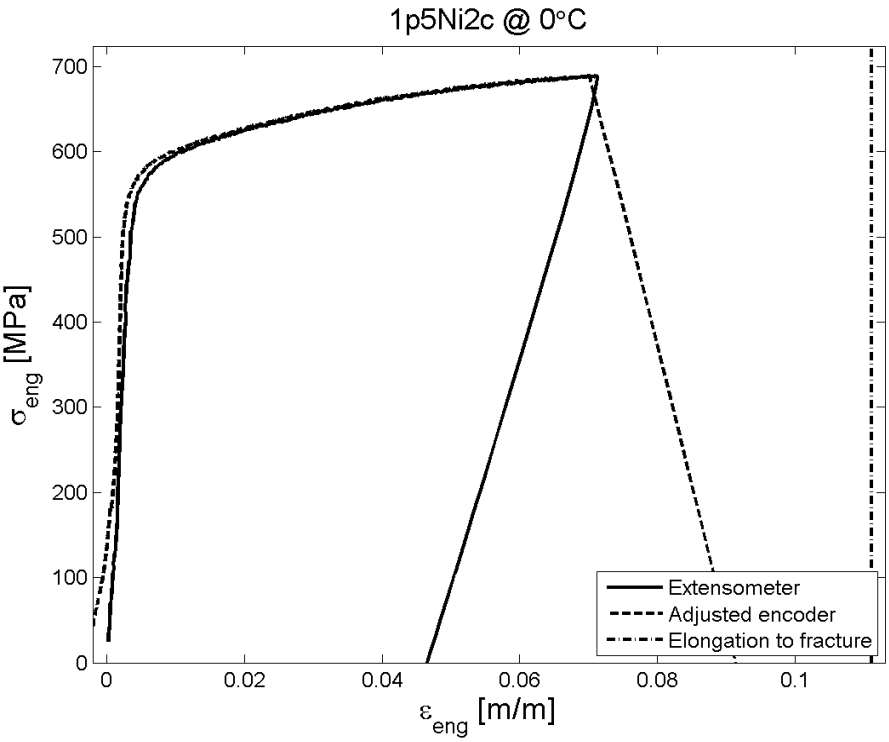


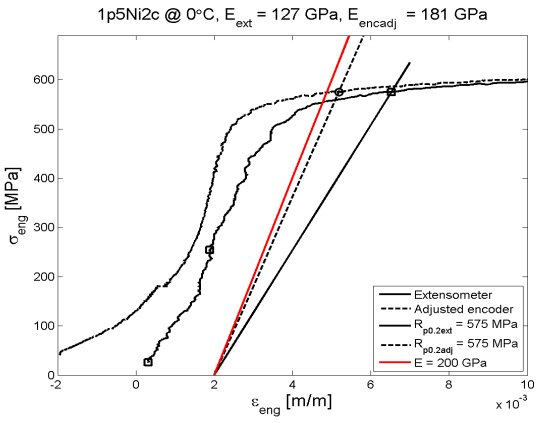


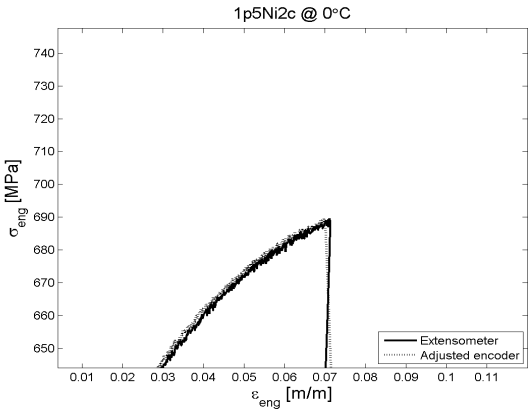

*5Ni weld at 0°C*

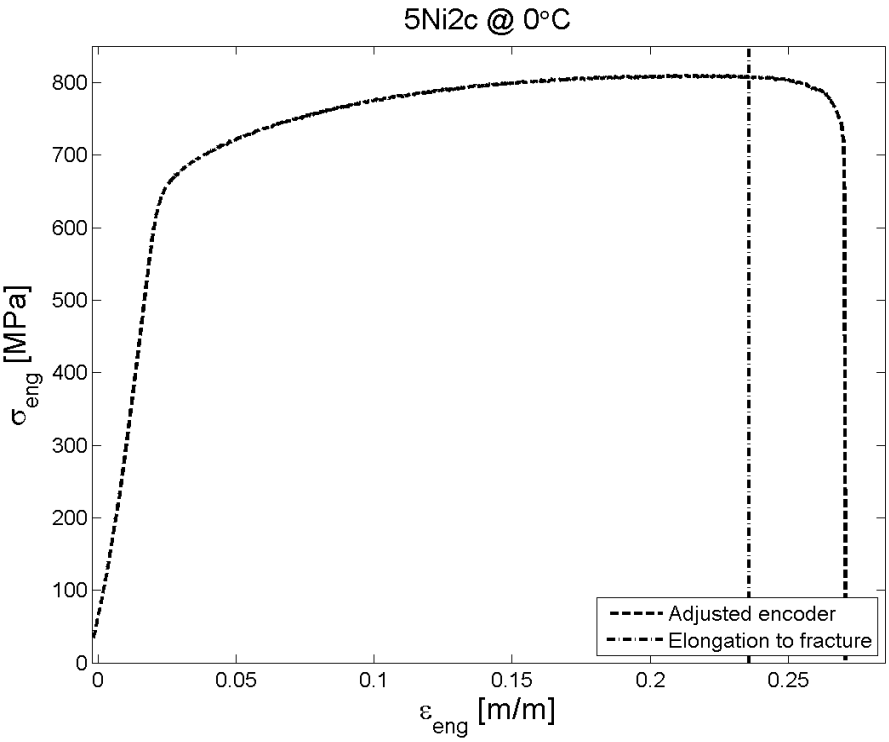


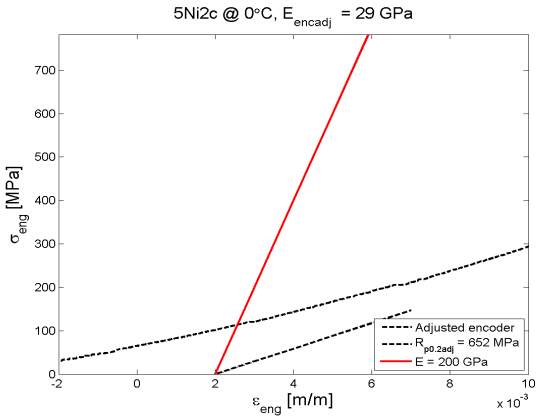


The extensometer does not work during this test: it is not possible elaborating the datas in the usual way. The compliance is taken as the average of those of *weld* specimens at 20°C.

*7Ni weld at 0°C ^*

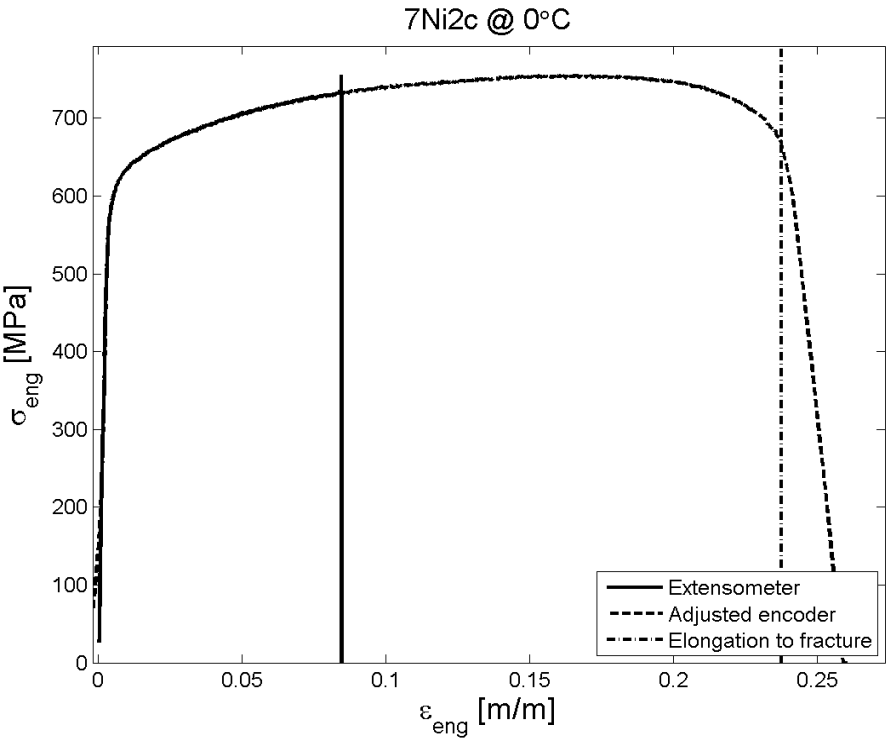


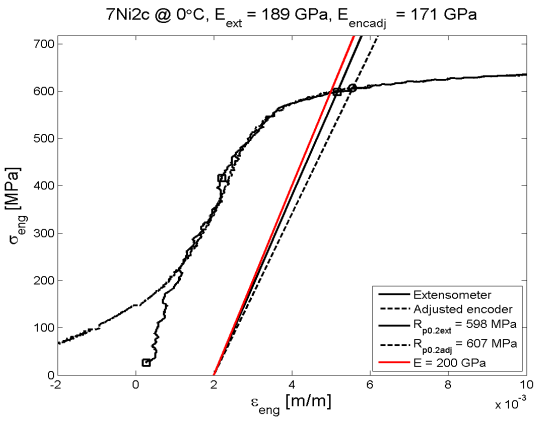


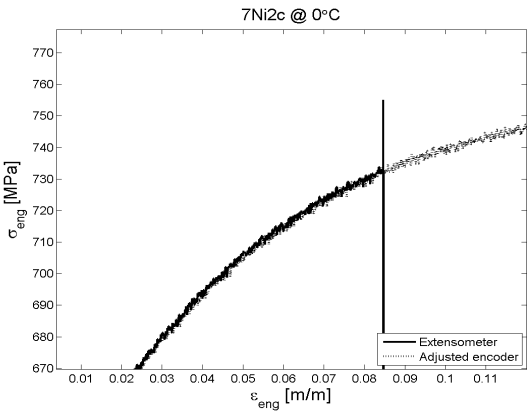

*Specimens at -20° C*

*1,5Ni surface cross weld at -20°C ^*

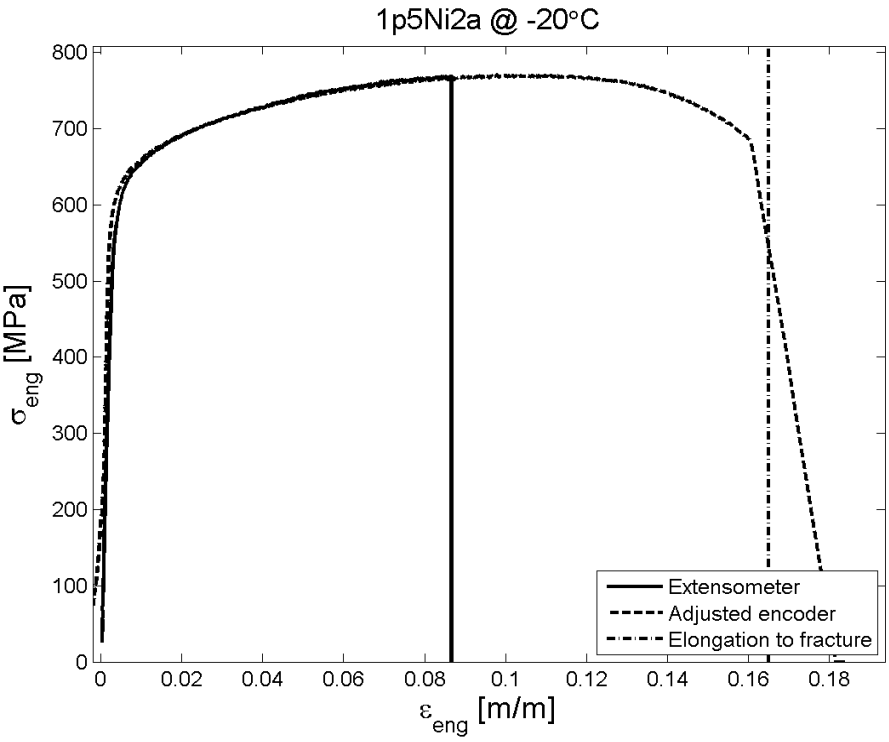


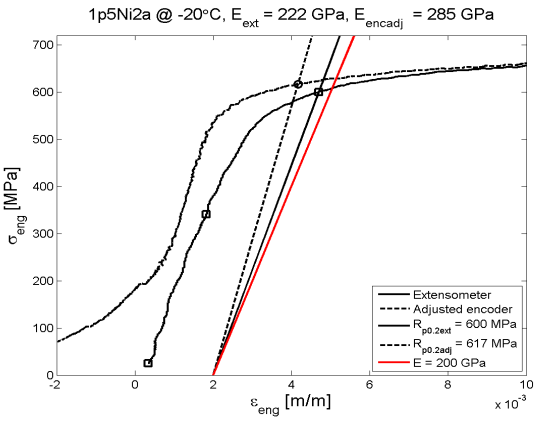


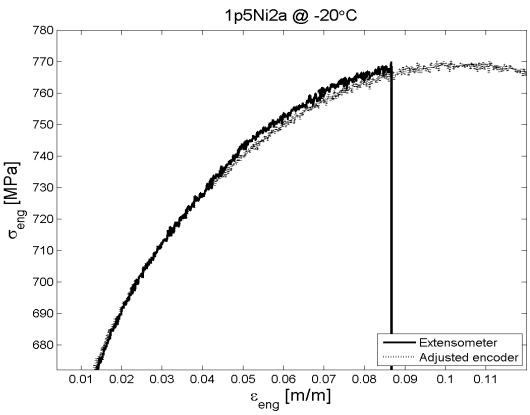

*5Ni surface cross weld at -20°C ^*

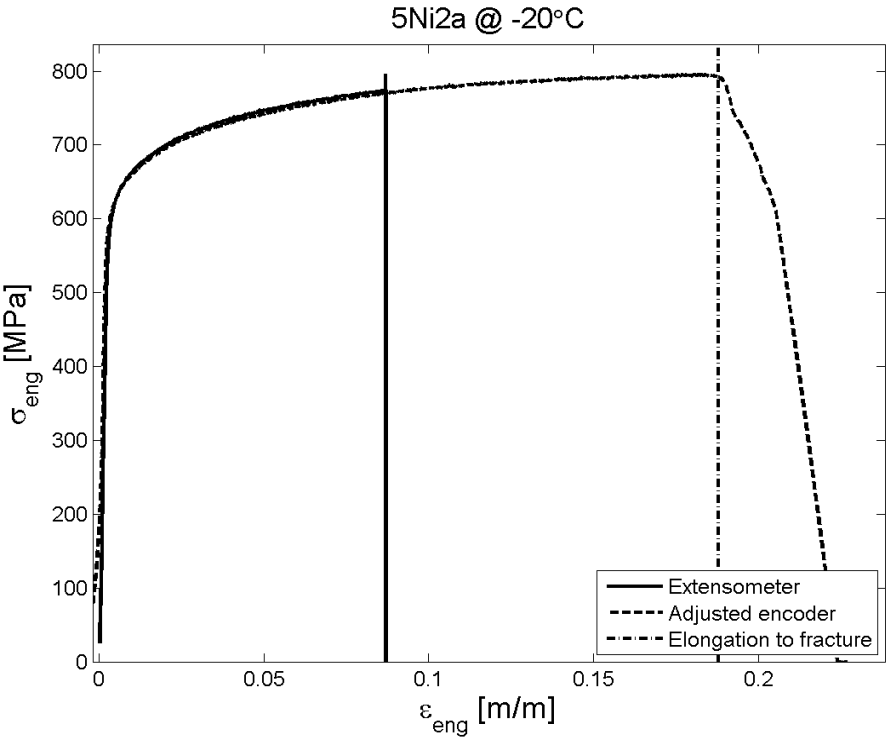


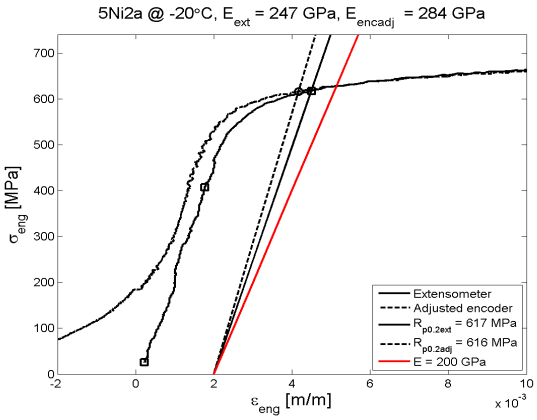


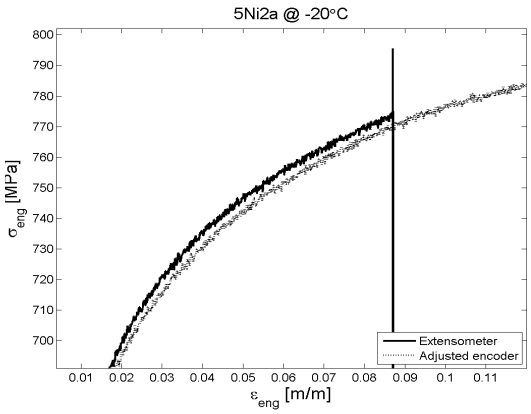

*7Ni surface cross weld at -20°C ^*

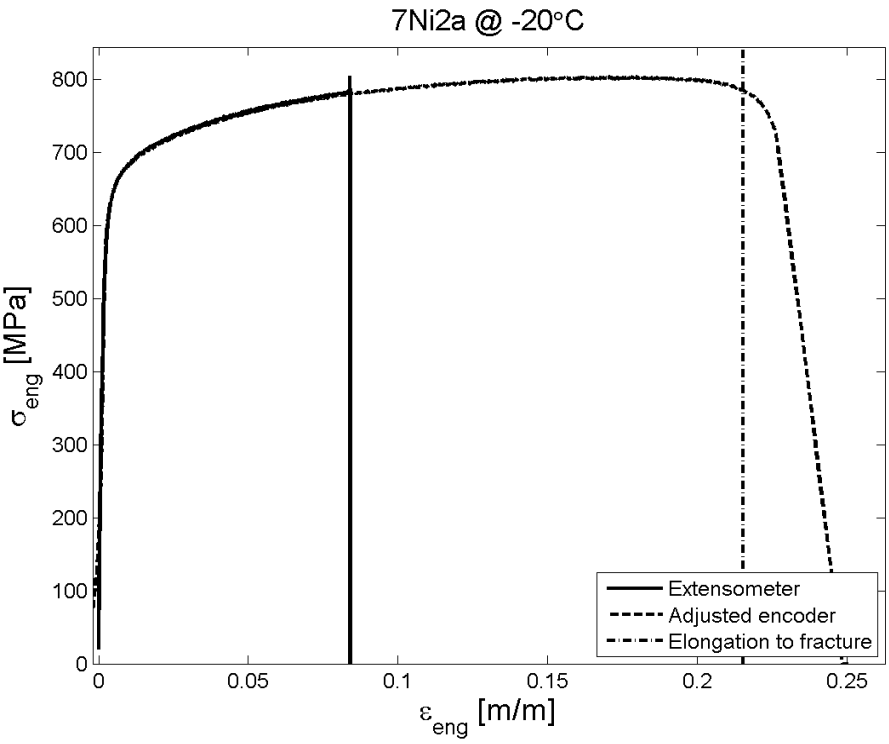


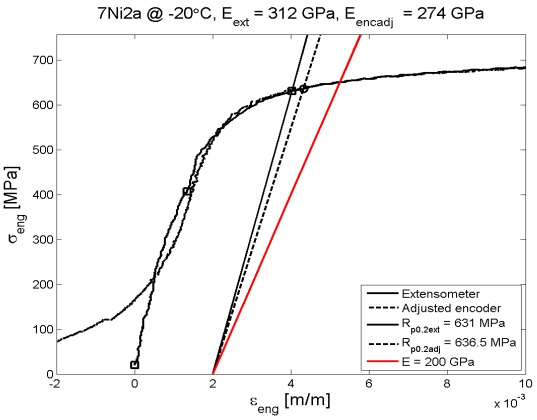


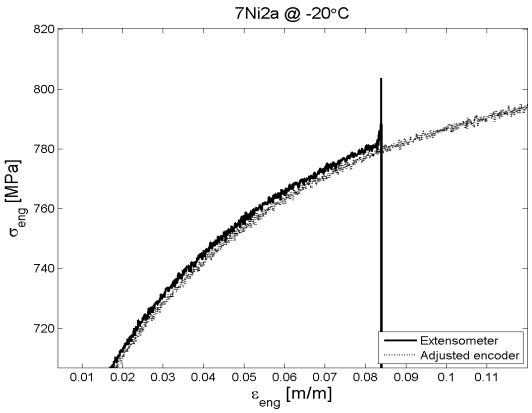


The test starts after 3 minutes at -20° C. The extensometer signal is quite stable before testing.

*1,5Ni root cross weld at -20°C ^*

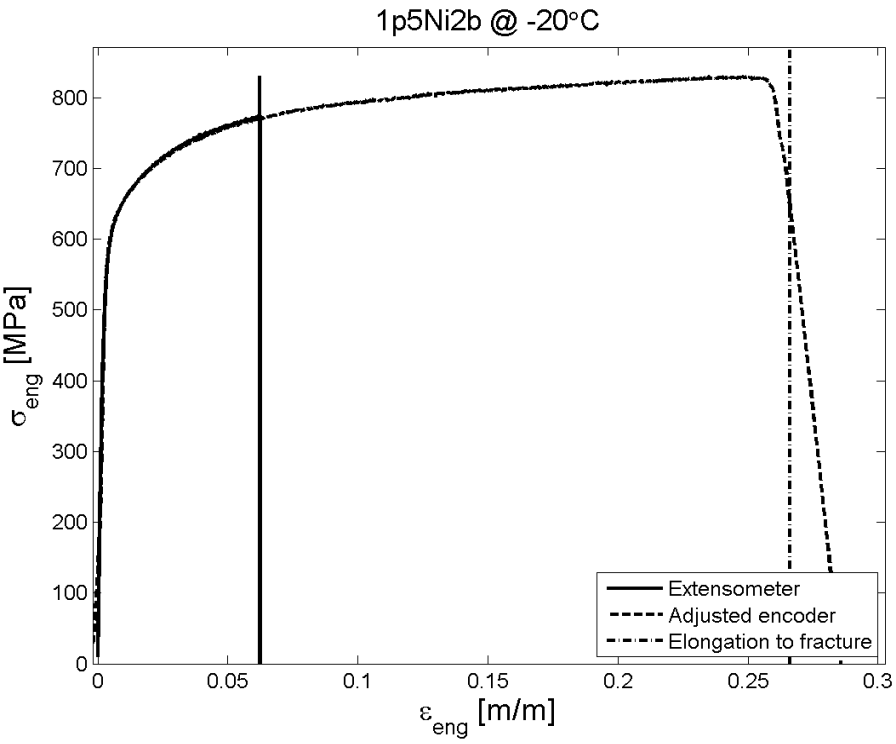


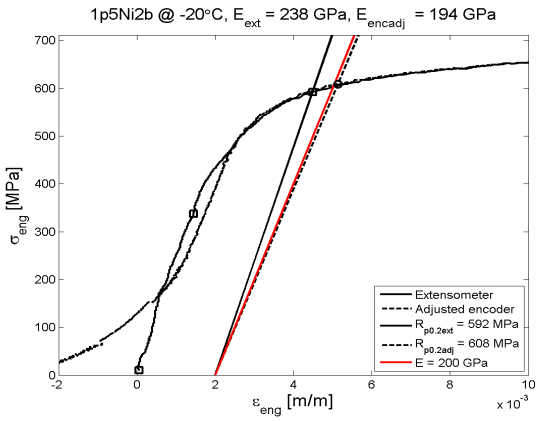


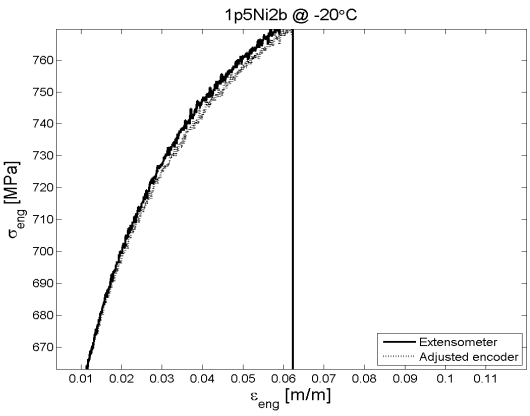

*5Ni root cross weld at -20°C ^*

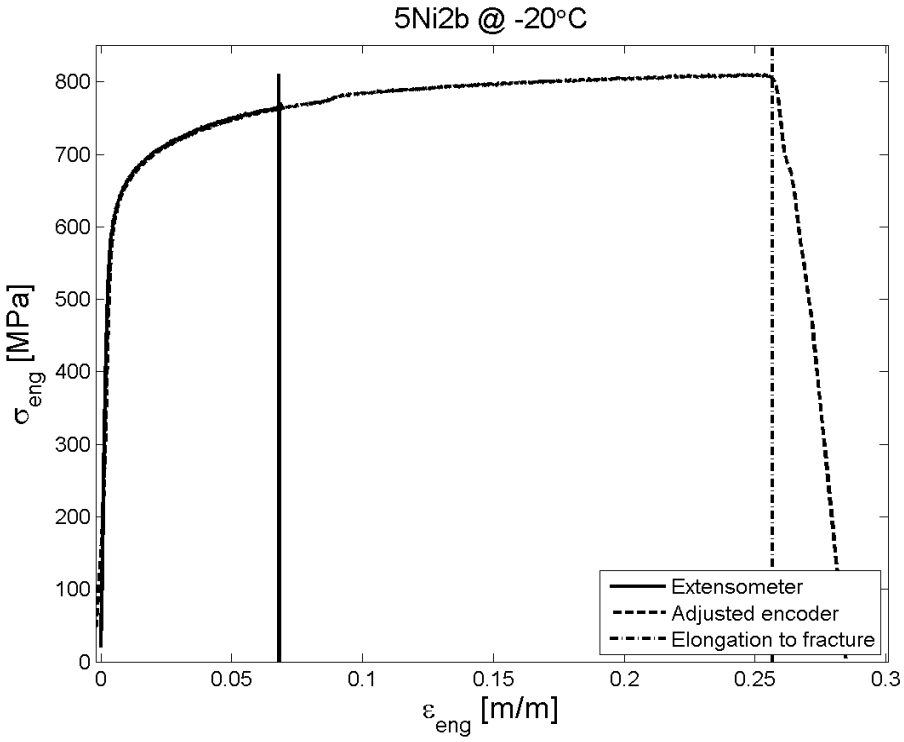


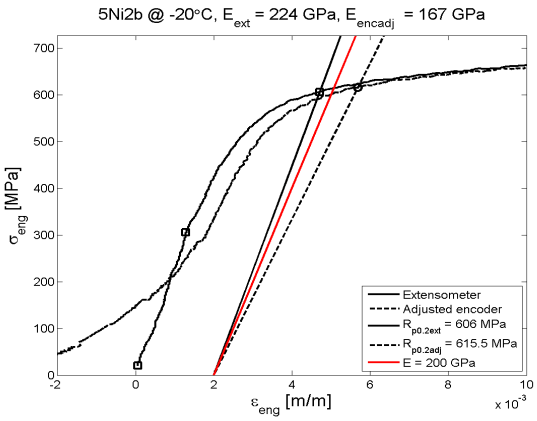


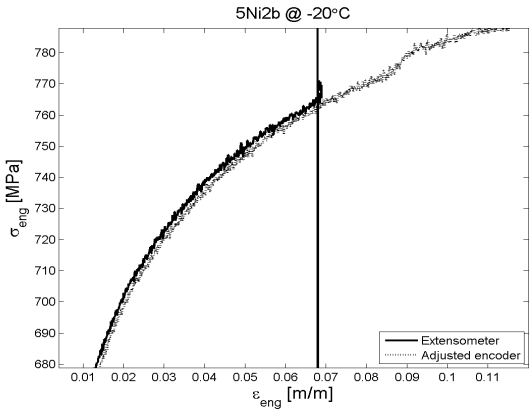


After the yield point, there is an extensometer slippage. The increase in load after the yield point is due to the temperature reduction to -20° C after it increased to -18° C. It is not possible keeping the temperature at -20° C after the start of the test because the stirrer would disturb the extensometer signal, see 5.3.

*7Ni root cross weld at -20°C ^*

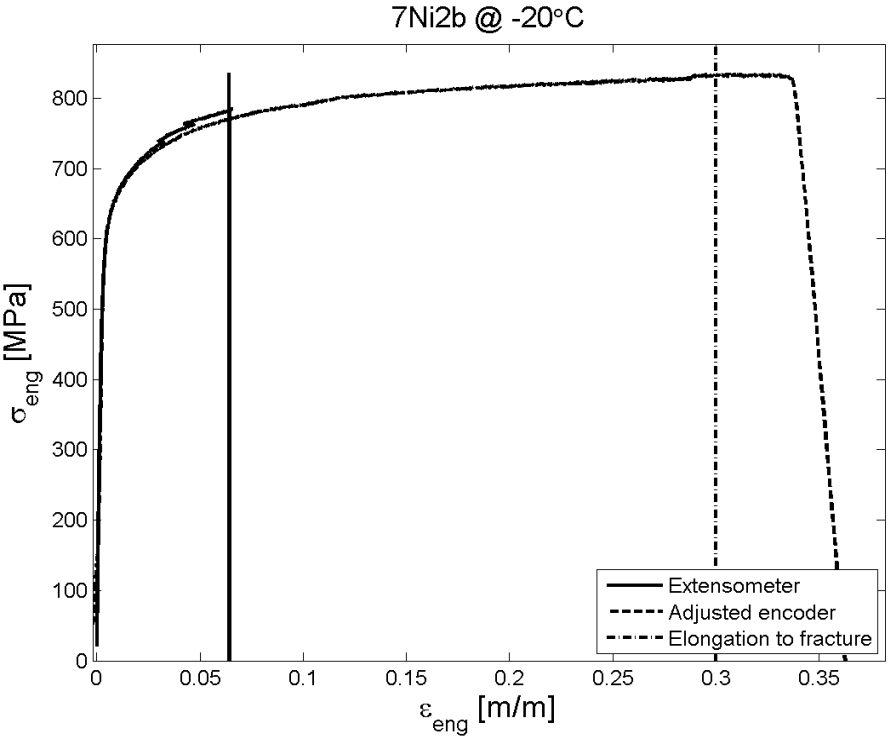


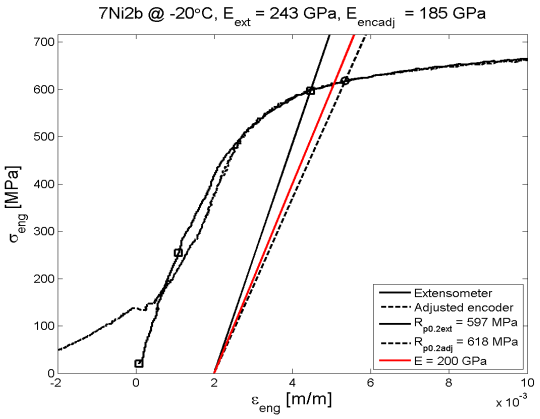


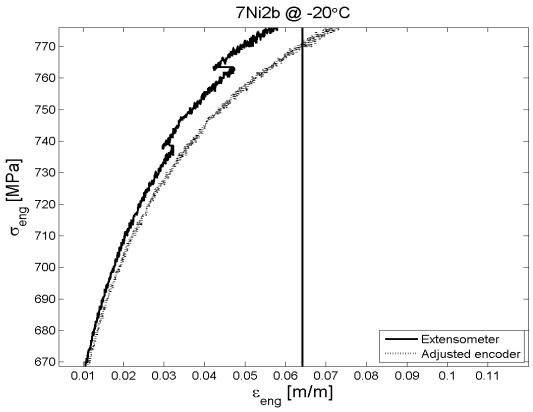


The extensometer slips more times after the elastic range; this causes mismatch between extensometer and encoder signal. Anyway, this does not affect the encoder adjustment because the compliance is found thanks to the signal in the elastic range only. Unfortunately, the extensometer signal is not so good even in the latter.

*1,5Ni weld at -20°C ^*

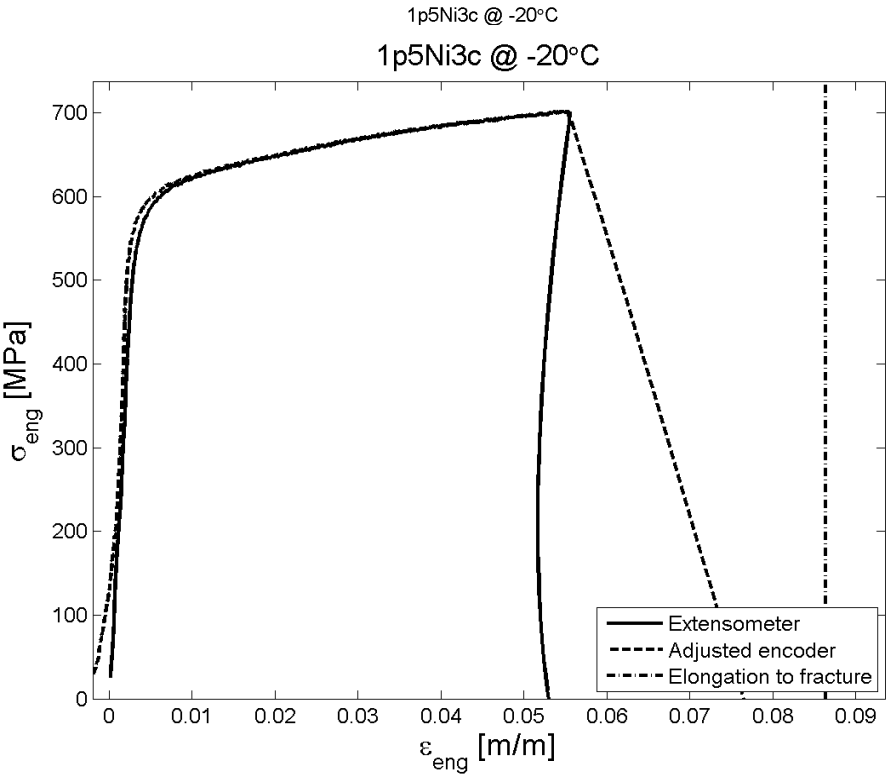


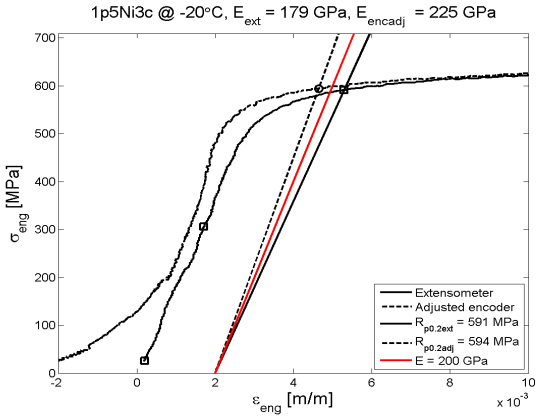


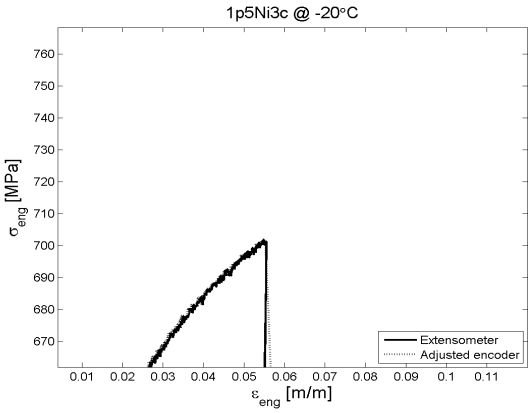


The failure is sudden so the extensometer springs back.

*5Ni weld at -20°C ^*

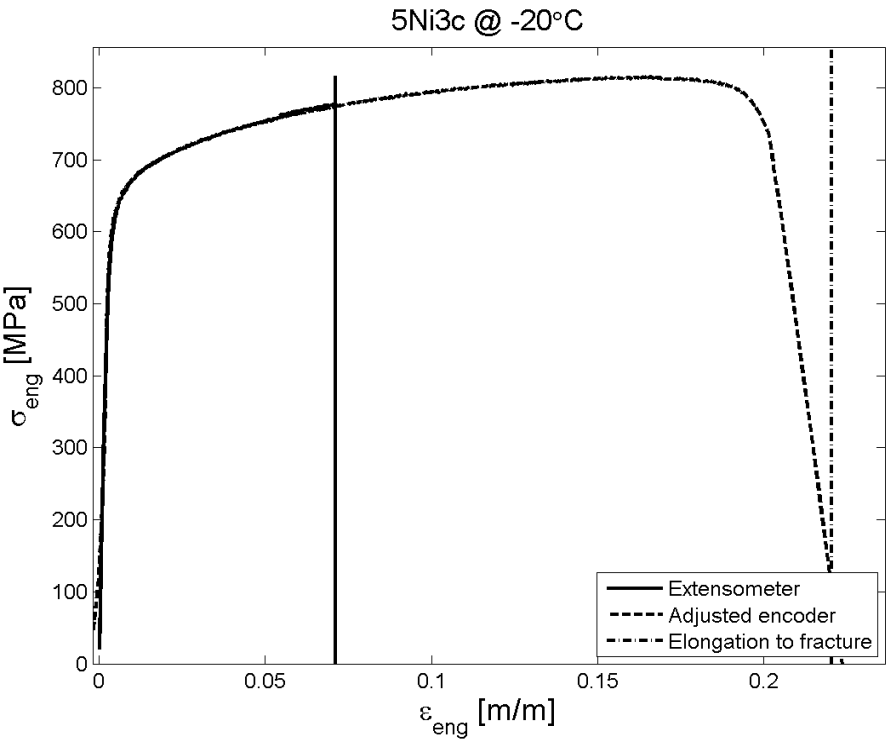


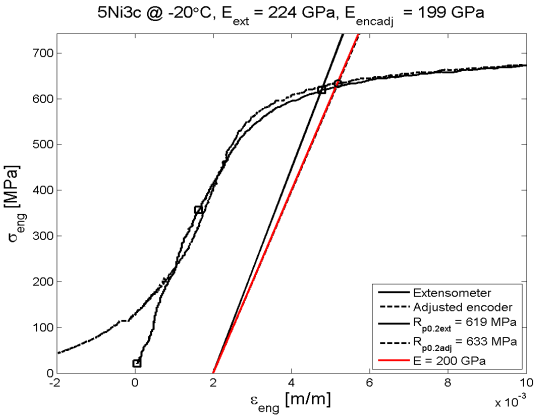


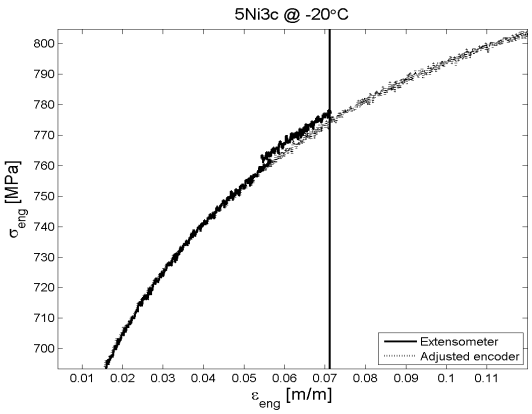


One infuser gets stuck in the nitrogen bucket, so in this test 3 infusers are used instead of 4: it is more difficult to keep the temperature stable. The yield point is still reached at -20°C, but then most of the test is performed at -19° and -18°C.

*7Ni weld at -20°C*

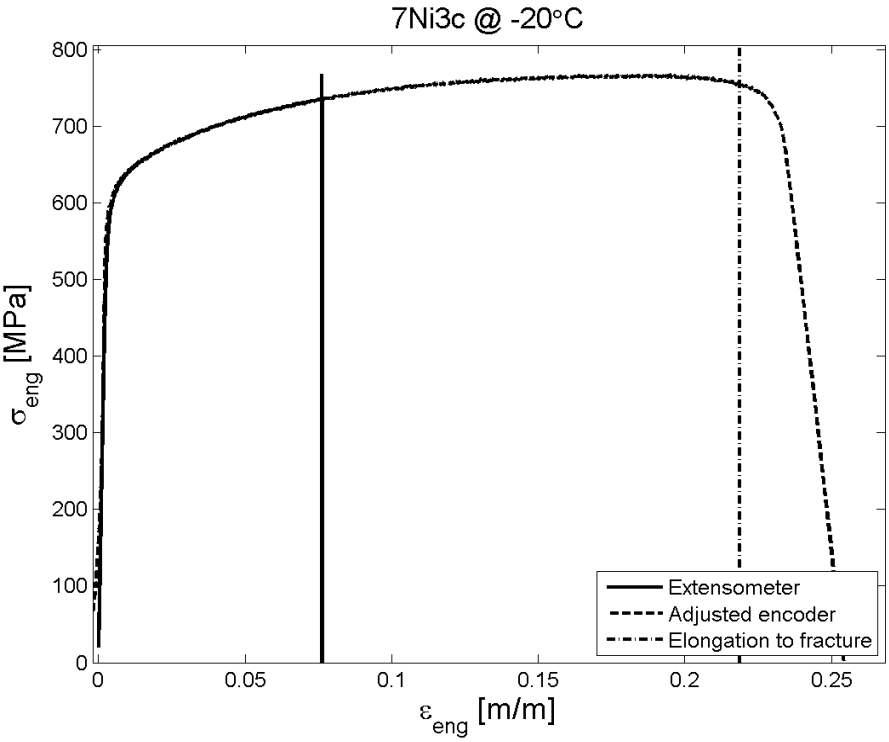


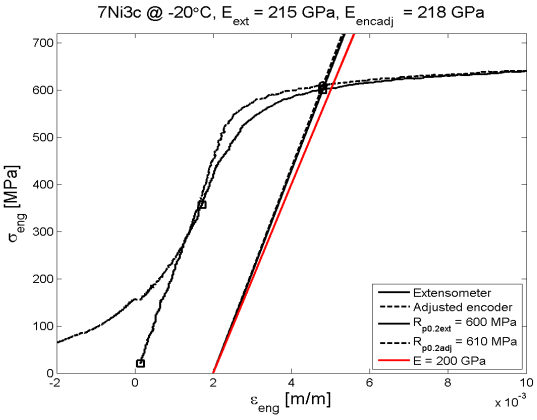


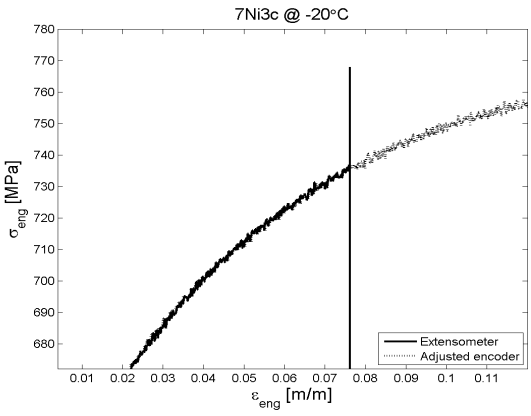


Same experimental problem as for the previous specimen. Moreover, due to nitrogen shortage during the test, the temperature cannot be well controlled and it rises slowly throughout the test, reaching -17°C at the end of the test.

*Specimens at -40° C*

*1,5Ni surface cross weld at -40°C*

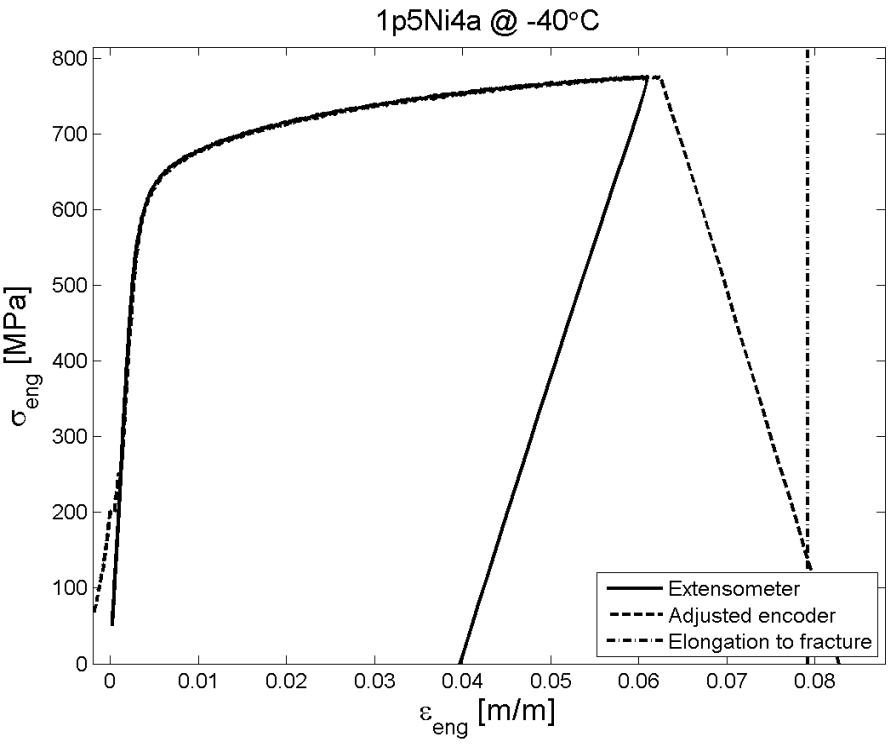


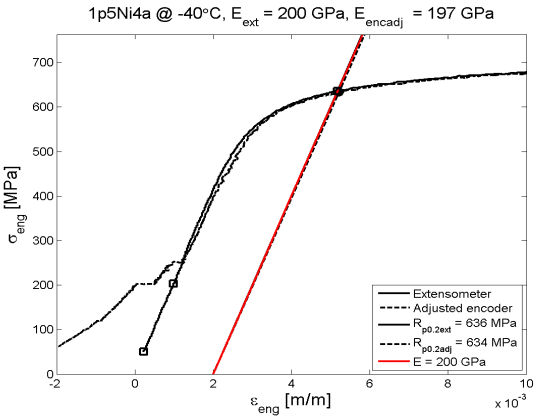


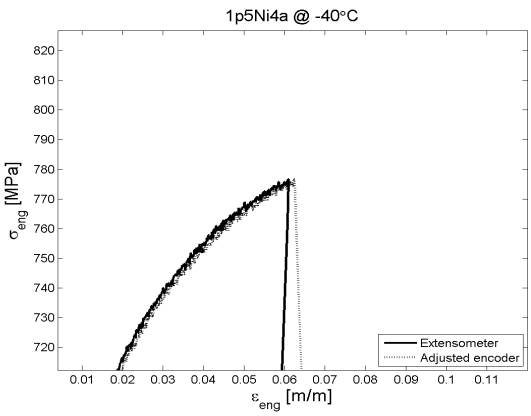


Before the test, the specimen is accidentally loaded 1,5 kN in compression for little time and promptly unloaded. That value should still be in the elastic range and the specimen does not look bent before testing. The specimen breaks little after the yield point. The extensometer signal is very stable, as during all tests at -40°C.

*5Ni surface cross weld at -40°C*

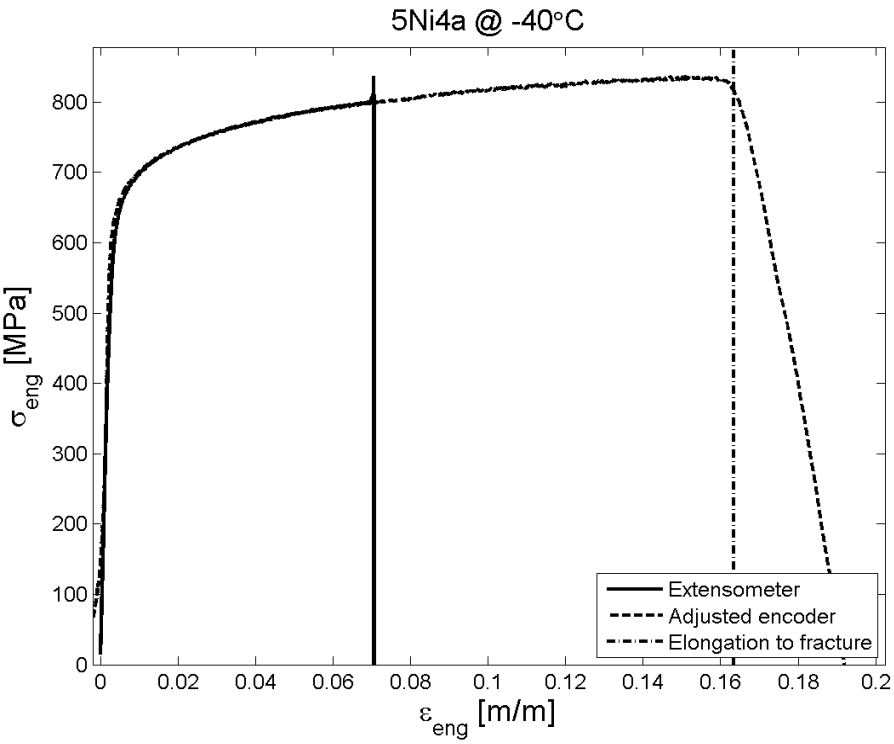


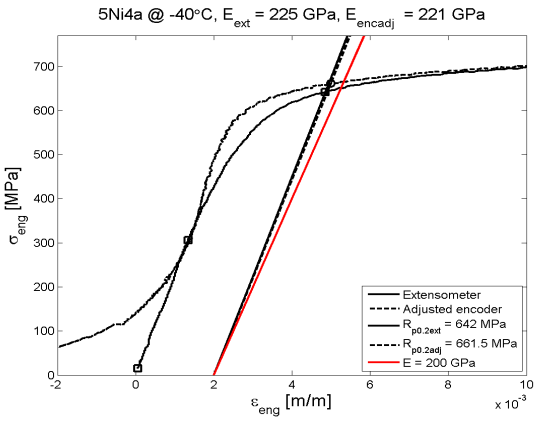


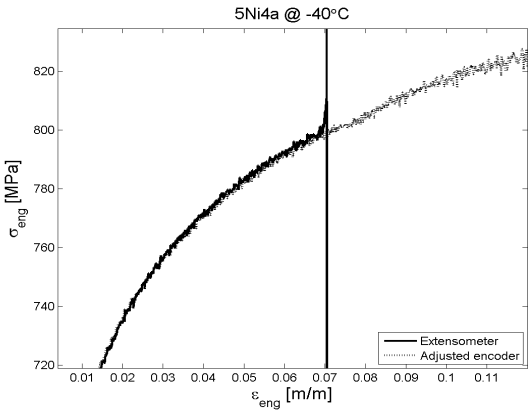


The temperature stays at -40° C till after the elastic range. Then, it increases to -39° and -38°C. When the extensometer reaches the maximum opening, the stirrer is speeded up and the temperature is brought back to -40° C until the end of the test. This increase in temperature causes a slight increase in stress level.

*7Ni surface cross weld at -40°C*

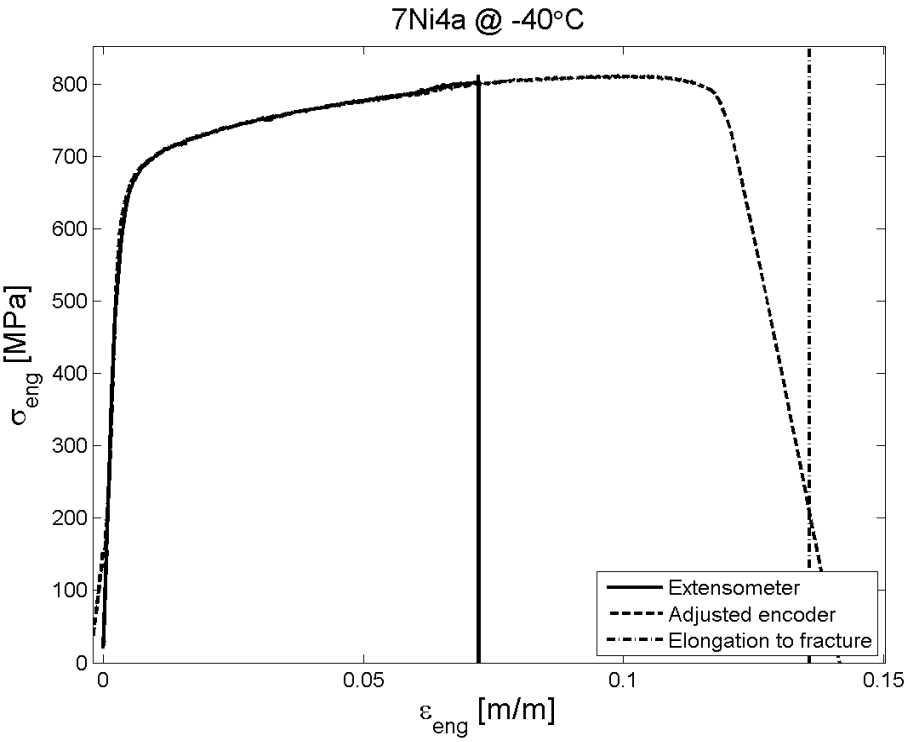


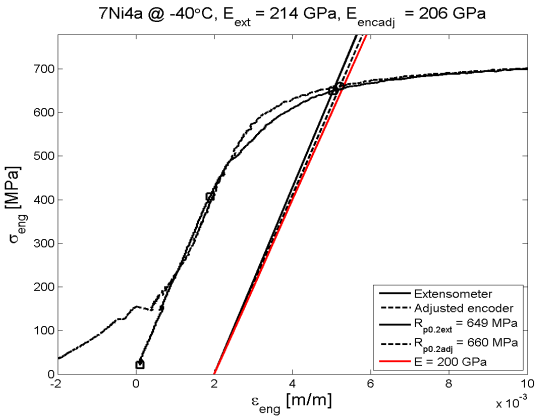


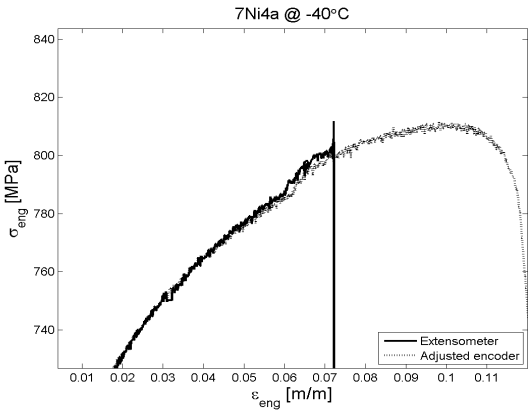


The extensometer shows slippages that should not affect any calculated property since they occur after the elastic range. Same experimental problem as for the previous specimen.

*1,5Ni weld at -40°C*

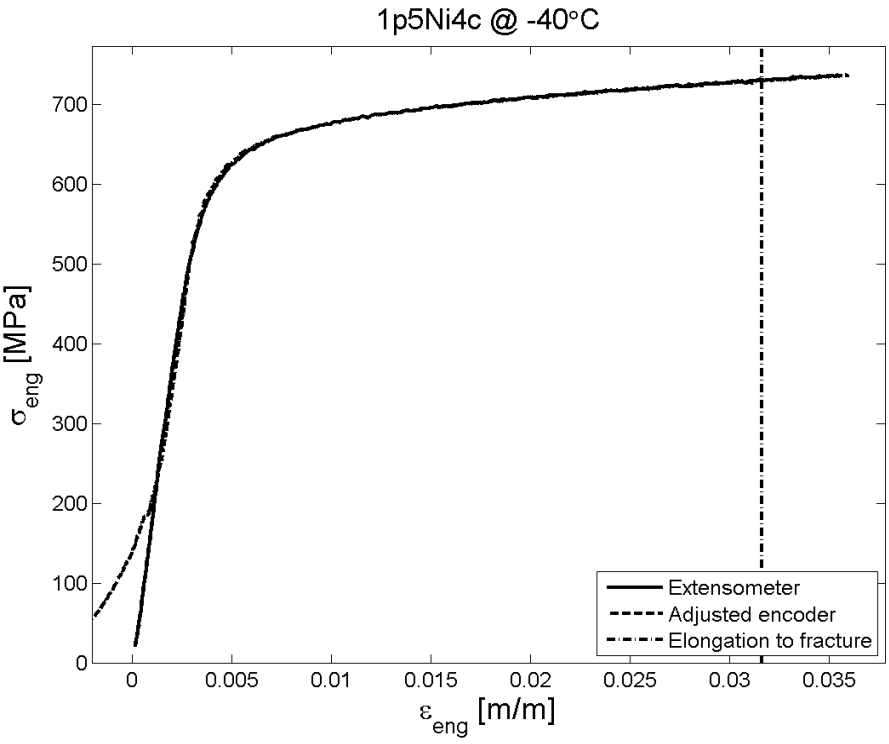


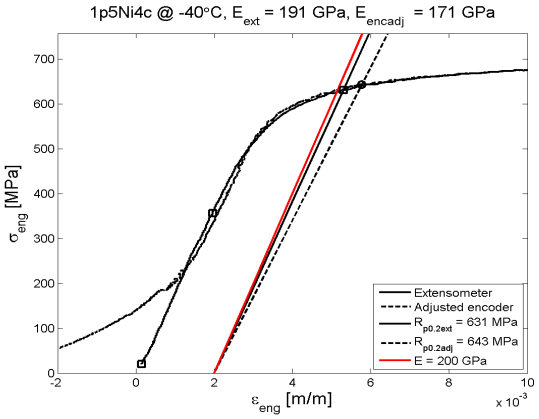


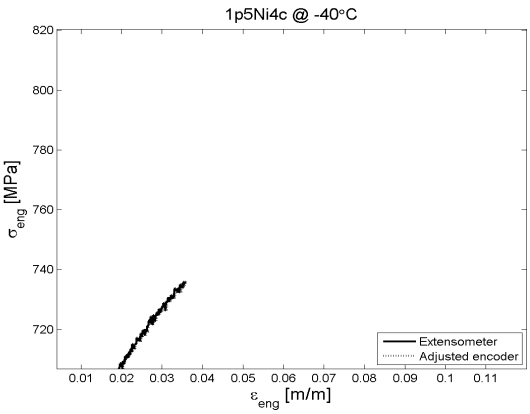


The specimen is preloaded at 0,5 kN and unloaded. Values about that are not registered. The matching between encoder and extensometer signal is perfect.

*5Ni weld at -40°C*

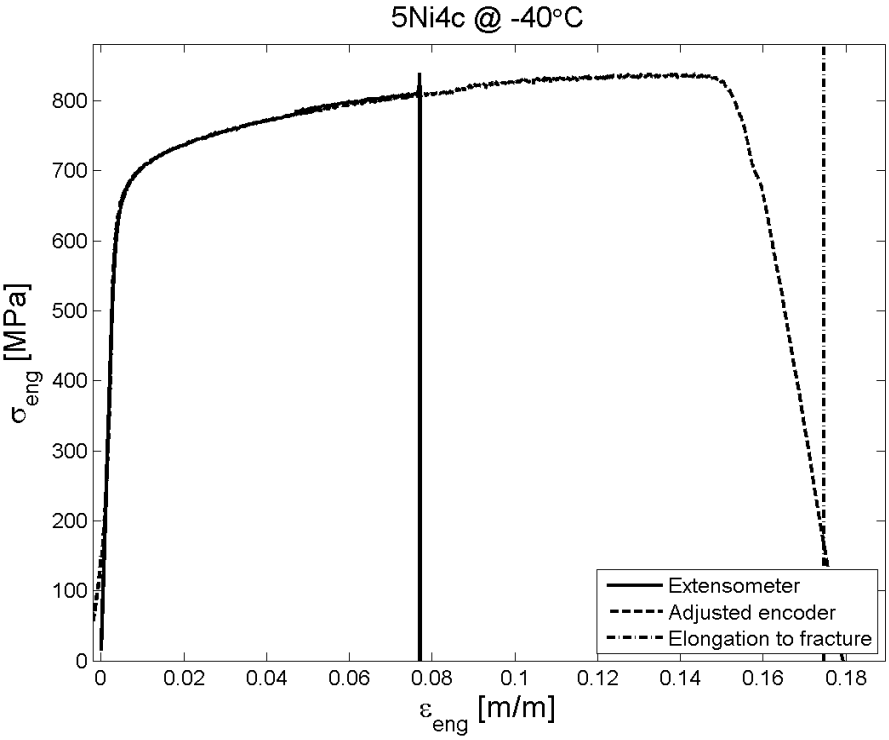


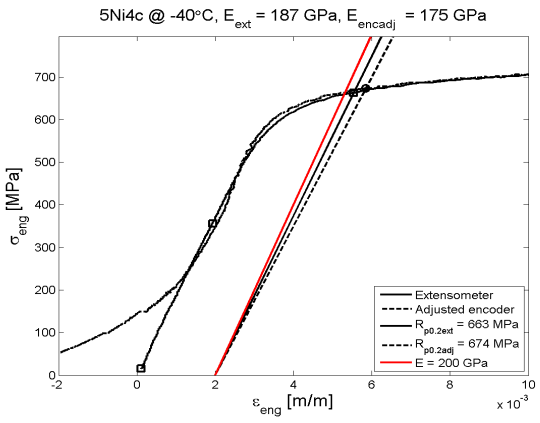


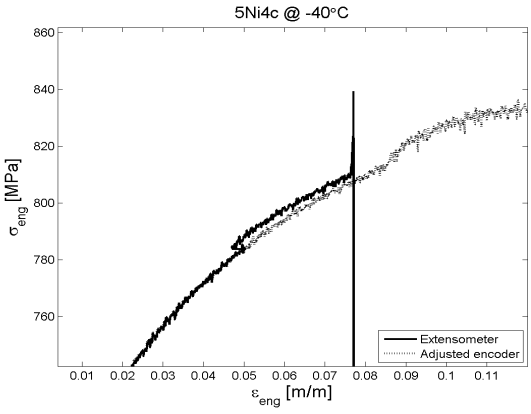


The specimen is preloaded at 0,5 kN and unloaded. Values about that are not registered. Same main experimental problem as for the *5Ni_surface cross weld* at -40°C.

*7Ni weld at -40°C*

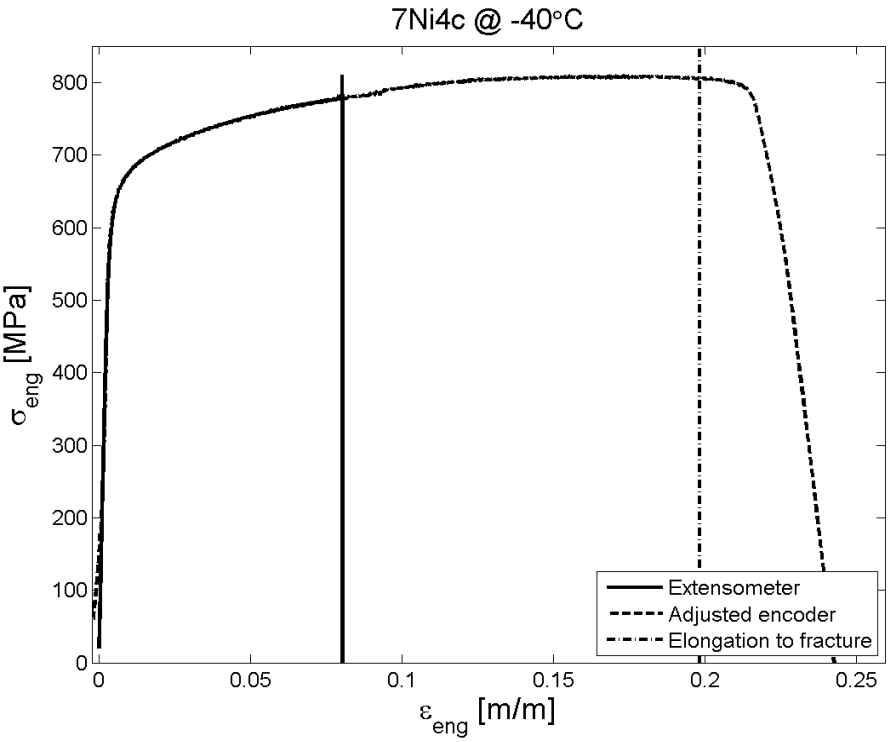


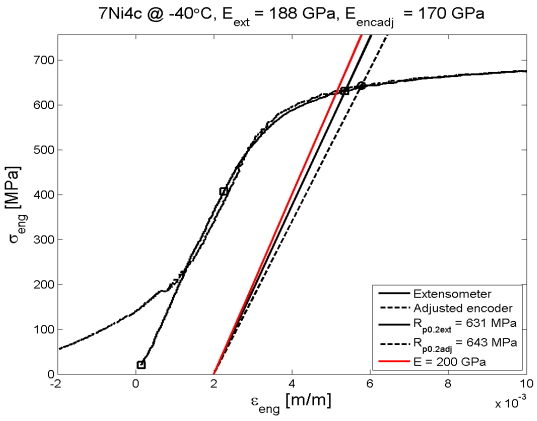


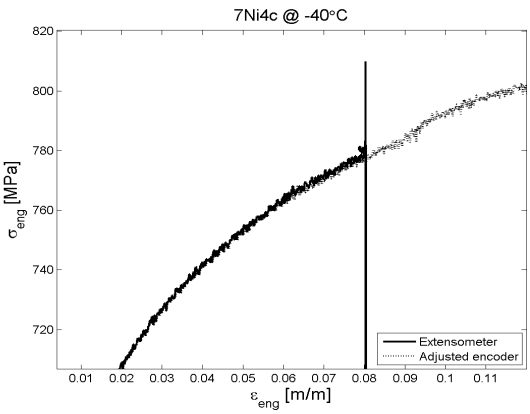


The specimen is preloaded at 0,5 kN and unloaded. Values about that are not registered. Same main experimental problem as for the *5Ni_surface cross weld* at -40°C.